

Comparative Analysis of the Physiological and Transport Functions of Various Sources of Renal Proximal Tubule Cells Under Static and Fluidic Conditions in PhysiMimix™ T12 Platform¹

Courtney Sakolish,¹ Haley L. Moyer,¹ Han-Hsuan D. Tsai,¹ Lucie C. Ford,¹

Allison N. Dickey², Piyush Bajaj³, Remi Villenave⁴, Philip Hewitt⁵,

Stephen S. Ferguson⁶, Jason Stanko⁶ and Ivan Rusyn¹

¹Department of Veterinary Physiology and Pharmacology, Texas A&M University, College Station, TX 77843, USA

²Bioinformatics Research Center, North Carolina State University, Raleigh, NC 27695, USA

³Global Investigative Toxicology, Preclinical Safety, Sanofi, Cambridge MA 02141, USA

⁴Roche Pharma Research and Early Development, Roche Innovation Center Basel, F. Hoffmann-La Roche Ltd, Basel, Switzerland

⁵Chemical and Preclinical Safety, Merck KGaA, Darmstadt, Germany

⁶Division of Translational Toxicology, National Institute of Environmental Health Sciences, Research Triangle Park, NC, 27709, USA

¹ This work was performed via the TEX-VAL Consortium collaboration funded by equitable monetary contributions from member organizations (American Chemistry Council, Bristol-Myers Squibb, Merck KGaA (Darmstadt, Germany), National Institute of Environmental Health Sciences, Sanofi, Unilever, Roche, and United States Environmental Protection Agency). This work was also supported, in part, by a grant from the National Institutes of Health U24 TR002633 and the United States Environmental Protection Agency (STAR RD84003201).

Running Title:

RPTEC qualification in a renal proximal tubule tissue chip

Corresponding author:

Ivan Rusyn, MD, PhD, Professor, Department of Veterinary Physiology and Pharmacology,
Texas A&M University, (979) 458-9866, irusyn@tamu.edu

Number of text pages:	35
Number of tables:	0
Number of figures:	8
Number of references:	71
Number of words in the Abstract:	250
Number of words in the Introduction:	712
Number of words in the Discussion:	3124

Nonstandard abbreviations:

Computer Fluid Dynamics (CFD), fluorescein isothiocyanate (FITC), para-aminohippurate (PAH), perfluorooctanoic acid (PFOA), phosphate buffered saline (PBS), principal component analysis (PCA), renal proximal tubule epithelial cells (RPTECs), Templated Oligonucleotide Sequencing Assay (TempO-Seq), transepithelial electrical resistance (TEER).

Abstract

In vitro models that can faithfully replicate critical aspects of kidney tubule function such as directional drug transport are in high demand in pharmacology and toxicology. Accordingly, development and validation of new models is underway. The objective of this study was to characterize physiological and transport functions of various sources of human renal proximal tubule epithelial cells (RPTECs). We tested TERT1-immortalized RPTEC, including OAT1-, OCT2- or OAT3-overexpressing variants, and primary RPTECs. Cells were cultured on transwell membranes in static (24-well transwells) and fluidic (transwells in PhysioMimix™ T12 organ-on-chip with 2 μ L/s flow) conditions. Barrier formation, transport, and gene expression were evaluated. We show that two commercially available primary RPTECs were not suitable for studies of directional transport on transwells because they formed a substandard barrier even though they exhibited higher expression of transporters, especially under flow. TERT1-parent, -OAT1 and -OAT3 cells formed robust barriers, but were unaffected by flow. TERT1-OAT1 cells exhibited inhibitable para-aminohippurate transport, it was enhanced by flow. However, efficient tenofovir secretion and perfluorooctanoic acid reabsorption by TERT1-OAT1 cells were not modulated by flow. Gene expression showed that TERT1 and TERT1-OAT1 cells were most correlated with human kidney than other cell lines, but that flow did not have noticeable effects. Overall, our data show that addition of flow to *in vitro* studies of the renal proximal tubule may afford benefits in some aspects of modeling kidney function, but that careful consideration of the impact such adaptations would have on the cost and throughput of the experiments is needed.

Significance Statement:

The topic of reproducibility and robustness of the complex microphysiological systems is looming large in the field of biomedical research; therefore, the uptake of these new models by the end-users is slow. This study systematically compared various RPTEC sources and experimental conditions, aiming to identify the level of model complexity needed for testing renal tubule transport. We demonstrate that while tissue chips may afford some benefits, their throughput and complexity need careful consideration in each context of use.

Introduction

Drugs and chemicals can have adverse effects on renal function by acting on a variety of cell types, potentially resulting in hemodynamic, inflammatory, and metabolic effects (Schreiner, 1965; Zager, 1997). While a number of kidney injury biomarkers have been recently proposed, and some have been qualified for clinical use (Vaidya et al., 2008; Bonventre et al., 2010), there is a continuous need for early prediction of nephrotoxicity in pre-clinical and safety pharmacology studies (Faria et al., 2019). Animal models of acute and chronic kidney injury and disease have been widely used but suffer from a number of limitations, primarily their high cost, species differences, low throughput, high complexity, and ethical reservations, as well as the lack of sensitivity of blood and urine biomarkers for mild to moderate kidney injury (Fuchs and Hewitt, 2011). To improve prediction of nephrotoxicity and to better characterize toxicity and disease mechanisms, many *in vitro* models of kidney have been proposed (Nieskens and Wilmer, 2016; Faria et al., 2019; Bejoy et al., 2022). A recent systematic literature review of *in vitro* models of drug-induced kidney injury concluded that advanced models have mainly been focused on mimicking the proximal tubules, with cytotoxicity as the common endpoint (Irvine et al., 2021).

Two principal modes of research for development for *in vitro* models for the proximal tubule are: (1) engineering of immortalized or pluripotent stem cell-derived cultures of various cell types known to constitute the tubule, both individually or as organoids (Balzer et al., 2022), and (2) improving the microphysiological environment in which these cells reside by modulating flow/shear stress and extracellular matrices (Chen et al., 2021). Shear stress via fluid flow is thought to be especially important for creating physiologically-relevant kidney models because the maintenance of directional transport of fluids, electrolytes, and chemicals is critical for both optimal function, polarization and response to drugs and other xenobiotics. Shear stress can be modelled *in vitro* by introducing lateral medium movement across a monolayer of cells which is critical for correct organization of renal proximal tubule epithelial cell (RPTEC) cytoskeleton and tight junctions (Duan et al., 2008). Indeed, most advanced 3D cultures of RPTECs focus on

introducing shear stress into either membrane-based (Gao et al., 2011; Jang et al., 2013; Kim et al., 2022; Shaughnessey et al., 2022; Specioso et al., 2022), or tubule-based (Weber et al., 2016; Vormann et al., 2018; Ross et al., 2021) microfluidic designs.

Many kidney-focused organ-on-chip devices have been created and tested with various drugs and disease conditions (e.g., ischemia-reperfusion), which span a very wide range of flow rates and shear stresses. Physiological ranges for shear stress *in vivo* range from 0.3 to 1.2 dyne/cm² in healthy individuals, with values <0.5 generally regarded as corresponding to renal disease (Ross et al., 2021). In continuous flow-based kidney-focused organ-on-chip devices, reported values vary from 6.5×10^{-4} (Specioso et al., 2022) to 0.7 dyne/cm² (Shaughnessey et al., 2022). In some tubule-based models, the shear could be highly intermittent, reaching as high as 1.7 dyne/cm² for a few seconds, then quickly decaying over the next 1–2 min to nearly static condition (Vormann et al., 2018). The differences in shear stress across models and studies, as well as the use of different RPTEC sources in different reports, make it difficult to determine the advantages that may be afforded by the flow on both physiological and transport functions of RPTEC. Based on a number of recent studies on flow-based systems for renal proximal tubules, which encompassed both static and fluidic conditions (with some involving varying fluid flow rates), it remains unclear whether the advantages of introducing flow are readily apparent (Kim et al., 2022; Lee et al., 2022; Specioso et al., 2022).

Therefore, the objective of this study was to investigate barrier formation, directional transport, and gene expression with various sources of human RPTECs that were cultured on transwell membranes in two conditions – static (conventional 24-well transwells) and fluidic (transwells placed into the PhysioMimix™ TC12 organ-on-chip platform with 2 μL/s flow). Multiple sources of RPTECs were used as prior studies in different organ-on-chip platforms indicated that cell source selection often introduces the greatest variability between experiments (Sakolish et al., 2018; Sakolish et al., 2023). For transparency, all data and protocols from this study are publicly available using the database links listed in **Supplemental Table 1**.

Materials and Methods

Cell Sources and Medium Information

Human RPTEC sources (TERT1, TERT1-OAT1, TERT1-OCT2, and TERT1-OAT3) were obtained from ATCC (#CRL-4031, CRL-4031-OAT1, CRL-4031-OCT2, and CRL-4031-OAT3; Manassas, VA). These cells were cultured in DMEM:F12 (ATCC #30-2006) supplemented with the hTERT Immortalized RPTEC Growth Kit (ATCC #ACS-4007), and a G418 supplement (final concentration of 0.1 mg/mL; Geneticin G418 Sulfate, Gibco, Billings, MT). Human primary RPTECs were obtained from Lonza (CC-2553, lot# 18TL117405; Basel, Switzerland), and were cultured in REGM™ Renal Epithelial Cell Growth Medium (CC-3190, Lonza) supplemented with the “BulletKit” (CC-4127, Lonza) containing fetal bovine serum (0.5%), human transferrin (10 mg/mL), hydrocortisone (0.5 mg/mL), insulin (5 mg/mL), triiodothyronine (5×10^{-12} M), epinephrine (0.5 mg/mL), epidermal growth factor (10 mg/mL), and antibiotics (100 U/mL penicillin and 100 mg/mL streptomycin). Another human primary RPTEC was obtained from Biopredic (HRPTECs, lot RPT101037; Saint Grégoire, France); these cells were cultured in a basal media consisting of 1:1 DMEM (11966-025, Life Technologies, Carlsbad, CA) and Ham’s F-12 nutrient mix (11765054, Life Technologies), supplemented with either the Biopredic “ADD582C” supplement for thawing media, or “ADD583C” supplement for seeding and culture media. Primary RPTECs were shipped from vendors at passage 2 and were expanded prior to testing for an additional 1-2 passages.

Cell Seeding and Culture Conditions

All RPTECs were cultured in their respective medium (see above) at 37°C and 5% CO₂ in Tissue Culture-treated 75 cm² flasks (CLS430641U, Corning, Corning, NY) prior to seeding onto Transwells (#3413, Corning). On the day of seeding, Transwells were coated in the top well (“top seeded conditions”), or inverted and coated on the bottom surface of the membrane (“bottom

seeded conditions”) with 90 μL of 100 $\mu\text{g}/\text{mL}$ fibronectin (# F1141-5MG Sigma-Aldrich, St. Louis, MO) in phosphate buffered saline (PBS; Gibco) for 1 hour at 37°C. After coating, excess solution was removed, and RPTECs were seeded onto the coated surface at a density of 625,000 cells/mL in their respective cell culture medium (50,000 cells in 80 μL) and allowed to attach for 4 hours at 37°C. In bottom seeded conditions, after this incubation, wells were re-inverted into the culture plates. Cell culture medium was added (750 μL to the bottom, and 150 μL to the top well) to all cell-seeded wells. Transwell cultures were incubated overnight, then either left in the plates as-is (“static culture conditions”) or transferred to the MPS-T12 Barrier plate (“fluidic culture conditions”, 2 $\mu\text{L}/\text{s}$ flow rate) of the PhysioMimix™ organ-on-chip platform (CNBio, Cambridge, UK). Cell culture media was exchanged in both static and fluidic cultures every 48 hours. **Figure 1** shows the timelines and other details of different experiments conducted in this study. A schematic of the device is shown in **Supplemental Figure 1**.

Simulations of the Shear Stress by Computer Fluid Dynamics (CFD)

Shear stress in the experiments using MPS-T12 Barrier plate (2 $\mu\text{L}/\text{s}$ flow rate) on the PhysioMimix™ organ-on-chip platform was calculated using 3D models based on measured dimensions of the transwells and T12 plate. These models were generated using SimFlow 4.0 CFD software (SIMFLOW Technologies, Warsaw, Poland; <https://sim-flow.com>). The software was used to perform the model flow simulations and estimate the flow rate at the bottom surface of the transwell membrane within the T12 plate. After creation of the 3D models, the SimFlow “MESH” panel was used to create a high-resolution mesh, defining the inner surfaces of the volumetric model. This mesh was loaded into the solver panel, and the SIMPLE (Semi-Implicit Method for Pressure Linked Equations) algorithm was selected for vector calculations with steady state and incompressible fluid settings. Turbulence modeling was not considered, as we assumed mostly laminar flow within the microfluidic system. The Newtonian transport model was utilized, using “water” as the input material for the simulation as the closest approximation for cell culture

medium. Lastly, the inlet “boundary condition” was set to 2 $\mu\text{L/s}$, matching the flow rate used in our testing with the proximal tubule model. Monitor “probes” were placed at 25 evenly spaced locations on the bottom surface of the transwell membrane to output the calculated X \times Y fluid vectors at each of these locations. This model was run until solution residuals converged (final residuals 3.01e-7 in 548 iterations), and raw vector values were exported from the CFD program. Vectors from iterations 100-548 (when model had reached steady state) were averaged, and shear stress was calculated as $FSS = 6\eta Q/h^2w$ with the following parameters: η , viscosity = 0.84 Pa/s; Q, volumetric flow rate was calculated from outputted CFD vectors; h, height = 2 mm; and w, width = 10 mm). Height and width were measured as the transwell membrane diameter, and the space between the bottom of the T12 plate well and the membrane, respectively. See **Supplemental Figure 2** for the description of the fluidic model and spatial distribution of the shear stress based on the modeled flow rates at different locations on the transwell in this device.

Evaluation of Barrier Formation

The barrier integrity of RPTEC monolayers was monitored over time by measuring the transepithelial electrical resistance (TEER) in Transwell experiments. TEER was tested using an epithelial voltmeter with Ag/AgCl probes (EVOM2 with STX-2 electrodes, World Precision Instruments, Sarasota, FL). TEER values were calculated by subtracting the resistance value (Ω) of blank membranes and multiplying by the growth area of the Transwells used herein (0.33 cm^2). TEER results are reported as $\Omega \cdot \text{cm}^2$.

Barrier function was also evaluated using fluorescein isothiocyanate (FITC)-tagged dextran (70 kDa; FD70S, Sigma-Aldrich). FITC-dextran was dissolved in corresponding cell source-specific medium (0.25 mg/mL) and added to the basolateral side (bottom well of “top seeded”, and top well of “bottom seeded” transwells), and fresh untreated culture medium was added to the apical side. Cells were cultured for 1 hr at 37°C and 5% CO_2 in either static or fluidic (2 $\mu\text{L/s}$) conditions. After this, medium was sampled from both sides of the membranes and

fluorescence was measured using a multi-mode microplate reader (SpectraMax iD3, Molecular Devices, San Jose, CA) at 485/535 nm. Results are reported as “% blank”, where FITC-dextran was added to the top or bottom well of cell-free Transwells, depending on the corresponding cell seeding configuration (top or bottom) and medium was collected after identical incubation period.

Immunocytochemistry Analysis of ZO-1, AQP1 and SGLT2 Expression

At the end of the experiments, medium was aspirated and Transwells were rinsed 2x with phosphate buffered saline (PBS), then incubated at room temperature for 10 minutes in 4% paraformaldehyde (10% formalin, J61899; Alfa Aesar, Haverhill, MA). After fixation, cells were permeabilized with 0.25% Triton X-100 (BP151-100; FisherScientific, Waltham, MA) in PBS for 10 minutes, then blocked with 2% bovine serum albumin (BSA) in PBS for one hour at room temperature. Primary antibodies against ZO-1 (33-9100; Invitrogen, Carlsbad, CA), and transporters AQP1 (TA502357, Life Technologies) and SGLT2 (PA5-101893, Life Technologies) were added to the cell-seeded side of membranes. All primary antibody solutions were added at 1:200 dilution in a 2% BSA solution, and cells incubated for two hours at 37°C. After incubation, cells were washed three times with PBS, and incubated for two hours at 37°C in the dark with a cocktail of secondary antibodies Goat anti-Mouse IgG (Alexa Fluor 488, A-11001; Life Technologies) and Donkey Anti-Rabbit IgG (Alexa Fluor® 647; ab150075; Abcam, Waltham, MA) at a 1:1000 dilution in a 2% BSA solution. Cells were rinsed 3x with PBS, then membranes were carefully cut from Transwells® using a scalpel and mounted on glass slides using ProLong™ Gold Antifade Mountant with DAPI (P36935, Life Technologies). Images were captured using ImageXpress Micro Confocal High-Content Imaging System (Molecular Devices). Images were quantified for positive staining by measuring average fluorescence per defined field in each fluorescent channel (FITC, Cy5) and normalizing to those in corresponding control conditions.

Water Transport

Throughout culture, it was observed that some of the RPTEC sources exhibited noticeable volumetric and colorimetric changes to the cell culture media in the top and bottom chambers. Concentration of phenol red in the cell culture medium was used to noninvasively monitor water transport across the membrane, as it appeared to be concentrated in the apical compartment as water was reuptaken by the cells from the basolateral compartment. Concomitantly, as water was pumped by cells into the basolateral compartment, absorbance was decreased as phenol red appeared to be diluted. Samples of media (50 μ L) from apical and basolateral compartments were collected, and the absorbance was measured at 560 nm using a multi-mode microplate reader (SpectraMax iD3, Molecular Devices). Results are reported as a ratio of the absorbances measured in the top and bottom chambers.

para-Aminohippurate (pAH) Secretion

Secretion of pAH was measured via two different methods. In the first experiment (**Figure 1A**), TERT1 lines (parent, -OAT1, -OCT2, -OAT3) and primary RPTECs (Lonza and Biopredic) were treated with 1 mM pAH on either the apical side, or basolateral side. After 2 hours of exposure at 37°C, media samples were collected and tested via colorimetric methods adapted from (Waugh and Beall, 1974). Briefly, samples were treated 1:10 in protein precipitant solution (1 M dichloroacetic acid (Sigma-Aldrich, D54702)), 0.3 M p-toluenesulfonic acid (Sigma-Aldrich, T35920), 0.85 M NaOH, pH 1.4) and incubated for 15 minutes at room temperature. Samples were centrifuged at 12,000 \times G for 10 minutes, and supernatants were collected to remove any protein precipitate. A 50 μ L sample of the supernatant was treated with an equal volume of 1% p-dimethylaminobenzaldehyde in 57% ethanol. The resulting yellow color was measured at an absorbance of 450 nm and compared against a standard curve of pAH created in culture media. Results are reported as “transport ratio” of moles of pAH secreted/moles of pAH reabsorbed

(B→A/A→B). If this ratio was equal to 1, then transport was equal in both directions, and if >1 transport was geared toward secretion.

In the second transport evaluation method (**Figure 1B**), pAH was added at the same concentration (5 μ M) to both the top and bottom compartments in the presence or absence of OAT1 inhibitor probenecid (100 μ M; Sigma-Aldrich, P8761). TERT1 and TERT1-OAT1 RPTECs were seeded on the bottom surface of Transwells and cultured in either static or fluidic conditions for 7 days prior to this experiment. Media were sampled from both compartments at 2, 4, 24, and 48 hours after addition of pAH, and concentrations were determined using LC-MS/MS methods as detailed below.

Bidirectional Chemical Transport Studies

To evaluate directional transport, tenofovir (100 μ M, Sigma-Aldrich, SML1795), cisplatin (10 μ M, Sigma-Aldrich, 1134357) or perfluorooctanoic acid (PFOA, 1 μ M, Sigma-Aldrich, 171468) were added to the bottom well (750 μ L, apical) or top well (200 μ L, basolateral) of the inverted RPTEC cultures (**Figure 1C**) after 10 days in culture. Fresh RPTEC culture medium was added to the opposite (recipient) well in either treatment configuration. Cultures were then returned to the incubator and cultured under static or fluidic (2 μ L/s) conditions. Media were sampled (50 μ L) and re-dosed at day 1, 2, 3, 5, and 7 of treatment. Chemical concentrations in the medium were determined as detailed below. After the final timepoint, cultures were removed from their respective platforms, all medium was removed, cells were rinsed with PBS, then lysed with TempO-Seq™ Enhanced Lysis Buffer (60 μ L, SU-01-100, BioSpyder Technologies, Carlsbad, CA) for 10 minutes at room temperature to collect lysates for gene expression studies. Media and lysate samples were stored at -20°C until analysis.

Analytical Chemistry Methods

C¹³-Caffeine was purchased from Supelco (C-082-1ML; Bellefonte, PA), and used as an internal standard for tenofovir. C¹³-PFOA was purchased from Wellington Labs (MPFOA, Guelph, Ontario, Canada), and used as an internal standard for PFOA. Bismuth (GF61155682) and acetaminophen (PHR1005) were purchased from Sigma-Aldrich and used as internal standards for cisplatin and pAH, respectively.

For the analysis of tenofovir, PFOA, and pAH samples were first extracted using liquid/liquid extraction with protein precipitation. Briefly, 50 μ L of spent culture media sample was added to 100 μ L of chilled acetonitrile (A998-4, FisherScientific) containing corresponding internal standard (0.1 μ M for PFOA, and 1 μ M for tenofovir and pAH), then vortexed before centrifuging and supernatant was transferred to new 1.5 mL microcentrifuge tube. The supernatant was then evaporated to dryness using a Savant SpeedVac (SPD1010, ThermoFisher) and reconstituted with 50 μ L of mobile phase A (see below). Samples were then transferred to autosampler vials containing 200 μ L fused inserts (A998-4, Ibis Scientific, Las Vegas, NV) and stored at -20°C until analysis.

Analysis was performed on a triple quadrupole mass spectrometer (Agilent 6470, Santa Clara, CA). For tenofovir and pAH, the instrument was operating in positive ion mode using an electrospray ionization source. For PFOA, analyses were performed using negative ion mode using an electrospray ionization source. Capillary voltage, sheath gas temperature, and sheath gas pressure were set to 4500V, 300°C and 50 psi respectively. Samples (10 μ L for pAH, 8 μ L for tenofovir, and 20 μ L for PFOA) were auto-injected onto a ZORBAX SSHD Eclipse Plus C18 column (3.0 \times 50 mm, 1.8 μ m, 959757-302, Agilent) with a guard column (2.1 \times 5 mm, 1.8 μ m, 821725-901, Agilent) using a 1290 Infinity II LC (Agilent).

For analysis of tenofovir and pAH, liquid chromatography flow rate was set to 0.4mL/min and the column temperature was 40°C with an initial condition of 90% mobile phase A (Water with 0.1% (v/v) formic acid) and 10% mobile phase B (Acetonitrile with 0.1% (v/v) formic acid). Initial conditions for sample injection were 90% mobile phase A (water with 0.1% (v/v) formic acid) and

10% mobile phase B (acetonitrile with 0.1% (v/v) formic acid). For analysis of tenofovir, after 3 minutes the gradient was increased to 80% mobile phase B until minute 4. Conditions then returned to 90% mobile phase A and 10% mobile phase B for the remainder of the run. For analysis of pAH, after 3 minutes, the gradient changed to 20% mobile phase A and 80% mobile phase B. At minute 4, binary pump conditions returned to 90% mobile phase A and 10% mobile phase B before the method ended at minute 6. The limits of quantitation were 0.0626 μM and 0.1 μM for pAH and tenofovir, respectively (based on the standard curves that were concurrent with samples).

For analysis of PFOA, column temperature was 50°C, flow rate was 0.4mL/min, and initial chromatographic conditions were 90% mobile phase A (HPLC-grade water containing 5 mM ammonium acetate) and 10% mobile phase B (95% MeOH with 5 mM ammonium acetate). At two minutes, mobile phase B increases to 30% until minute 14 when this increases to 95%. At 14.5 minutes, this was changed to 100% mobile phase B before returning to 10% at 15.5 minutes. This condition remained for the rest of the method which ended at 17 minutes. The limit of quantitation for PFOA in these experiments was 0.078 μM .

For cisplatin (Pt) analyses, samples were first digested by adding 2.4 mL of 1% nitric acid (Omnitrace Ultra Nitric acid) spiked with 10 ng/mL bismuth internal standard. The samples were shaken with loose covering to allow any gases to escape in a ventilated chemical safety hood. Then the samples were allowed to stand overnight at room temperature to ensure complete digestion. Cisplatin calibration standards were freshly prepared daily from certified standards in cell culture media to adjust for any matrix effects. Calibration concentrations ranged from 0 to 100 μM , and blanks containing media only (100 μL) and acid (2.4 mL) were analyzed with each sample batch. To avoid carryover, 2% nitric acid was used as a wash between sample analyses. Continuing calibration standard checks were performed after every 15 samples followed by a blank analysis. Samples and calibration standards were analyzed on an Inductively Coupled Plasma-Mass Spectrophotometer Nexlon 300 (Perkin Elmer, Waltham, MA). Concentrations

were determined as Pt¹⁹⁵, the most abundant isotope, to provide most optimal sensitivity and were based on a near-linear calibration curve ($r^2 > 0.99$). Sample concentrations were then determined based on the calibration curve considering the sample dilution factor (1:25). The method's quantitation limit in these experiments was 0.013 μ M.

Gene Expression Library Preparation and Sequencing

Cell lysates (see preparation above) were used for the Templated Oligonucleotide Sequencing Assay (TempO-Seq™, BioSpyder Technologies, Carlsbad, CA) as the mRNA quantitation technology of choice (House et al., 2017). Detailed protocols for TempO-seq are provided by the manufacturer and were previously detailed elsewhere (House et al., 2022). TempO-seq libraries were prepared using the human S1500+ targeted transcriptome panel (Mav et al., 2018) consisting of 2,982 transcripts according to the manufacturer's instructions. Briefly, hybridization of the mRNA content of cell lysates was achieved by incubating 2 μ L of the lysate with 2 μ L hybridization mix as follows: 10 min at 70°C, cooling ramp from 70°C to 45°C for 49 min, and 1 min at 45°C. Excess oligonucleotides were then digested in a nuclease catalyzed reaction for 90 min at 37°C. Next, hybridization products were incubated with DNA ligase for 60 min at 37°C. Nuclease and ligase were then denatured using a heat denaturation step (80°C for 30 min). A total of 10 μ L of each ligation product were then mixed with an equal volume of PCR amplification mix and amplified in a LightCycler 96 (Roche, Basel, Switzerland) using the manufacturer recommended settings. Amplicon samples (5 μ L) were then pooled and purified using a commercial PCR clean-up kit (Clontech, Mountain View, CA). Pooled libraries were sequenced in 75 single-end read mode dual index run with custom primers using NextSeq 550 sequencing (Illumina, San Diego, CA).

Gene Expression Data Analysis

The raw sequencing reads for each pooled sample, which included four lanes of single-end sequencing reads that were 76 base pairs in length, were combined to generate a single FASTQ file for each sample. Then, we used Fastp (version 0.21.0) approach (Chen et al., 2018) to process the FASTQ files, trimming the sequencing reads to 50 base pairs with default parameters. These processed FASTQ files served as input for the TempO-Seq data analysis pipeline (House et al., 2017), which utilized the human S1500+ probe manifest file. To facilitate further analyses, we aggregated the resulting raw count matrix data to the gene level if a gene was associated with more than one probe in the TempO-seq assay. The FASTQ files were uploaded to Gene Expression Omnibus (GEO; accession #GSE246180; reviewer token wdsdsgayfnkrjcv).

Before conducting differential gene expression or other transcriptomic analyses, quality control steps were applied to filter the raw counts: (i) exclusion of samples with fewer than 200,000 total counts and (ii) removal of genes with average counts lower than 5% of the number in the remaining samples, except for the genes listed in **Supplemental Table 2** that were retained for subsequent analyses. Following these steps, principal component analysis (PCA) was employed for sample grouping visualization and potential outlier identification using the built-in R function *prcomp*. PCA analysis did not reveal any additional sample outliers and the final dataset contained a total of 69 samples ($n = 30$ for fluidic and $n = 39$ for static conditions) and 2,311 genes. The count data was visualized with clustering using the R package *pheatmap*.

Differential expression analysis was performed using the DEseq2 package in R (Love et al., 2014) through a two-step approach. Initially, the full model was employed to investigate the apical-basolateral effects of each chemical treatment compared to the corresponding untreated samples, while controlling for platform and cell line differences. The results of these apical-basolateral effects for chemical treatments guided the formulation of a final model. While no apparent variances in differential gene expression between apical and basolateral treatments were observed for PFOA and cisplatin, tenofovir, when added basolaterally, exhibited

considerable effects in the fluidic conditions with TERT1-OAT1 cells (**Supplemental Figure 3**). Several cisplatin-treated samples were not available for transcriptomic analyses; therefore, the effects of cisplatin in fluidic experiments for TERT1-OAT1 cells could not be evaluated. Consequently, samples treated with tenofovir and cisplatin in the fluidic condition for TERT1-OAT1 were excluded from all subsequent modeling. The final model combined apical and basolateral treatments of the same chemical for differential expression analysis to evaluate platform effects and controlled for cell line and treatment differences. This model resulted in five pairwise comparisons for differential expression between platforms in the following conditions (i) TERT1-OAT1 treated with PFOA; (ii) TERT1-OAT1 untreated; (iii) TERT1 treated with cisplatin; (iv) TERT1 treated with PFOA, and (v) TERT1 untreated. Significant differentially expressed genes (DEGs) for each of these pair-wise comparisons were determined using the DESeq2 *result* function, specifying the contrast groups, and applying cutoffs of false discovery q-values <0.05 and absolute \log_2 -fold-change values >1.5 . The union of DEGs (normalized counts) was utilized for clustering and visualization of the DEGs between platforms using the R package *pheatmap*. To interpret clusters of DEGs through pathway analyses, the *xgr* package version 1.1.8 in R (Fang et al., 2016) was employed, considering all pathways (ontology = "MsigdbC2CPall") as gene sets. The background gene list for this analysis comprised all genes retained after low-count removal (2,311 genes; see above for selection).

In addition, to compare the transcriptional profiles obtained in our study with those reported by the GTEx Consortium across various human tissues (GTEx Consortium, 2017), rank-based (Spearman) correlation analysis was performed between platforms for TERT1 and TERT1-OAT1 cells. This involved comparing the mean expression levels of individual genes across different experimental conditions (24-well transwells in static or fluidic condition, and cell sources) with the mean expression levels observed in various human tissues from the GTEx Portal (GTEx Consortium, 2017). Additionally, previously published Spearman correlation coefficients similar

analyses conducted with TERT1 and TERT1-OAT1 cells cultured in 384-well plates (Sakolish et al., 2023) were compared with the results of the current study.

Results

Figure 1 shows the experimental designs and timelines for the studies described herein that compared RPTEC cultured on Transwells® under static conditions or flow enabled by the PhysioMimix™ T12 platform. These studies were conducted to address the context of investigating chemical transport/drug effects in an *in vitro* model replicating the proximal tubule of the human kidney. Specifically, we investigated (i) barrier formation, (ii) water secretory function (tested with pAH), (iii) directional transport of chemicals (tested using cisplatin, tenofovir, and PFOA), and (iv) gene expression profiles as an indicator of the physiological state of RPTEC.

Effects of media flow on epithelial barrier formation with various sources of RPTECs

A number of immortalized and primary human RPTEC sources are available for *in vitro* studies of the proximal tubule. In this study, we first aimed to compare the widely used TERT1-immortalized RPTEC lines (parent line and OAT1-, OCT2-, and OAT3-overexpressing cells) as well as several sources of primary RPTECs (Biopredic and Lonza). Immortalized cells were cultured under either static or fluidic (2 μ L/s) conditions for up to 8 days, while primary RPTECs were cultured for 14 days to account for differences in growth rates among the immortalized cell lines that are proliferating more rapidly than primary cells (**Figure 1A**). Computationally estimated values of the peak shear stress in the fluidic conditions were estimated at the cell surface to be 0.126 dyne/cm² with an average shear of 0.053 dyne/cm² across the entire membrane (**Supplemental Figure 2**). In additional experiments, cells were seeded on either the upper or lower surface of the membranes in both static and fluidic conditions to assess whether growing cells in the direct path of fluid flow (as enabled by PhysioMimix™ T12 platform) influenced barrier formation and/or molecular transport. Subsequent experiments detailed in **Figures 1B-C** were

streamlined to include only "bottom-seeded" cultures and only TERT1 and TERT1-OAT1 RPTECs to enable the throughput required for compound exposures and additional endpoints as detailed below.

Figure 2 shows representative examples of membrane coverage by different cell sources on days 8 (TERT1 lines) and 14 (primary RPTECs) for cultures grown in static or fluidic conditions, as well as when cells were seeded on the top (**Figure 2A**) or bottom (**Figure 2B**) surface of the membranes. In all conditions, TERT1 RPTEC lines grew to a confluent and uniform monolayer by day 8. By contrast, primary RPTECs from 2 commercial sources appeared clustered and failed to form contiguous monolayers, except for Biopredic primary RPTECs in static conditions (both top and bottom seeded conditions). The addition of fluid flow (in the bottom chamber only) appeared to induce cell clumping of Biopredic primary RPTECs, even when cells were grown on the top surface of membranes and out of the direct path of fluid flow. Lonza primary RPTECs exhibited a "patchy" morphology in all tested culture conditions.

Transepithelial electrical resistance (TEER) measurements are a common method used to evaluate barrier function of a cell monolayer and a widely accepted indicator of the confluence of an epithelial layer. We evaluated TEER prior to media changes every 48 hours in all conditions detailed above (**Figure 3A**). TERT1-immortalized RPTEC lines rapidly attained TEER levels that are considered physiological in the proximal tubule (Wieser et al., 2008; Secker et al., 2019) within the first 8 days of culture, with the exception of the OCT2-overexpressing line which showed a trend of increasing TEER but lagged behind other lines. Primary RPTECs did not exceed a TEER level of $20 \Omega \cdot \text{cm}^2$ in any culture condition, even after 14 days of culture, likely due to the "patchy" nature of the cell layer (**Figure 2**). TERT1, TERT1-OAT1, and TERT1-OAT3 RPTECs exhibited similar patterns in TEER values, albeit the values were generally higher in static culture conditions as compared to fluidic conditions and in "bottom-seeded" cells as compared to "top-seeded" ones.

In addition to TEER measurements, we used FITC-dextran (70 kDa) permeability to assess barrier formation. These experiments were performed on day 8 for TERT1 lines and day

14 for primary RPTECs (**Figure 3B**). The results are presented as “% blank” where acellular, extracellular matrix-coated membranes in either static or fluidic conditions were treated with the same dextran solution through either the top or bottom chambers as a direct point of comparison. TERT1-immortalized cells showed the lowest permeability (greatest barrier), regardless of culture condition. One exception was the TERT1-OAT3 line that did not form as tight of a barrier when seeded on top of the membrane in either static or fluidic conditions. Both primary RPTECs showed patterns similar to that of TERT1-OAT3 cells but their barrier formation was generally lower than that of TERT1-immortalized cells. These differences were less pronounced in the fluidic condition. When comparing static and fluidic conditions in only the “bottom seeded” cells, on the side of the membrane where cells would experience fluid movement, permeability appeared slightly lower in fluidic conditions, albeit not reaching statistical significance.

At the end of these experiments (**Figure 1A**), cells were fixed and stained for ZO-1, AQP1, and SGLT2 to investigate tight junction formation and membrane-bound transporter expression under the various growth conditions (**Figure 4**). **Figure 4A** shows monochromatic images for each stain in bottom-seeded TERT1 and Lonza RPTECs as representative cell sources (images for other experiments can be viewed using the links to the full data repository as shown in **Supplemental Table 1**). Both static and fluidic conditions are presented. Qualitative evaluation of microscopy images revealed a uniform and well-defined ZO-1 staining at the cell junctions of TERT1 cells. In Lonza cell cultures, because of the non-uniformity of the cell coverage, there were several areas of higher staining, but cell borders were still clearly marked throughout. AQP1 and SGLT2 staining was uniformly distributed across the monolayer in TERT1 cells, but similar to ZO-1 patterns these displayed areas of high staining across the entire field of view. Expression of all three markers appeared to be greater in Lonza cells, especially under fluidic conditions.

Quantitative image analysis was performed by measuring total probe-specific fluorescence per field (**Figure 4B**). Data was normalized to TERT1 cells under static growth conditions and expressed as relative image intensity for other groups. This image analysis was

performed for all RPTEC sources and statistical comparisons were made within cell source between static and fluidic conditions. In all TERT1 cell lines (TERT1, TERT1-OAT1, TERT1-OCT2, and TERT1-OAT3), the expression levels of ZO1, AQP1, and SGLT2 were comparable between static and fluidic conditions and were largely uniform across all TERT1 lines. By contrast, in primary RPTECs, ZO-1 and SGLT2 expression (in Lonza RPTEC only) as well as AQP1 (in both Lonza and Biopredic RPTEC) was significantly greater. This significant increase was only observed in “bottom seeded” conditions and was not evident in “top seeded” conditions (data not shown). These findings suggest that fluidic conditions may induce polarization and increase transporter expression in primary RPTECs when they are positioned directly in the path of fluid flow; however, because normalization could not be performed to the cell number and monolayers in primary RPTECs appeared thicker, the difference in staining intensity could be due to differences in the cell number between conditions.

Effects of media flow on RPTECs secretory functions

RPTECs secretory functions were then assessed (**Figure 1A**); directional transport of water (Secker et al., 2019) and para-aminohippurate (pAH) (Chasis et al., 1945) were tested. Cell culture media were exchanged in all cultures every 48 hours, and noticeable changes in media volumes were observed between top and bottom media chambers in cells of different source (**Figures 5A-C**). To quantify these changes, samples of media were collected, and absorbance was tested at 590 nm (absorbance of phenol red), because a noticeable concentration of phenol red pH indicator was observed concomitantly with changes in media volume (**Figure 5D**). These changes in absorbance are depicted in **Figure 5E** as a ratio of absorbance between the apical and basolateral chambers. An increase in the ratio of apical/basolateral absorbance was indicative of water reabsorption by the cells. Water transport was observed in TERT1 and TERT1-OAT1, and to some extent in TERT1-OCT2 cells. In contrast, TERT1-OAT3, Lonza, and Biopredic RPTEC cultures exhibited an absorbance ratio of approximately 1, suggesting a lack of water

transport. The lack of noticeable water transport in primary RPTECs was inconsistent with our finding of the substantial expression of AQP1 in fluidic cultures of these cells (**Figure 4**). We attribute this to the suboptimal barrier formation by these cells demonstrated by TEER and FITC-dextran permeability.

Comparable trends were evident in experiments with pAH, which was also detected using colorimetric methods. Here, pAH (1 mM) was added to either the apical or basolateral chambers, and the transport ratio was measured (**Figure 5F**, ratio of B→A transport/A→B transport in nmols of pAH) after a 2 hour incubation. A ratio of 1 is indicative of passive diffusion (no active transport in either direction), a ratio >1 is indicative of active secretion by the cells. The results indicate that only TERT1 and TERT1-OAT1 cells exhibited active secretion of pAH, with 15-20% higher secretion under fluidic conditions (significant only in TERT1 cells).

A major limitation of the typical pAH transport studies is the high concentration (1 mM) required to detect pAH transport using colorimetric methods and the limited dynamic range of the assay. Therefore, a follow-up pAH transport study (**Figure 1B**) was conducted at a lower concentration (5 μ M) utilizing LC-MS/MS detection; this study also tested whether pAH transport was inhibited by probenecid (Hosoyamada et al., 2004). Based on the outcome of the studies detailed in **Figures 2-5**, the number of conditions was reduced to include only static and fluidic “bottom seeded” ones. We also proceeded with testing two cell sources, TERT1 and TERT1-OAT1 because the primary RPTECs did not form an acceptable barrier on transwells, limiting the utility of these cells for transport studies. In this experiment, pAH, with and without inhibitor probenecid (100 μ M) was added in equal concentrations to both the top and bottom chambers, and media were sampled from both sides at 2, 4, 24, and 48 hours to determine if RPTECs could establish directional transport of pAH. **Figure 6** shows the transport ratio apical/basolateral concentrations normalized to TERT1 without inhibitor in either static or fluidic conditions at 2 hours. TERT1 cells showed no pAH gradient in either static or fluidic condition and addition of the inhibitor appeared to non-significantly increase the pAH gradient with time. In contrast,

TERT1-OAT1 cells showed a robust response indicating directional pAH secretion to the apical side of cells that was inhibited by probenecid. The transport ratio increased to >40 at 24 hours, and >50 by 48 hours in static condition, and was as high as 166 at 48 hours in fluidic condition, indicating that flow contributed to the function of over-expressed OAT1, but had no effect on the TERT1 cells.

Effects of media flow on RPTEC directional transport of chemicals

We tested directional transport of the drugs tenofovir and cisplatin, both known to be secreted into the kidney tubule (Filipski et al., 2009; Kohler et al., 2011), as well as a ubiquitous environmental pollutant PFOA that is known to be efficiently reabsorbed in the human kidney (Harada et al., 2005) (**Figure 1C**). TERT1 and TERT1-OAT1 cells were grown on the bottom surface of membranes in static or fluidic conditions for 10 days prior to addition of these compounds at concentrations known to be without overt adverse effect on RPTECs (as determined through earlier dose-response testing, data not shown). Tenofovir (100 μ M), cisplatin (10 μ M) or PFOA (1 μ M) were added to the apical or basolateral side of the transwells, and were re-dosed during media collections on days 1, 2, 3, 5, and 7. At each of the sampling times, medium from both sides was collected and transport rates were measured using LC-MS/MS (pmol/hr). The net secretion, reported in **Figure 7** as [secretion – reabsorption], was determined by subtracting reabsorption (A→B) from secretion (B→A). A net secretion of zero suggests a bidirectional transport of the compound at comparable rates, indicative of a more passive transport mechanism. When the net secretion was negative, the compound was being actively reabsorbed by the cells; conversely, a net positive secretion indicates active secretion of the compound by the cells.

For tenofovir, we observed some reabsorption in the fluidic conditions at early time points (days 1-2) in TERT1 cells, but by the end of the week-long exposure a net secretion of 0 was

measured. Conversely, TERT1-OAT1 cells indicated strong secretion of tenofovir (observed only in static conditions), which was expected given that tenofovir is an OAT1 substrate (Kohler et al., 2011). Cisplatin was initially secreted in the TERT1 line; however, this secretion was not maintained over the week of exposure. A lower rate of secretion was observed in the TERT-OAT1 overexpressing line, but this effect was not sustained beyond the initial 48 hours of exposure. Cisplatin is an OCT2 substrate (Filipski et al., 2009), and neither TERT1 nor TERT1-OAT1 lines express sufficiently high levels of this cationic transporter to enable secretion of cisplatin. Lastly, the addition of PFOA in the TERT1 cells did not result in transport in either direction under both static and fluidic conditions. However, in both static and fluidic cultures of the TERT1-OAT1 cells, PFOA was actively re-absorbed, favoring transport in the A→B direction, as indicated by a negative net secretion. This result is aligned with the long half-life of PFOA in humans (Olsen et al., 2007), a phenomenon that is largely attributed to efficient renal re-uptake in the proximal tubule (Harada et al., 2005; Loccisano et al., 2011).

Effects of media flow on RPTECs gene expression profiles

Finally, we used gene expression profiling to evaluate the differences between cell sources (TERT1 and TERT1-OAT1), chemical treatments, and the effects of shear stress. We correlated (**Figure 8A**) overall gene expression profiles of these two cell sources when cultured in 384-well plates [data from (Sakolish et al., 2023)], or in transwells without and with flow, with gene expression profiles of various human tissues (GTEx Consortium, 2017). Rank-based Spearman correlation indicated that TERT1 and TERT1-OAT1 cells most closely resembled the transcriptome of human kidney medulla (kidney cortex was the fifth-top correlated tissue type). Furthermore, while there was not a large difference in correlation coefficients between static and fluidic transwell cultures, both of these conditions correlated better with human kidney medulla than the same RPTECs cultured in 384-well plates. Correlation coefficients of TERT1 cells were consistently higher than those of TERT1-OAT1 cells.

Principal component analysis of gene expression data (**Figure 8B**) showed that individual samples clustered primarily based on the cell source (TERT1 vs TERT1-OAT1) but showed little difference between static and fluidic conditions, except for tenofovir-treated TERT1-OAT1 cells under flow. Clustering analysis of the gene expression data from all samples and genes (**Supplemental Figure 4**) showed overall similarity in gene expression patterns; nevertheless, the differences between cell sources were the primary driver in clustering of the samples. Secondary grouping by assay condition (static vs fluidic) was also evident within each cell source. Tenofovir samples in TERT1-OAT1 cells were also clustered. Because the main goal of these analyses was to determine whether a transcriptomic signature could be established between static and fluidic cultures, we further examined if chemical-induced effects were evident or whether samples could be combined to increase statistical power. **Supplemental Figure 3** shows that only tenofovir-treated samples exhibited marked transcriptional effects; for other treatments, the differences between apical and basolateral addition of a chemical were negligible. Therefore, we excluded tenofovir-treated samples from further analyses and combined apical and basolateral-treated samples for PFOA and cisplatin separately in further analyses.

Figure 8C shows an unsupervised clustering heatmap from the analysis of the differentially expressed genes (DEGs). A total of 257 genes that were differentially expressed between static and fluidic conditions (in pair-wise analyses among 5 comparison groups: (i) TERT1-OAT1 treated with PFOA; (ii) TERT1-OAT1 untreated; (iii) TERT1 treated with cisplatin; (iv) TERT1 treated with PFOA, and (v) TERT1 untreated) were included. While it is not surprising that the samples within each of these comparisons clustered into groups, the uniformity of transcription patterns among samples in each group is notably showing consistency of the effects between experimental replicates. Among these 257 DEGs, we examined whether static or fluidic condition had a greater effect on gene expression. **Figure 8D** shows that within each comparison group, static cultures showed consistently higher numbers of DEGs as compared to fluidic cultures. A total of 24 DEGs were shared among at least 3 comparison groups (**Figure 8E**). These

genes are expressed in human kidney to a moderate or high extent and are known to play several physiological roles (**Supplemental Table 3**). A pathway analysis of the transcripts in each of the comparison groups also showed that glycolysis/gluconeogenesis, cell signaling, and hypoxia inducible response were enriched in static cultures (**Supplemental Table 4**). Finally, we examined expression of xenobiotic metabolism and transporter genes separately as they did not appear in the DEGs. **Supplemental Figure 5** shows that little difference was evident between static and fluidic cultures within each cell source, with the exception of much higher expression of three transporters (*SLC22A6* (*OAT1*), *SLC10A2* and *SLCO1B1*) in TERT1-OAT1 cells, but independent of flow. It is notable that according to the gene expression data across human tissues (GTEx Consortium, 2017), *SLC22A6* and *SLC10A2* are expressed in the proximal kidney tubules (*SLC10A2* is expressed the most in the small intestine); however, *SLCO1B1* is a liver transporter with lower expression in the proximal tubules at the physiological state. The observed marked induction of *SLC10A2* and *SLCO1B1* in TERT-OAT1 cells may thus be the result of the well-known phenomenon of dynamic expression of the functionally-relevant transporters in the kidney upon injury or drug treatment (Nigam et al., 2015), or in this case supra-physiological levels of *SLC22A6* expression.

Discussion

Many organ-on-chip models of the renal proximal tubule aim to create a perfused tubule lined with RPTEC by using various device designs where a hollow tubule is created using a gel substrate (Weber et al., 2016; Wilmer et al., 2016; Vormann et al., 2018; Lin et al., 2019; Ross et al., 2021). An alternative is to introduce media movement into a membrane-based system where RPTEC are seeded on the side of the membrane where lateral flow is introduced (Gao et al., 2011; Jang et al., 2013; Kim et al., 2022; Shaughnessey et al., 2022; Specioso et al., 2022). Indeed, most advanced 3D cultures of RPTEC focus on enabling shear stress in either membrane-based, or in-gel tubule microfluidic designs. The amount of shear stress in each model

is dependent not only on the flow rate, but also on the configuration of the device and can vary by more than an order of magnitude across studies. It is also noteworthy that while the consumables and peripherals for some of the published kidney organ-on-chip models are commercially available, others may not be easily accessible. Consequently, the degree of standardization of each model, and their accessibility to the wider scientific community, or to the end-users in the pharmaceutical and chemical companies, also varies. Together, these factors represent serious barriers to the wide adoption of these organ-on-chip models because their reproducibility, robustness and utility to specific contexts of use remains uncertain (Marx et al., 2020; Ewart and Roth, 2021; Hargrove-Grimes et al., 2021).

Kidney organ-on-chip models may have utility in a number of drug development and safety contexts and are of great interest to both drug developers and regulators (Phillips et al., 2020). Prospective end-users are interested in the overall technical feasibility of implementing these models in their laboratories, model reproducibility, as well as the functionality in terms of kidney-specific features such as physiological and transport function, and response to xenobiotics (Phillips et al., 2020). Commercially-available models are typically more attractive to the end-users because of easier access to the devices and associated equipment, as well as greater quality assurance of the manufacturing process and experimental conditions (e.g., flow rates). However, the need to standardize the protocols and demonstrate the model's utility in specific contexts remained out of reach for many individual manufacturers and has typically been conducted by industry consortia (Phillips et al., 2020; Rusyn et al., 2022). With regards to the kidney organ-on-chip models, studies of reproducibility and robustness of several commercial platforms have demonstrated that careful consideration of the cell sources and intra-study comparisons of various organ-on-chip and multi-well plate conditions, accompanied by the transparency with data access, provide important information for the end-users and fitness to a specific purpose (Sakolish et al., 2018; Maass et al., 2019; Sakolish et al., 2020; Sakolish et al., 2023). Therefore, the studies detailed herein aimed to evaluate the PhysioMimix™ T12 plate, a

commercially available flow-enabled transwell system. In this study, the platform was characterized with respect to its reproducibility, robustness, and human translational relevance as a flow-enabled model of the renal proximal tubule in several regulatory-focused contexts of use (Avila et al., 2023). These included testing of the effects of shear stress and RPTEC cell sources on barrier formation, directional transport of water and small molecules, and similarity to human kidney gene expression profiles.

By comparing different cell sources and culture conditions, we observed considerable differences in monolayer formation between different RPTECs. While TERT1 lines demonstrated efficient growth and achieved a confluent, even monolayer by day 8, primary RPTECs faced difficulty with monolayer formation when grown on transwells, and the introduction of fluid flow appeared to further exacerbate this issue. In addition, primary cells exhibited significant “clumping” on the membrane, which contributed to the challenge in forming an even monolayer. This variability in monolayer formation was confirmed through TEER measurements. Reported TEER values for mouse and rat isolated tubules range from 5-20 $\Omega \cdot \text{cm}^2$ (Bello-Reuss, 1986; Plain et al., 2020). In cell culture, primary RPTECs and immortalized cell lines exhibit an even wider range of TEER, from 5-170 $\text{Ohm} \cdot \text{cm}^2$ (Brown et al., 2008; Wieser et al., 2008; King et al., 2017; Secker et al., 2019; Shaughnessey et al., 2022). In general, primary cells exhibit lower TEER values while RPTEC lines achieve higher TEER values, aligning with our own observations. Notably, we found higher TEER values when cells were seeded on the bottom or the transwell; however, medium recirculation did not improve the barrier, in fact, static cultures showed higher TEER. Additionally, permeability to 70 kDa FITC-dextran was lower in bottom-seeded cultures and higher in primary RPTECs, aligning with the data on TEER.

A comparative analysis of cellular markers ZO-1, AQP1, and SGLT2 in TERT1 lines and primary RPTEC provided further insights into the response to fluid shear stress. In TERT1 lines, the expression of these markers was relatively consistent across all cell lines, indicating that fluid shear stress did not affect transporter expression (in the case of SGLT2, it appeared that fluid

shear stress decreased expression). However, in primary RPTEC, exposure to fluid shear stress resulted in an increase in ZO-1, AQP1, and SGLT2 staining. Previous publications suggested that fluid shear stress may have differential effects on these markers. In our study, ZO-1 expression increased with the addition of flow, whereas other publications report a more fragmented, depolarized expression of ZO-1 under shear conditions (Maggiorani et al., 2015) or no effect (Jang et al., 2013). Conversely, AQP1 and SGLT2 showed significantly increased abundance under fluidic conditions in our study, aligning with previous reports (Jang et al., 2013; Pohl et al., 2015).

The proximal tubule is responsible for the reabsorption of over 70% of water filtered through the kidneys (Feraille et al., 2022) and recreation of this physiological process *in vitro* serves as important evidence of human relevance. Previous studies showed TERT1 cells cultures without flow are able to reabsorb water (Secker et al., 2019). The observed water transport, evident through changes in media color is a simple, non-destructive technique that shows that as water is being reabsorbed (apical→basolateral), phenol red is either left behind or is possibly even secreted (basolateral→apical), leading to the increase in media absorbance that we are observing on the apical side. It was shown that AQP1 plays a role in water transport (Pohl et al., 2015); however, we found that AQP1 staining was not concordant with water transport efficiency – TERT1 lines showed similar staining for AQP1 but only TERT1 and TERT1-OAT1 lines showed the greatest reabsorption of water, and this was further increased by the presence of fluid flow. Furthermore, even though primary RPTEC showed higher AQP1 expression than TERT1 lines and even larger increases in the fluidic conditions, this did not translate to the actual transport of water. While it is likely that the primary RPTECs are capable of water transport, the leaky monolayer (as previously indicated by clumping cells, low TEER, and higher FITC-dextran permeability) may have allowed for a backflow by gravity.

To study the secretion of pAH, we employed two approaches. In a colorimetric method, pAH concentrations were high (1 mM) to allow for quantitation in the recipient channel. As

expected, pAH secretion was highest in the TERT1-OAT1 line, but secretion was also appreciable in the parent line. Other TERT1 lines, and primary RPTEC showed negligible pAH secretion. Indeed, it is well known that primary RPTECs rapidly lose function of many transporters, including OATs (Caetano-Pinto et al., 2022). However, the use of MPS has been demonstrated to recover some of the transport function, though to a limited extent, and in primary RPTECs (Weber et al., 2016; Caetano-Pinto and Stahl, 2023). Additionally, it should be acknowledged that other groups have demonstrated robust and inhibitable OAT expression in fresh primary human RPTECs when cultured directly post-isolation (Brown et al., 2008). In the context of these experiments, it is possible that the high treatment concentration of pAH could result in the inhibition/ suppression of transport, so testing with pAH in the other experiments was performed at much lower concentrations, utilizing an LC-MS/MS analytical detection method. Because all our previous studies showed that primary RPTEC were less suitable for studies of the proximal tubule barrier and transport, in subsequent experiments of directional transport we used only TERT1 and TERT1-OAT1 cells. pAH secretion was investigated in static and fluidic cultures with a lower test concentration of pAH (5 μ M) and addition of pAH to both the apical and basolateral side. This design aimed to establish a measurable, polarized concentration gradient. Significant secretion of pAH was observed exclusively in TERT1-OAT1 cells, with the most pronounced effect occurring in the fluidic culture conditions. This effect could be inhibited by the addition of the OAT1 inhibitor probenecid. These results confirm the influence of fluid shear stress on renal proximal tubule secretion. These data are consistent with reports of increased OAT1 and other transporter-mediated absorption efficiency in fluidic models of the renal proximal tubule, including both membrane-based (Jing et al., 2022) and tubule-based (Sakolish et al., 2023). Our observations suggest that the augmented secretion of pAH under fluidic conditions is likely due to heightened activity in influx (OAT1) and efflux (MRP) pathways, as pAH secretion involves both basolateral uptake through OAT1 and apical release through MRP2, the latter also known to be affected by shear stress (Vriend et al., 2020).

As renal clearance of tenofovir and cisplatin exceeds glomerular filtration rate (due to active cellular secretion), concentrations in the tubule often significantly exceed serum C_{max} concentrations. Human serum tenofovir C_{max} concentrations are around 1.35 μM [401 $\mu\text{g/L}$ (Fonsart et al., 2017)]; however, due to water reabsorption and active tubular secretion, urinary tenofovir concentrations are typically 100 \times higher (Drain et al., 2020). Cisplatin urinary concentrations can also exceed serum C_{max} [8.3 μM , 2.5 $\mu\text{g/mL}$ (Ikeda et al., 1998)] concentrations by 10-100 \times fold (Fukushima et al., 2018); however, we observed significant cytotoxicity in RPTEC cultures treated with cisplatin at 100 μM and thus a lower concentration of was selected. In the case of PFOA, human C_{max} in different human cohorts has been reported to range from 0.03-0.5 μM [11.8-241 ng/mL ; (Seals et al., 2011)], so a test concentration of 1 μM was selected.

Our data show that TERT1-OAT1 cells can efficiently secrete tenofovir, commensurate with known accumulation of this drug in proximal renal tubular cells and primarily elimination through both active tubular secretion and glomerular filtration (Zimmermann et al., 2006). We found this only under static conditions and only in OAT1 overexpressing cells. Conversely, cisplatin, a chemotherapy agent expected to undergo secretion in renal tubules through an OCT2-mediated pathway (Filipski et al., 2009), showed limited transport outside of some early (day 1) secretion in the TERT1 parent line. This observation could be attributed to the absence of appreciable OCT2 expression in TERT1 cells, and the further reduction of OCT2 in the transporter overexpressing line. This effect has been previously reported in ciPTEC lines where overexpression of OAT1 or OAT3 led to a reduced sensitivity to cisplatin (Nieskens et al., 2018). Regarding perfluorooctanoic acid (PFOA) transport, our study demonstrated sustained reuptake of PFOA in both static and fluidic cultures of the OAT1-overexpressing cells, data supporting efficient renal reuptake and long half-life of this environmental chemical in humans (Harada et al., 2005; Loccisano et al., 2011). Although OAT1 is primarily involved in basolateral uptake, the

overexpression of OAT1 in this cell line is associated with upregulated expression of other transporters (Sakolish et al., 2023). Specifically, the involvement of OAT4-mediated uptake is the likely mechanism, given previous studies demonstrating its participation in renal re-uptake of perfluorinated compounds (Yang et al., 2010). Overall, these drug and chemical transport studies showed that shear stress in this model may not have resulted in improved directional transport and that a deeper characterization of the transcriptional profiles of RPTECs in static and fluidic conditions is needed.

Previous transcriptomic studies of TERT1 RPTEC showed that they express kidney-specific genes playing a role in transport, tight junction formation, and energy metabolism (Limonciel et al., 2018). Another recent transcriptomics study of different types of RPTECs cultured in 384-well plates or in a tubule-based device (OrganoPlate 3-lane 40) with intermittent medium flow (Sakolish et al., 2023) showed that while primary RPTECs were most concordant in terms of their gene expression to the human kidney transcriptome, there was little evidence of the microfluidic conditions in that experimental setup in making RPTECs more physiologically relevant. Here, we conducted similar experiments to examine transcriptional profiles of TERT1 and TERT-OAT1 cells and compared them to each other, to different human tissues, and between static and fluidic conditions. We found that when these two cell sources were cultured on transwell membranes, their gene expression was most concordant to human kidney medulla and to a somewhat lesser degree cortex; however, the effect of fluidic condition was not apparent. In fact, there were more kidney-relevant genes and pathways expressed in static transwell cultures. One other gene expression study that evaluated gene expression effects of fluid shear stress on TERT1 RPTEC (Ross et al., 2021) observed higher expression of a number of transporters and xenobiotic metabolism under fluidic conditions (0.1-0.5 dyne/cm²); however, an almost equal number of transcripts, most also important for renal function, were profoundly down-regulated. The authors described the transcriptomic effects as “dynamic” and highly dependent on the shear stress with lower (0.1 dyne/cm²) flow having greater effects than high flow (0.5 dyne/cm²). Overall,

our data, and those from other published transcriptomic studies, do not provide clear evidence of an advantage that may be afforded by fluid flow on the gene expression profiles of RPTECs.

Previous studies have examined fluidic membrane models similar in design to the PhysioMimix™ T12 plate used herein, with (Lee et al., 2022) and (Kim et al., 2022) utilizing custom injection-molded polycarbonate chips housing fluidic transwell membranes. Their studies utilized primary RPTECs cultured on either the upper (Lee et al., 2022) or lower (Kim et al., 2022) surfaces of the membranes. In their model, fluid flow (0.13 dyne/cm²) was only present in the lower chamber, exposing cells on the lower side to fluid shear stress. When static and fluidic conditions were compared (Lee et al., 2022), RPTECs exhibited comparable viability, glucose reabsorption, and transporter gene expression to controls. A subsequent study (Kim et al., 2022) showed that relocating RPTECs to the lower (fluidic) side of the membrane improved TEER, glucose reabsorption, and reduced permeability, emphasizing the need to position RPTECs directly in the path of flow. Another pertinent study (Specioso et al., 2022), examined the effects of fluid shear stress when primary RPTECs were cultured on the bottom of transwell inserts, exposing them directly to fluid shear stress (Vitrofluid device). The results indicated shear stress-associated decreased RPTEC proliferation, accompanied by an increase in ciliary length, suggesting a more "mature" cellular phenotype. Notably, while these changes in cell morphology were observed, barrier function, transporter gene expression, and responses to colistin toxicity remained largely similar between static and fluidic conditions. However, it is important to note the authors of this study acknowledged that the shear stress in their model was considerably lower than the physiological levels (6.5×10⁻⁴ dyne/cm² reported). By contrast, others have investigated higher shear stress levels (ranging from 0.1 to 1 dyne/cm²) (Duan et al., 2008; Jang et al., 2013; Ross et al., 2021) and reported favorable outcomes. Collectively, the choice of RPTEC culture location, shear stress levels, and duration of culture in fluidic models can considerably influence cell behavior and functional outcomes. However, the optimal conditions for replicating the proximal tubule microenvironment warrant further investigation, with a focus on achieving a

balance between mimicking physiological shear stress and maintaining cellular viability and function. In this respect, we acknowledge several limitations to our study. While healthy physiological shear stress typically ranges between 0.3 and 1.2 dyne/cm² (Ross et al., 2021), the maximum shear stress achieved in the fluidic model used in these studies was only 0.126 dyne/cm², with an average of 0.053 dyne/cm² across the entire membrane. Although adjustments in the volume at the bottom of the transwell may enhance the average shear stress to 0.1 dyne/cm², this would still fall within the range considered as "disease levels" (<0.5 dyne/cm²). Therefore, the PhysioMimix platform may not be the optimal choice for the modeling of the proximal tubule shear stress under "healthy" conditions. An additional limitation of this study was the use of "off the shelf" media recommended by the cell providers, it contains serum (0.2-0.5%) and high D-glucose levels (~3.15 g/L, standard DMEM:F12). Previous studies have demonstrated that the presence of serum proteins (2% serum) may elicit secretion of proinflammatory cytokines, leading to tubular injury and fibrosis (Lidberg et al., 2022). Additionally, similar effects have been observed in RPTECs cultured in media with high levels of D-glucose. For example, a study in RPTEC/TERT1 cells in media containing 5 mM or 30 mM (0.9 and 5.4 g/L, respectively) D-glucose found that the high glucose condition induced expression of inflammation-related transcripts (Islam et al., 2019). While investigation of media formulation effects on the cells cultured in different flow- or static conditions was beyond the scope of this study, these previous reports consideration in future cell characterization studies, particularly in scenarios such as disease modeling or renal toxicity.

Overall, this study systematically compared various RPTEC sources and experimental (cell seeding and flow) conditions, aiming to identify the optimal configuration for transport testing. We show that primary RPTECs may not be suitable for studies of directional transport on transwell membranes even though they show generally more relevant expression of key transporters, especially when shear stress is present. Studies of TERT1 PRTECs showed that both the parent line and -OAT1 and -OAT3 overexpressing lines form robust barrier, that TERT1-OAT1 cells

exhibit robust and inhibitable pAH transport, and that shear stress increases pAH transport function of these cells. However, we also found that tenofovir secretion and PFOA reabsorption by TERT1-OAT1 cells are not improved by shear stress. With respect to gene expression profiles, we found that both TERT1 and TERT1-OAT1 cells exhibit human kidney-like transcriptomes, but that shear stress does not result in an apparent enhancement of the kidney phenotype. Overall, our data show that addition of flow to *in vitro* studies of the renal proximal tubule may afford benefits in some aspects of kidney physiological function, but that careful consideration of the impact such studies would have on the cost and throughput of the experiments is needed. As reported previously, RPTEC source remains the most impactful choice with respect to the utility of the *in vitro* models and that cryopreserved primary cells may not be the most optimal choice despite their more human-like phenotypes. Careful comparison of RPTEC sources and experimental conditions may be necessary depending on the context of use and in many instances the use of immortalized RPTEC lines in static cultures may represent the most appropriate *in vitro* model.

Acknowledgments

The authors greatly appreciate useful discussions and technical support from TEX-VAL Consortium members. This work does not represent policy or product endorsement by TEX-VAL Consortium member organizations (American Chemistry Council, Bristol-Myers Squibb, Merck KGaA (Darmstadt, Germany), National Institute of Environmental Health Sciences, Sanofi, Unilever, Roche, and the United States Environmental Protection Agency).

Data Availability

The data presented in this study are openly available and can be found on the EveAnalytics Platform (previously the MPS-Database). Direct links for each study are listed in **Supplemental Table 1**. Gene expression data are available on GEO (Accession # GSE246180, reviewer token: wdsdsgayfnkrjcv).

Conflicts of Interest

This work was performed via the TEX-VAL Consortium collaboration funded by equitable monetary contributions from member organizations (American Chemistry Council, Bristol-Myers Squibb, Merck KGaA (Darmstadt, Germany), National Institute of Environmental Health Sciences, Sanofi, Unilever, Roche, and United States Environmental Protection Agency). Some of the authors are affiliated with these organizations.

Authorship Contributions

Participated in research design: Sakolish, Bajaj, Villenave, Hewitt, Ferguson, Stanko, Rusyn.

Conducted experiments: Sakolish, Moyer, Tsai, Ford, Dickey.

Performed data analysis: Sakolish, Moyer, Tsai, Ford, Dickey, Rusyn.

Wrote or contributed to the writing of the manuscript: Sakolish, Moyer, Tsai, Ford, Dickey, Bajaj, Villenave, Hewitt, Ferguson, Stanko, Rusyn.

References

- Avila AM, Bebenek I, Mendrick DL, Peretz J, Yao J, and Brown PC (2023) Gaps and challenges in nonclinical assessments of pharmaceuticals: An FDA/CDER perspective on considerations for development of new approach methodologies. *Regul Toxicol Pharmacol* **139**:105345.
- Balzer MS, Rohacs T, and Susztak K (2022) How Many Cell Types Are in the Kidney and What Do They Do? *Annu Rev Physiol* **84**:507-531.
- Bejoy J, Qian ES, and Woodard LE (2022) Tissue Culture Models of AKI: From Tubule Cells to Human Kidney Organoids. *J Am Soc Nephrol* **33**:487-501.
- Bello-Reuss E (1986) Cell membranes and paracellular resistances in isolated renal proximal tubules from rabbit and *Ambystoma*. *J Physiol* **370**:25-38.
- Bonventre JV, Vaidya VS, Schmouder R, Feig P, and Dieterle F (2010) Next-generation biomarkers for detecting kidney toxicity. *Nat Biotechnol* **28**:436-440.
- Brown CD, Sayer R, Windass AS, Haslam IS, De Broe ME, D'Haese PC, and Verhulst A (2008) Characterisation of human tubular cell monolayers as a model of proximal tubular xenobiotic handling. *Toxicol Appl Pharmacol* **233**:428-438.
- Caetano-Pinto P, Justian N, Dib M, Fischer J, Somova M, Burchardt M, and Wolff I (2022) In Vitro Characterization of Renal Drug Transporter Activity in Kidney Cancer. *Int J Mol Sci* **23**:10177.
- Caetano-Pinto P and Stahl SH (2023) Renal Organic Anion Transporters 1 and 3 In Vitro: Gone but Not Forgotten. *Int J Mol Sci* **24**:15419.
- Chasis H, Redish J, Goldring W, Ranges HA, and Smith HW (1945) The use of sodium p-Aminohippurate for the functional evaluation of the human kidney. *J Clin Invest* **24**:583-588.
- Chen S, Zhou Y, Chen Y, and Gu J (2018) fastp: an ultra-fast all-in-one FASTQ preprocessor. *Bioinformatics* **34**:i884-i890.

- Chen WY, Evangelista EA, Yang J, Kelly EJ, and Yeung CK (2021) Kidney Organoid and Microphysiological Kidney Chip Models to Accelerate Drug Development and Reduce Animal Testing. *Front Pharmacol* **12**:695920.
- Drain PK, Kubiak RW, Siriprakaisil O, Klinbuayaem V, Quame-Amaglo J, Sukrakanchana PO, Tanasri S, Punyati P, Sirirungsi W, Cressey R, Bacchetti P, Okochi H, Baeten JM, Gandhi M, and Cressey TR (2020) Urine Tenofovir Concentrations Correlate With Plasma and Relate to Tenofovir Disoproxil Fumarate Adherence: A Randomized, Directly Observed Pharmacokinetic Trial (TARGET Study). *Clin Infect Dis* **70**:2143-2151.
- Duan Y, Gotoh N, Yan Q, Du Z, Weinstein AM, Wang T, and Weinbaum S (2008) Shear-induced reorganization of renal proximal tubule cell actin cytoskeleton and apical junctional complexes. *Proc Natl Acad Sci U S A* **105**:11418-11423.
- Ewart L and Roth A (2021) Opportunities and challenges with microphysiological systems: a pharma end-user perspective. *Nat Rev Drug Discov* **20**:327-328.
- Fang H, Knezevic B, Burnham KL, and Knight JC (2016) XGR software for enhanced interpretation of genomic summary data, illustrated by application to immunological traits. *Genome Med* **8**:129.
- Faria J, Ahmed S, Gerritsen KGF, Mihaila SM, and Masereeuw R (2019) Kidney-based in vitro models for drug-induced toxicity testing. *Arch Toxicol* **93**:3397-3418.
- Feraille E, Sassi A, Olivier V, Arnoux G, and Martin PY (2022) Renal water transport in health and disease. *Pflugers Arch* **474**:841-852.
- Filipski KK, Mathijssen RH, Mikkelsen TS, Schinkel AH, and Sparreboom A (2009) Contribution of organic cation transporter 2 (OCT2) to cisplatin-induced nephrotoxicity. *Clin Pharmacol Ther* **86**:396-402.
- Fonsart J, Saragosti S, Taouk M, Peytavin G, Bushman L, Charreau I, Hance A, Goldwirt L, Morel S, Mammano F, Loze B, Capitant C, Clavel F, Mahjoub N, Meyer L, Anderson PL, Delaugerre C, and Molina JM (2017) Single-dose pharmacokinetics and

- pharmacodynamics of oral tenofovir and emtricitabine in blood, saliva and rectal tissue: a sub-study of the ANRS IPERGAY trial. *J Antimicrob Chemother* **72**:478-485.
- Fuchs TC and Hewitt P (2011) Biomarkers for drug-induced renal damage and nephrotoxicity- an overview for applied toxicology. *AAPS J* **13**:615-631.
- Fukushima K, Okada A, Oe H, Hirasaki M, Hamori M, Nishimura A, Shibata N, and Sugioka N (2018) Pharmacokinetic-Pharmacodynamic Analysis of Cisplatin with Hydration and Mannitol Diuresis: The Contribution of Urine Cisplatin Concentration to Nephrotoxicity. *Eur J Drug Metab Pharmacokinet* **43**:193-203.
- Gao X, Tanaka Y, Sugii Y, Mawatari K, and Kitamori T (2011) Basic structure and cell culture condition of a bioartificial renal tubule on chip towards a cell-based separation microdevice. *Anal Sci* **27**:907-912.
- GTEEx Consortium (2017) Genetic effects on gene expression across human tissues. *Nature* **550**:204-213.
- Harada K, Inoue K, Morikawa A, Yoshinaga T, Saito N, and Koizumi A (2005) Renal clearance of perfluorooctane sulfonate and perfluorooctanoate in humans and their species-specific excretion. *Environ Res* **99**:253-261.
- Hargrove-Grimes P, Low LA, and Tagle DA (2021) Microphysiological systems: What it takes for community adoption. *Exp Biol Med (Maywood)* **246**:1435-1446.
- Hosoyamada M, Ichida K, Enomoto A, Hosoya T, and Endou H (2004) Function and localization of urate transporter 1 in mouse kidney. *J Am Soc Nephrol* **15**:261-268.
- House JS, Grimm FA, Jima DD, Zhou YH, Rusyn I, and Wright FA (2017) A Pipeline for High-Throughput Concentration Response Modeling of Gene Expression for Toxicogenomics. *Front Genet* **8**:168.
- House JS, Grimm FA, Klaren WD, Dalzell A, Kuchi S, Zhang SD, Lenz K, Boogaard PJ, Ketelslegers HB, Gant TW, Rusyn I, and Wright FA (2022) Grouping of UVCB

substances with dose-response transcriptomics data from human cell-based assays.

ALTEX **39**:388-404.

Ikeda K, Terashima M, Kawamura H, Takiyama I, Koeda K, Takagane A, Sato N, Ishida K, Iwaya T, Maesawa C, Yoshinari H, and Saito K (1998) Pharmacokinetics of cisplatin in combined cisplatin and 5-fluorouracil therapy: a comparative study of three different schedules of cisplatin administration. *Jpn J Clin Oncol* **28**:168-175.

Irvine AR, van Berlo D, Shekhani R, and Masereeuw R (2021) A systematic review of models of drug-induced kidney injury. *Current Opinion in Toxicology* **27**:18-26.

Islam MN, Griffin TP, Sander E, Rocks S, Qazi J, Cabral J, McCaul J, McMorro T, and Griffin MD (2019) Human mesenchymal stromal cells broadly modulate high glucose-induced inflammatory responses of renal proximal tubular cell monolayers. *Stem Cell Res Ther* **10**:329.

Jang KJ, Mehr AP, Hamilton GA, McPartlin LA, Chung S, Suh KY, and Ingber DE (2013) Human kidney proximal tubule-on-a-chip for drug transport and nephrotoxicity assessment. *Integr Biol (Camb)* **5**:1119-1129.

Jing B, Yan L, Li J, Luo P, Ai X, and Tu P (2022) Functional Evaluation and Nephrotoxicity Assessment of Human Renal Proximal Tubule Cells on a Chip. *Biosensors (Basel)* **12**:718.

Kim H, Lee JB, Kim K, and Sung GY (2022) Effect of shear stress on the proximal tubule-on-a-chip for multi-organ microphysiological system. *Journal of Industrial and Engineering Chemistry* **115**:279-286.

King SM, Higgins JW, Nino CR, Smith TR, Paffenroth EH, Fairbairn CE, Docuayan A, Shah VD, Chen AE, Presnell SC, and Nguyen DG (2017) 3D Proximal Tubule Tissues Recapitulate Key Aspects of Renal Physiology to Enable Nephrotoxicity Testing. *Front Physiol* **8**:123.

- Kohler JJ, Hosseini SH, Green E, Abuin A, Ludaway T, Russ R, Santoianni R, and Lewis W (2011) Tenofovir renal proximal tubular toxicity is regulated by OAT1 and MRP4 transporters. *Lab Invest* **91**:852-858.
- Lee JB, Kim H, Kim S, and Sung GY (2022) Fabrication and Evaluation of Tubule-on-a-Chip with RPTEC/HUVEC Co-Culture Using Injection-Molded Polycarbonate Chips. *Micromachines (Basel)* **13**:1932.
- Lidberg KA, Muthusamy S, Adil M, Mahadeo A, Yang J, Patel RS, Wang L, Bammler TK, Reichel J, Yeung CK, Himmelfarb J, Kelly EJ, and Akilesh S (2022) Serum Protein Exposure Activates a Core Regulatory Program Driving Human Proximal Tubule Injury. *J Am Soc Nephrol* **33**:949-965.
- Limonciel A, Ates G, Carta G, Wilmes A, Watzele M, Shepard PJ, VanSteenhouse HC, Seligmann B, Yeakley JM, van de Water B, Vinken M, and Jennings P (2018) Comparison of base-line and chemical-induced transcriptomic responses in HepaRG and RPTEC/TERT1 cells using TempO-Seq. *Arch Toxicol* **92**:2517-2531.
- Lin NYC, Homan KA, Robinson SS, Kolesky DB, Duarte N, Moisan A, and Lewis JA (2019) Renal reabsorption in 3D vascularized proximal tubule models. *Proc Natl Acad Sci U S A* **116**:5399-5404.
- Loccisano AE, Campbell JL, Jr., Andersen ME, and Clewell HJ, 3rd (2011) Evaluation and prediction of pharmacokinetics of PFOA and PFOS in the monkey and human using a PBPK model. *Regul Toxicol Pharmacol* **59**:157-175.
- Love MI, Huber W, and Anders S (2014) Moderated estimation of fold change and dispersion for RNA-seq data with DESeq2. *Genome Biol* **15**:550.
- Maass C, Sorensen NB, Himmelfarb J, Kelly EJ, Stokes CL, and Cirit M (2019) Translational Assessment of Drug-Induced Proximal Tubule Injury Using a Kidney Microphysiological System. *CPT Pharmacometrics Syst Pharmacol* **8**:316-325.

- Maggiorani D, Dissard R, Belloy M, Saulnier-Blache JS, Casemayou A, Ducasse L, Gres S, Belliere J, Caubet C, Bascands JL, Schanstra JP, and Buffin-Meyer B (2015) Shear Stress-Induced Alteration of Epithelial Organization in Human Renal Tubular Cells. *PLoS One* **10**:e0131416.
- Marx U, Akabane T, Andersson TB, Baker E, Beilmann M, Beken S, Brendler-Schwaab S, Cirit M, David R, Dehne EM, Durieux I, Ewart L, Fitzpatrick SC, Frey O, Fuchs F, Griffith LG, Hamilton GA, Hartung T, Hoeng J, Hogberg H, Hughes DJ, Ingber DE, Iskandar A, Kanamori T, Kojima H, Kuehnl J, Leist M, Li B, Loskill P, Mendrick DL, Neumann T, Pallocca G, Rusyn I, Smirnova L, Steger-Hartmann T, Tagle DA, Tonevitsky A, Tsyb S, Trapecar M, Van de Water B, Van den Eijnden-van Raaij J, Vulto P, Watanabe K, Wolf A, Zhou X, and Roth A (2020) Biology-inspired microphysiological systems to advance patient benefit and animal welfare in drug development. *ALTEX* **37**:365-394.
- Mav D, Shah RR, Howard BE, Auerbach SS, Bushel PR, Collins JB, Gerhold DL, Judson RS, Karmaus AL, Maull EA, Mendrick DL, Merrick BA, Sipes NS, Svoboda D, and Paules RS (2018) A hybrid gene selection approach to create the S1500+ targeted gene sets for use in high-throughput transcriptomics. *PLoS One* **13**:e0191105.
- Nieskens TT and Wilmer MJ (2016) Kidney-on-a-chip technology for renal proximal tubule tissue reconstruction. *Eur J Pharmacol* **790**:46-56.
- Nieskens TTG, Peters JGP, Dabaghie D, Korte D, Jansen K, Van Asbeck AH, Tavraz NN, Friedrich T, Russel FGM, Masereeuw R, and Wilmer MJ (2018) Expression of Organic Anion Transporter 1 or 3 in Human Kidney Proximal Tubule Cells Reduces Cisplatin Sensitivity. *Drug Metab Dispos* **46**:592-599.
- Nigam SK, Bush KT, Martovetsky G, Ahn SY, Liu HC, Richard E, Bhatnagar V, and Wu W (2015) The organic anion transporter (OAT) family: a systems biology perspective. *Physiol Rev* **95**:83-123.

- Olsen GW, Burris JM, Ehresman DJ, Froehlich JW, Seacat AM, Butenhoff JL, and Zobel LR (2007) Half-life of serum elimination of perfluorooctanesulfonate, perfluorohexanesulfonate, and perfluorooctanoate in retired fluorochemical production workers. *Environ Health Perspect* **115**:1298-1305.
- Phillips JA, Grandhi TSP, Davis M, Gautier JC, Hariparsad N, Keller D, Sura R, and Van Vleet TR (2020) A pharmaceutical industry perspective on microphysiological kidney systems for evaluation of safety for new therapies. *Lab Chip* **20**:468-476.
- Plain A, Pan W, O'Neill D, Ure M, Beggs MR, Farhan M, Dimke H, Cordat E, and Alexander RT (2020) Claudin-12 Knockout Mice Demonstrate Reduced Proximal Tubule Calcium Permeability. *Int J Mol Sci* **21**:2074.
- Pohl M, Shan Q, Petsch T, Styp-Rekowska B, Matthey P, Bleich M, Bachmann S, and Theilig F (2015) Short-term functional adaptation of aquaporin-1 surface expression in the proximal tubule, a component of glomerulotubular balance. *J Am Soc Nephrol* **26**:1269-1278.
- Ross EJ, Gordon ER, Sothers H, Darji R, Baron O, Haithcock D, Prabhakarandian B, Pant K, Myers RM, Cooper SJ, and Cox NJ (2021) Three dimensional modeling of biologically relevant fluid shear stress in human renal tubule cells mimics in vivo transcriptional profiles. *Sci Rep* **11**:14053.
- Rusyn I, Sakolish C, Kato Y, Stephan C, Vergara L, Hewitt P, Bhaskaran V, Davis M, Hardwick RN, Ferguson SS, Stanko JP, Bajaj P, Adkins K, Sipes NS, Hunter ES, Baltazar MT, Carmichael PL, Sadh K, and Becker RA (2022) Microphysiological Systems Evaluation: Experience of TEX-VAL Tissue Chip Testing Consortium. *Toxicol Sci* **188**:143-152.
- Sakolish C, Chen Z, Dalaijamts C, Mitra K, Liu Y, Fulton T, Wade TL, Kelly EJ, Rusyn I, and Chiu WA (2020) Predicting tubular reabsorption with a human kidney proximal tubule tissue-on-a-chip and physiologically-based modeling. *Toxicol In Vitro* **63**:104752.

- Sakolish C, Moyer HL, Tsai HD, Ford LC, Dickey AN, Wright FA, Han G, Bajaj P, Baltazar MT, Carmichael PL, Stanko JP, Ferguson SS, and Rusyn I (2023) Analysis of Reproducibility and Robustness of a Renal Proximal Tubule Microphysiological System OrganoPlate(R) 3-lane 40 for In Vitro Studies of Drug Transport and Toxicity. *Toxicol Sci*.
- Sakolish C, Weber EJ, Kelly EJ, Himmelfarb J, Mouneimne R, Grimm FA, House JS, Wade T, Han A, Chiu WA, and Rusyn I (2018) Technology Transfer of the Microphysiological Systems: A Case Study of the Human Proximal Tubule Tissue Chip. *Sci Rep* **8**:14882.
- Schreiner GE (1965) Toxic Nephropathy: Adverse Renal Effects Caused by Drugs and Chemicals. *JAMA* **191**:849-850.
- Seals R, Bartell SM, and Steenland K (2011) Accumulation and clearance of perfluorooctanoic acid (PFOA) in current and former residents of an exposed community. *Environ Health Perspect* **119**:119-124.
- Secker PF, Schlichenmaier N, Beilmann M, Deschl U, and Dietrich DR (2019) Functional transepithelial transport measurements to detect nephrotoxicity in vitro using the RPTEC/TERT1 cell line. *Arch Toxicol* **93**:1965-1978.
- Shaughnessey EM, Kann SH, Azizgolshani H, Black LD, 3rd, Charest JL, and Vedula EM (2022) Evaluation of rapid transepithelial electrical resistance (TEER) measurement as a metric of kidney toxicity in a high-throughput microfluidic culture system. *Sci Rep* **12**:13182.
- Specioso G, Bovard D, Zanetti F, Maranzano F, Merg C, Sandoz A, Titz B, Dalcanale F, Hoeng J, Renggli K, and Suter-Dick L (2022) Apical Medium Flow Influences the Morphology and Physiology of Human Proximal Tubular Cells in a Microphysiological System. *Bioengineering (Basel)* **9**:516.
- Vaidya VS, Ferguson MA, and Bonventre JV (2008) Biomarkers of acute kidney injury. *Annu Rev Pharmacol Toxicol* **48**:463-493.

- Vormann MK, Gijzen L, Hutter S, Boot L, Nicolas A, van den Heuvel A, Vriend J, Ng CP, Nieskens TTG, van Duinen V, de Wagenaar B, Masereeuw R, Suter-Dick L, Trietsch SJ, Wilmer M, Joore J, Vulto P, and Lanz HL (2018) Nephrotoxicity and Kidney Transport Assessment on 3D Perfused Proximal Tubules. *AAPS J* **20**:90.
- Vriend J, Peters JGP, Nieskens TTG, Skovronova R, Blaimschein N, Schmidts M, Roepman R, Schirris TJJ, Russel FGM, Masereeuw R, and Wilmer MJ (2020) Flow stimulates drug transport in a human kidney proximal tubule-on-a-chip independent of primary cilia. *Biochim Biophys Acta Gen Subj* **1864**:129433.
- Waugh WH and Beall PT (1974) Simplified measurement of p-aminohippurate and other arylamines in plasma and urine. *Kidney Int* **5**:429-436.
- Weber EJ, Chapron A, Chapron BD, Voellinger JL, Lidberg KA, Yeung CK, Wang Z, Yamaura Y, Hailey DW, Neumann T, Shen DD, Thummel KE, Muczynski KA, Himmelfarb J, and Kelly EJ (2016) Development of a microphysiological model of human kidney proximal tubule function. *Kidney Int* **90**:627-637.
- Wieser M, Stadler G, Jennings P, Streubel B, Pfaller W, Ambros P, Riedl C, Katinger H, Grillari J, and Grillari-Voglauer R (2008) hTERT alone immortalizes epithelial cells of renal proximal tubules without changing their functional characteristics. *Am J Physiol Renal Physiol* **295**:F1365-1375.
- Wilmer MJ, Ng CP, Lanz HL, Vulto P, Suter-Dick L, and Masereeuw R (2016) Kidney-on-a-Chip Technology for Drug-Induced Nephrotoxicity Screening. *Trends Biotechnol* **34**:156-170.
- Yang CH, Glover KP, and Han X (2010) Characterization of cellular uptake of perfluorooctanoate via organic anion-transporting polypeptide 1A2, organic anion transporter 4, and urate transporter 1 for their potential roles in mediating human renal reabsorption of perfluorocarboxylates. *Toxicol Sci* **117**:294-302.
- Zager RA (1997) Pathogenetic mechanisms in nephrotoxic acute renal failure. *Semin Nephrol* **17**:3-14.

Zimmermann AE, Pizzoferrato T, Bedford J, Morris A, Hoffman R, and Braden G (2006)

Tenofovir-associated acute and chronic kidney disease: a case of multiple drug interactions. *Clin Infect Dis* **42**:283-290.

Figure Legends

Figure 1. General study designs for the experiments performed. See detailed experimental protocols for each experiment detailed in **Supplemental Table 1**. Day -1 corresponded to the day when the cells were seeded onto membranes, and day 0 was the day of initiation of fluid flow (in fluidic models). Medium changes were performed every 48 hours, and timing for assays and endpoints are indicated (see symbol legends). RPTECs and seeding condition (top/bottom) are shown for each study design. **(A)** The study design used to evaluate 6 RPTEC sources. Cells were seeded on either the top or bottom of membranes. **(B)** The study design used to evaluate the renal transport of para-aminohippurate (pAH) by TERT1 and TERT1-OAT1 cells. pAH was added on day 7 of culture, and sampled at 2, 4, 24, and 48 hours. **(C)** The study design used to evaluate the renal transport of various compounds (cisplatin, tenofovir, and PFOA) by TERT1 and TERT1-OAT1 cells. Cells were seeded on the bottom of transwells, and compounds were added apically (“lumen”) or basolaterally (“blood”). Treatment day 0 was on day 10 of culture and exposures were carried out for 1 week.

Figure 2. Nuclear (DAPI) staining of RPTECs to illustrate cell morphology in top **(A)** and bottom **(B)** seeded conditions with and without media flow. All TERT lines were imaged on day 8, and primary RPTECs (BioPredic and Lonza) were imaged on day 14. All images were captured at 4x magnification (scale bar = 500 μ m).

Figure 3. Barrier formation by TERT1 and TERT1-OAT1 cells under static or fluidic conditions. **(A)** TEER was measured every 48 hours of culture in each seeding condition. TERT lines were cultured until day 8, and primary RPTECs were cultured until day 14. **(B)** FITC-dextran permeability (70 kDa) is shown as “% Blank” (transwells with no cells – permeability was 9.4% in static and 13.2% in fluidic conditions). All values shown are mean \pm SD (n = 6 for TEER and n = 3

for FITC-dextran). Asterisks (*, **, and ****) denote statistical differences ($p < 0.05$, $p < 0.01$, and $p < 0.0001$, respectively) between seeding condition within each group using two-way ANOVA followed by Šídák's multiple comparisons test.

Figure 4. Immunocytochemistry on TERT1 and Lonza primary RPTECs in static and fluidic conditions (bottom seeded). (A) Representative monochromatic images of immunostaining of TERT1 and Lonza RPTECs for tight junctions (ZO-1), and transporters (AQP1 and SGLT2) with and without media flow. Scale bar = 200 μm . (B) Image quantitation shows mean \pm SD ($n = 3$) fluorescence per field, normalized to TERT1/static transwell conditions. Asterisks (*, **, and ****) denote statistical differences ($p < 0.05$, $p < 0.01$, and $p < 0.0001$, respectively) between seeding condition within each cell source using two-way ANOVA followed by Šídák's multiple comparisons test.

Figure 5. Water transport functionality of different RPTECs in static and fluidic condition. (A-B) Schematic diagram of cell seeding and expected media movement if RPTECs are functioning to transport water between chambers in a transwell. (C) Representative photographs of the transwells in which TERT1 cells were seeded on either side of the membrane as indicated by the legend and incubated for 48 hrs. (D) Representative photograph of the medium collected from either side of the transwell displays difference in both volume and color (dilution of Phenol Red). (E) Absorbance ratio of medium (590 nm) in apical/basolateral chambers of transwells in various seeding conditions (RPTEC source indicated in a legend to each chart, top vs bottom seeded, static (open bars) vs fluidic (gray bars)). (F) pAH transport is shown as a ratio of secretion (Basolateral \rightarrow Apical) to absorbance (Apical \rightarrow Basolateral). All bar graphs show mean \pm SD ($n = 6$ for water transport and $n = 3$ for pAH secretion). Asterisks (*, **, and ****) denote statistical differences ($p < 0.05$, $p < 0.01$, and $p < 0.0001$, respectively) between conditions within each group using either two-way ANOVA followed by Šídák's multiple comparisons test (E), or t-tests (F).

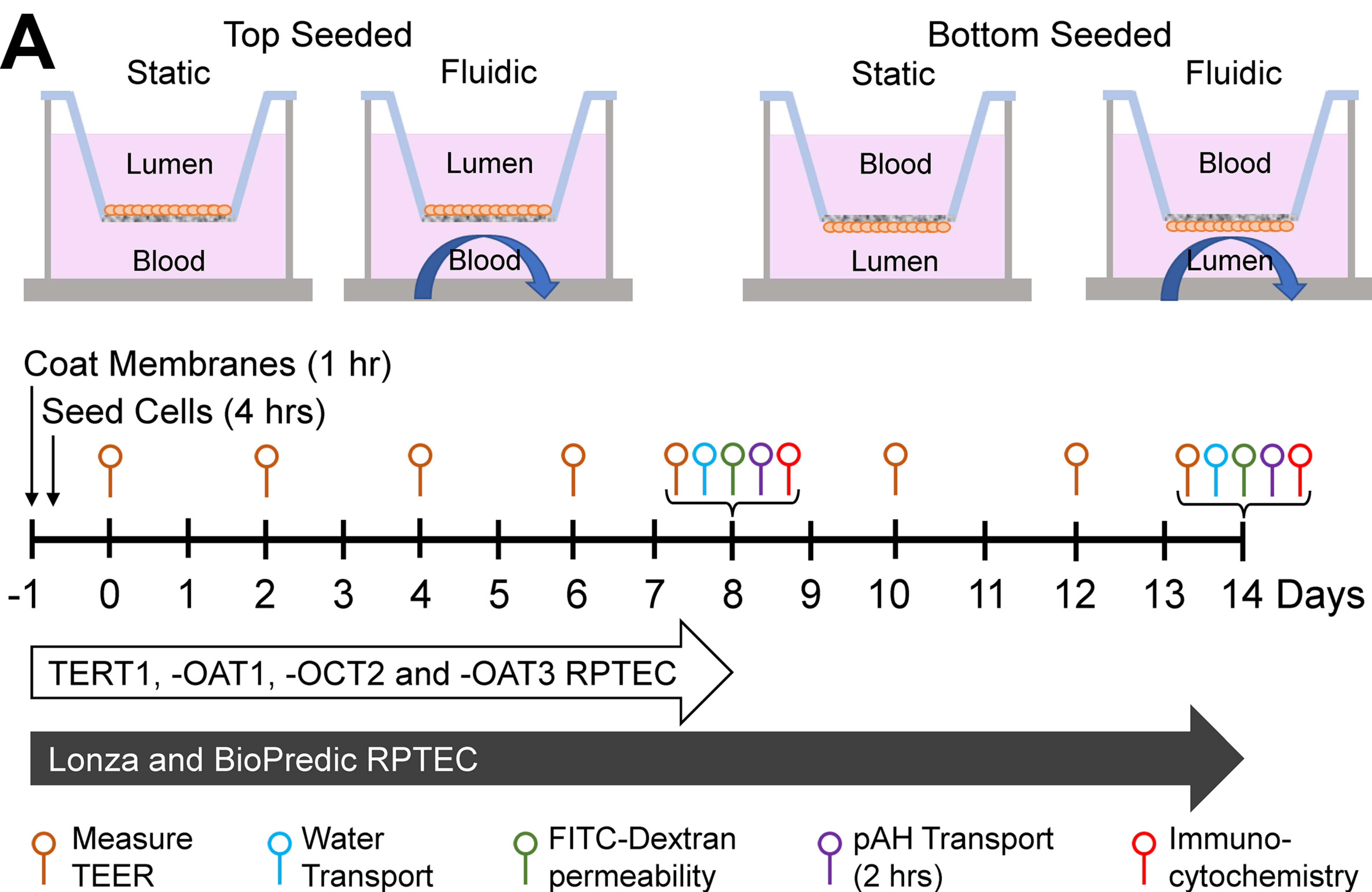
Figure 6. Secretion of para-aminohippurate (pAH) by TERT1 and TERT1-OAT1 cells in static and fluidic condition. pAH was added to the top and bottom wells in equal concentration (5 μM pAH \pm 100 μM probenecid [Inh]), and the medium was sampled at 2, 4, 24, and 48 hours to monitor pAH concentrations. Results are shown as a ratio of apical to basolateral concentration, where values >1 indicate active secretion by the cells. Values (mean \pm SD, $n = 3$) are normalized to the TERT1 line at 2 hours for each culture condition (static vs fluidic). Asterisks (***, and ****) denote statistical differences ($p < 0.001$ and $p < 0.0001$, respectively) between exposure conditions within each group using two-way ANOVA followed by Tukey's multiple comparisons test.

Figure 7. Directional transport of drugs and chemicals by TERT1 and TERT1-OAT1 cells in static and fluidic condition. Net secretion of tenofovir (100 μM), cisplatin (10 μM), and PFOA (1 μM) was studied in two RPTEC sources that were bottom seeded in transwells with and without flow. Net secretion rate (pmol/hr) was calculated as detailed in Methods. Values shown are mean \pm SD ($n = 8$ to 10).

Figure 8. Gene expression analyses for TERT1 and TERT1-OAT1 cells cultured either without flow in transwells (TW) or 384-well plates (384WP), or in transwells with flow (CN). **(A)** Rank-based (Spearman) correlation between transcriptional profiles of TERT1 and TERT1-OAT1 cells (depicted in different colors) in transwells with flow (circles), transwells without flow (squares), or 384-well plates without flow (triangles) and human tissues [data from (GTEx Consortium, 2017)]. **(B)** Principal component analysis of gene expression data. Symbols depict chemical treatments and culture conditions as indicated in the legend. Cell sources (TERT1 and TERT-OAT1) are depicted in solids or open symbols, respectively. **(C)** An unsupervised (average linkage clustering)

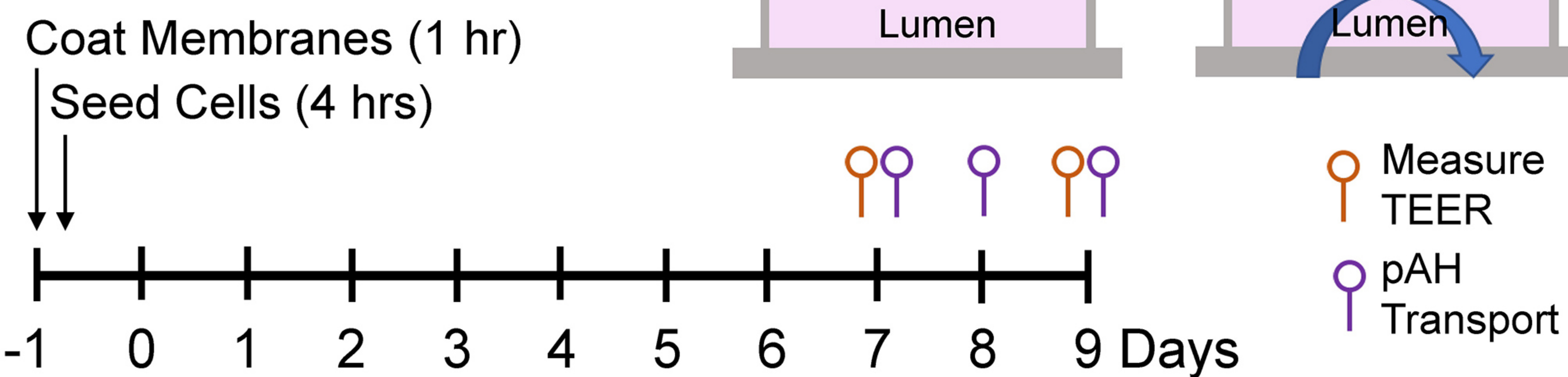
heatmap visualizing expression of 257 genes that were differentially expressed between fluidic (CN) and static (TW) cultures of TERT1 and TERT1-OAT1 cells treated with cisplatin (10 μ M, Cisp), PFOA (1 μ M) or untreated (Untr). Colors depict Z-score values for normalized data. Cell sources and culture conditions (vertical-colored bars) are indicated in the legend. **(D)** Bar plots show the number of genes that were differentially expressed between static (TW) and fluidic (CN) conditions for each cell source/treatment. **(E)** Bar plots displaying common differentially expressed genes from a comparison shown in (D). Shades represent the mean fold difference in expression (on \log_2 scale) across all conditions as indicated in the color bar.

Figure 1



B Cell Types Used:

- TERT1 RPTEC
- TERT1-OAT1 RPTEC



C Cell Types Used:

- TERT1 RPTEC
- TERT1-OAT1 RPTEC

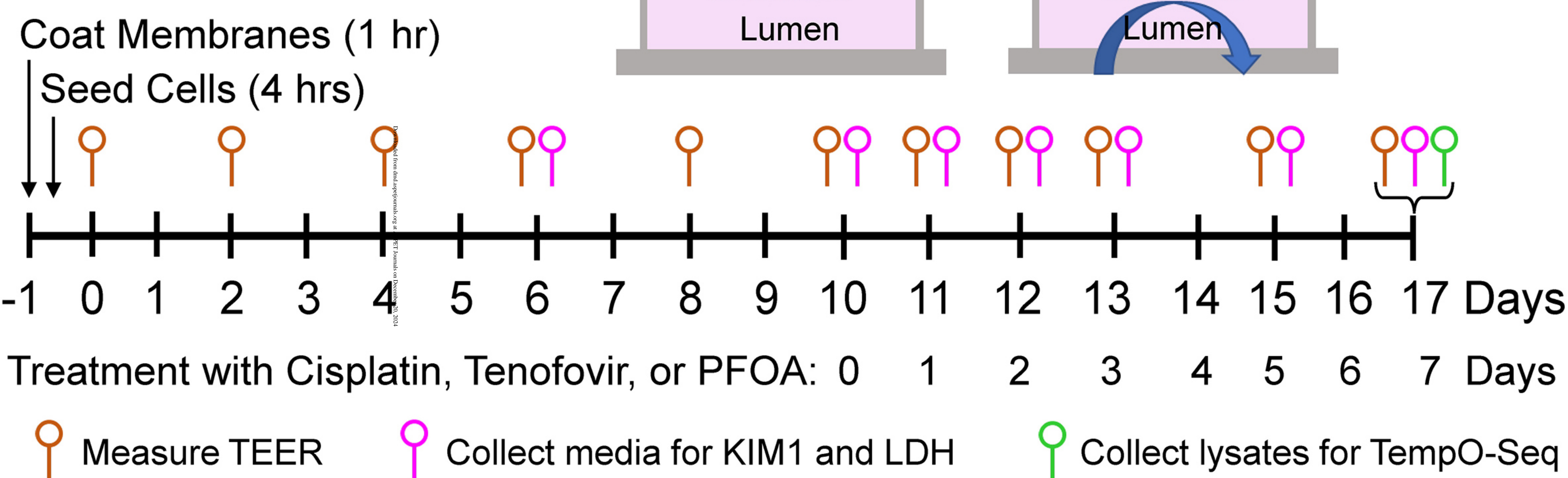


Figure 2

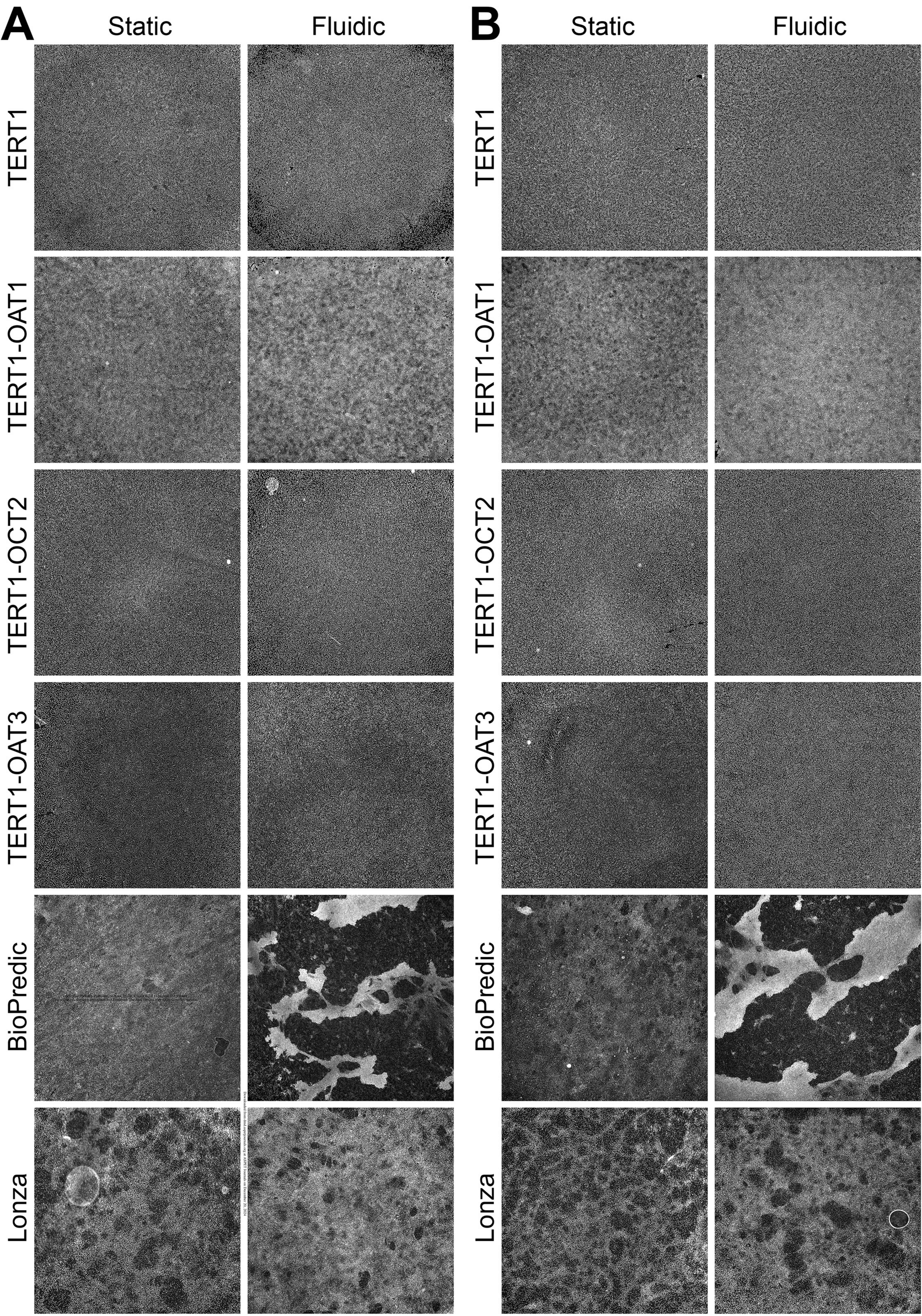


Figure 3

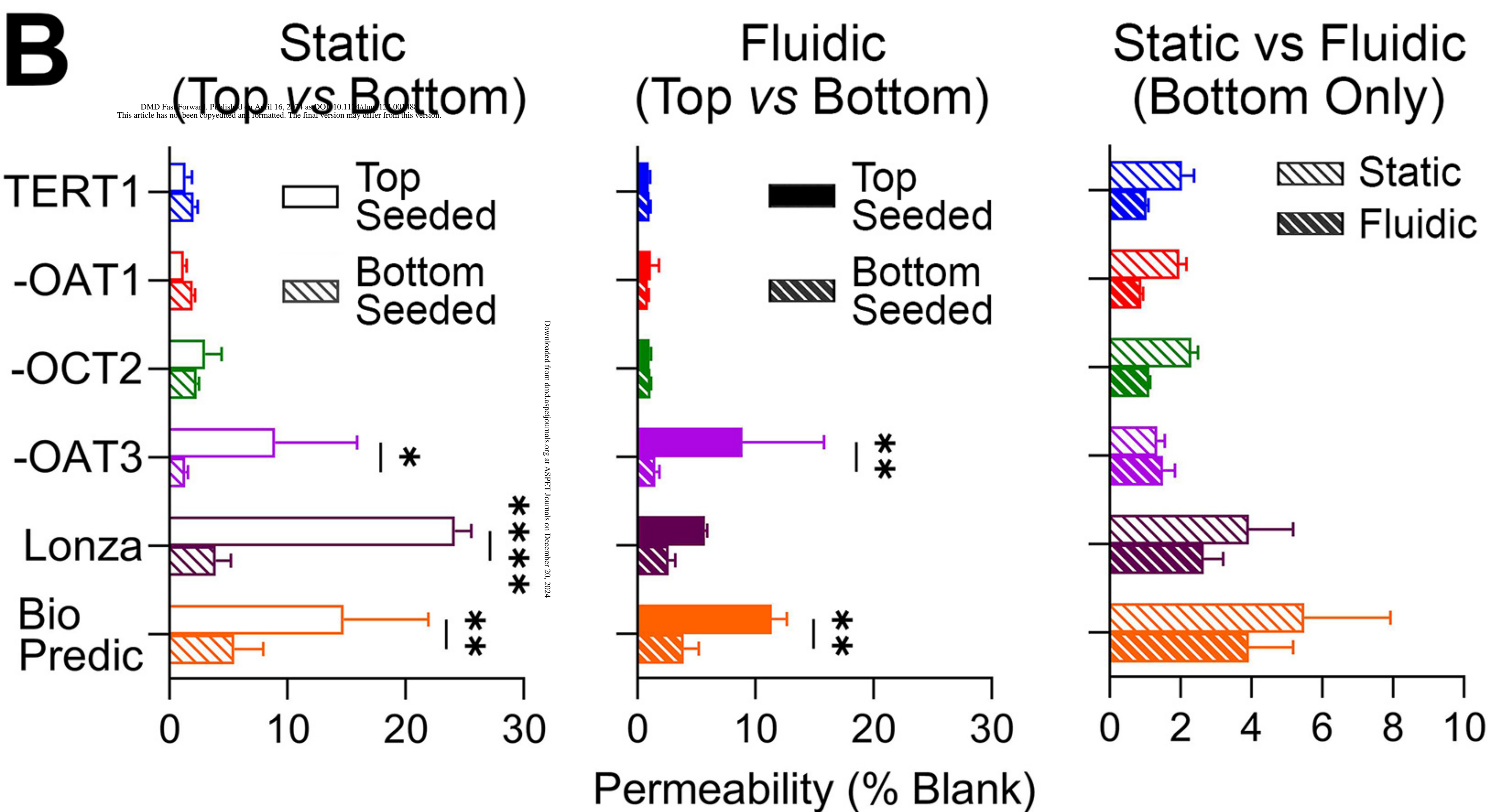
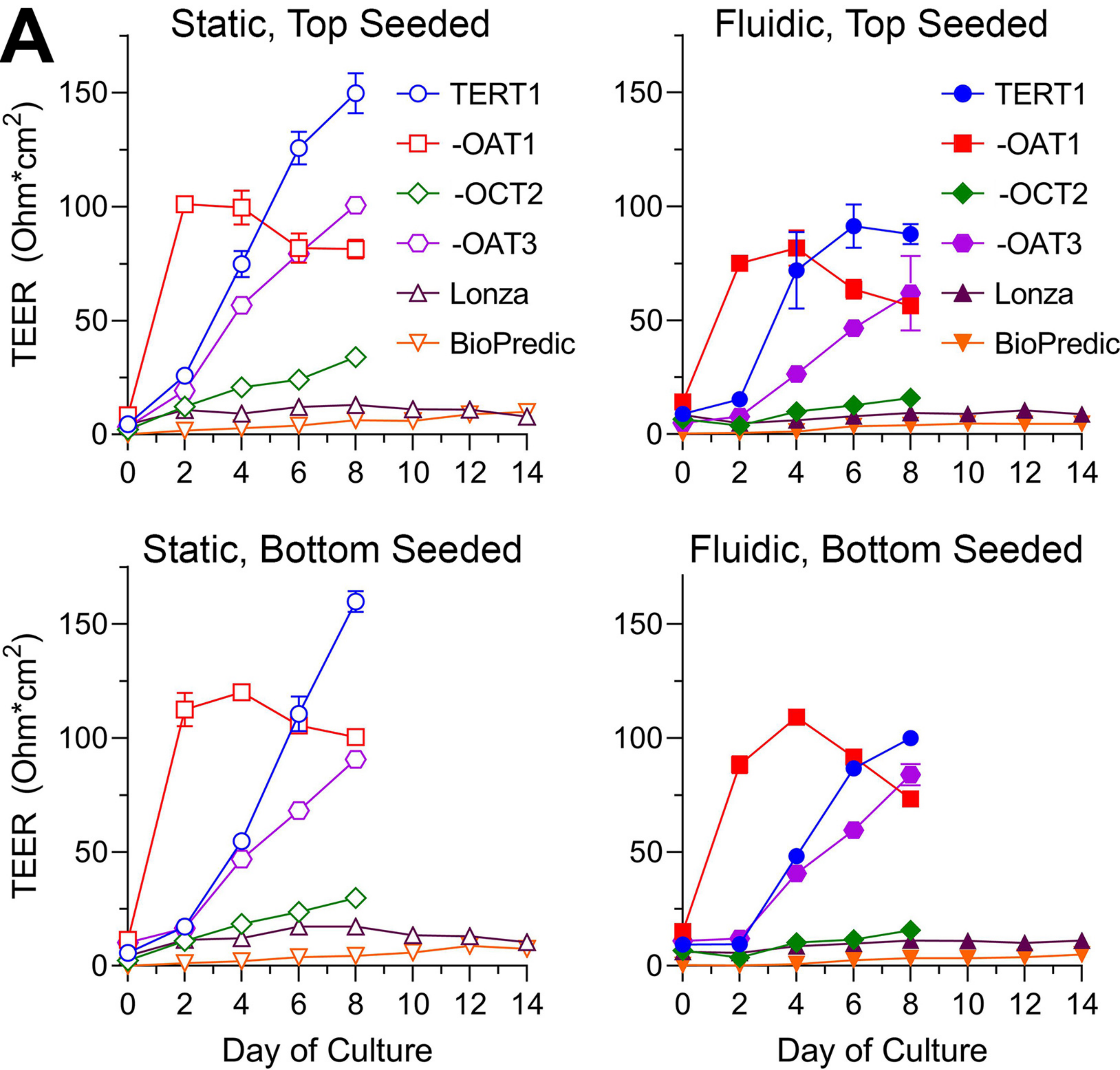
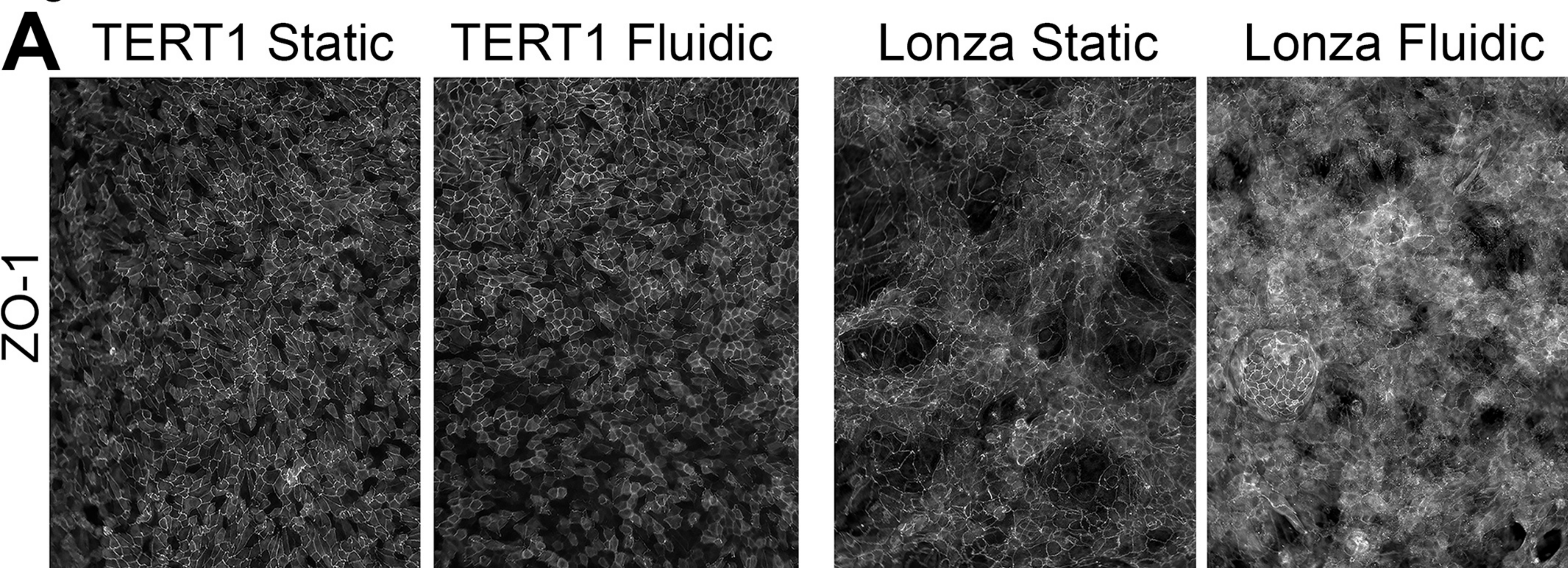
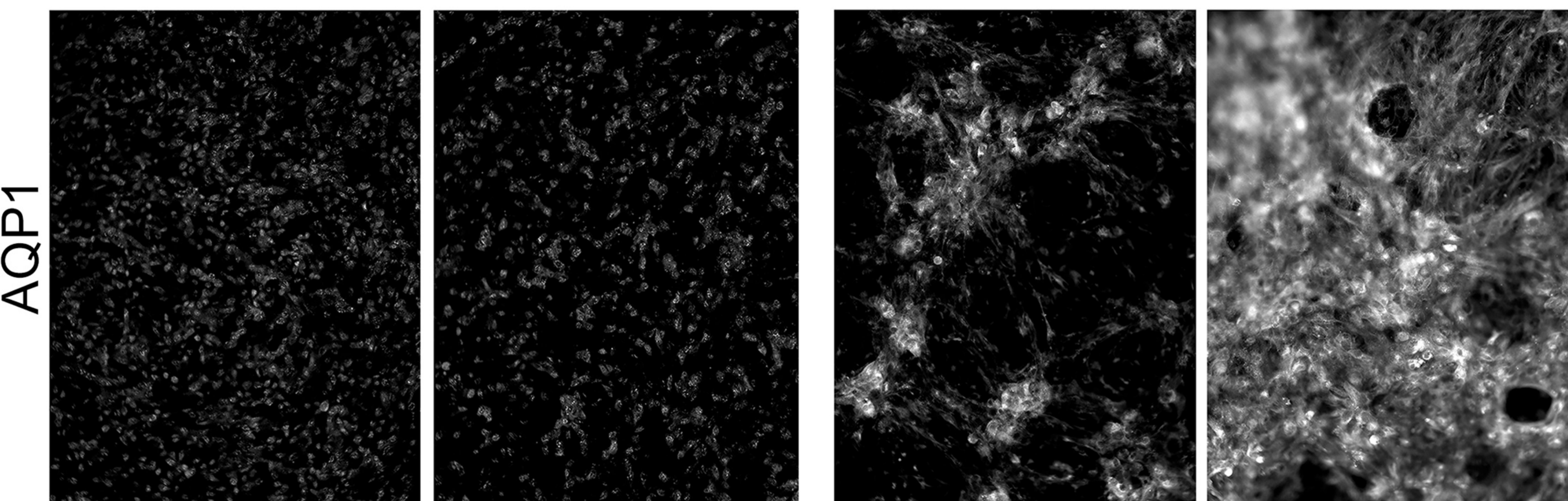
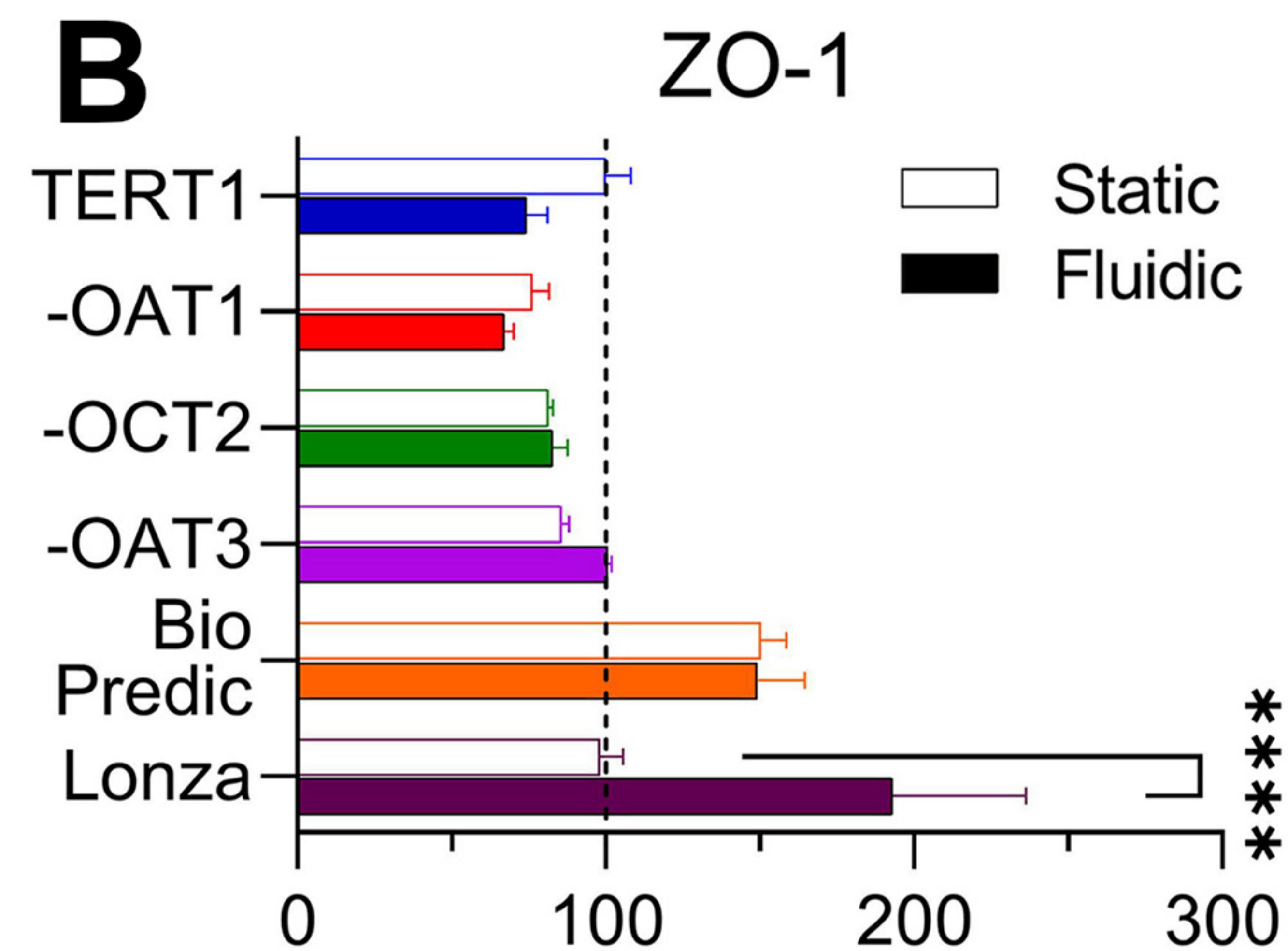


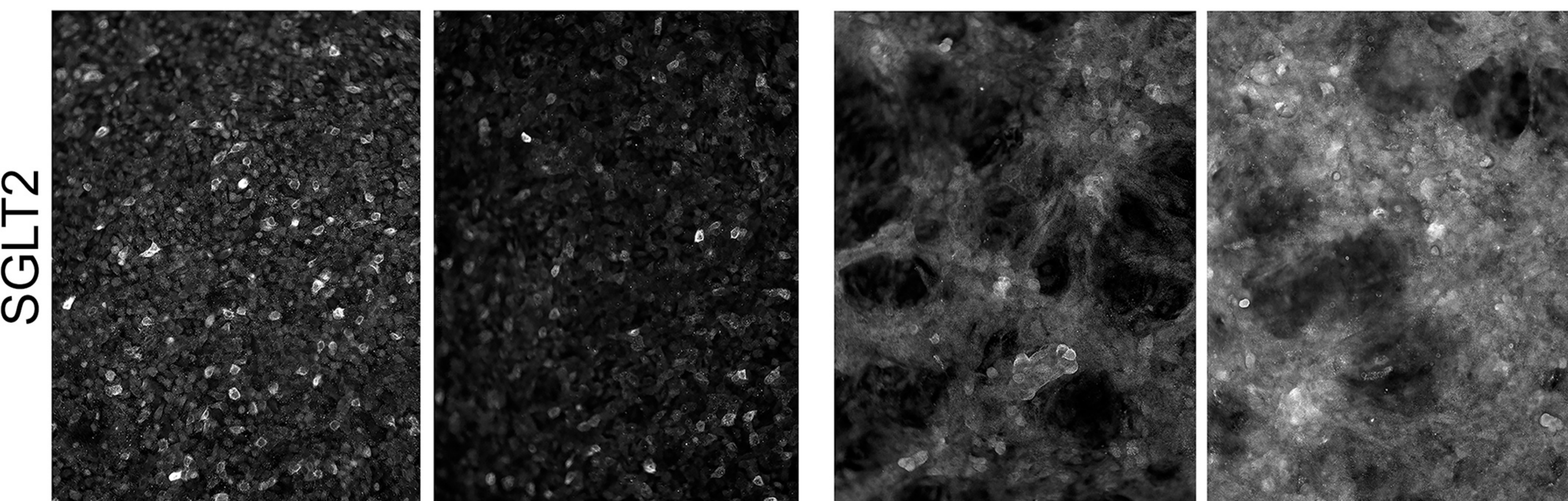
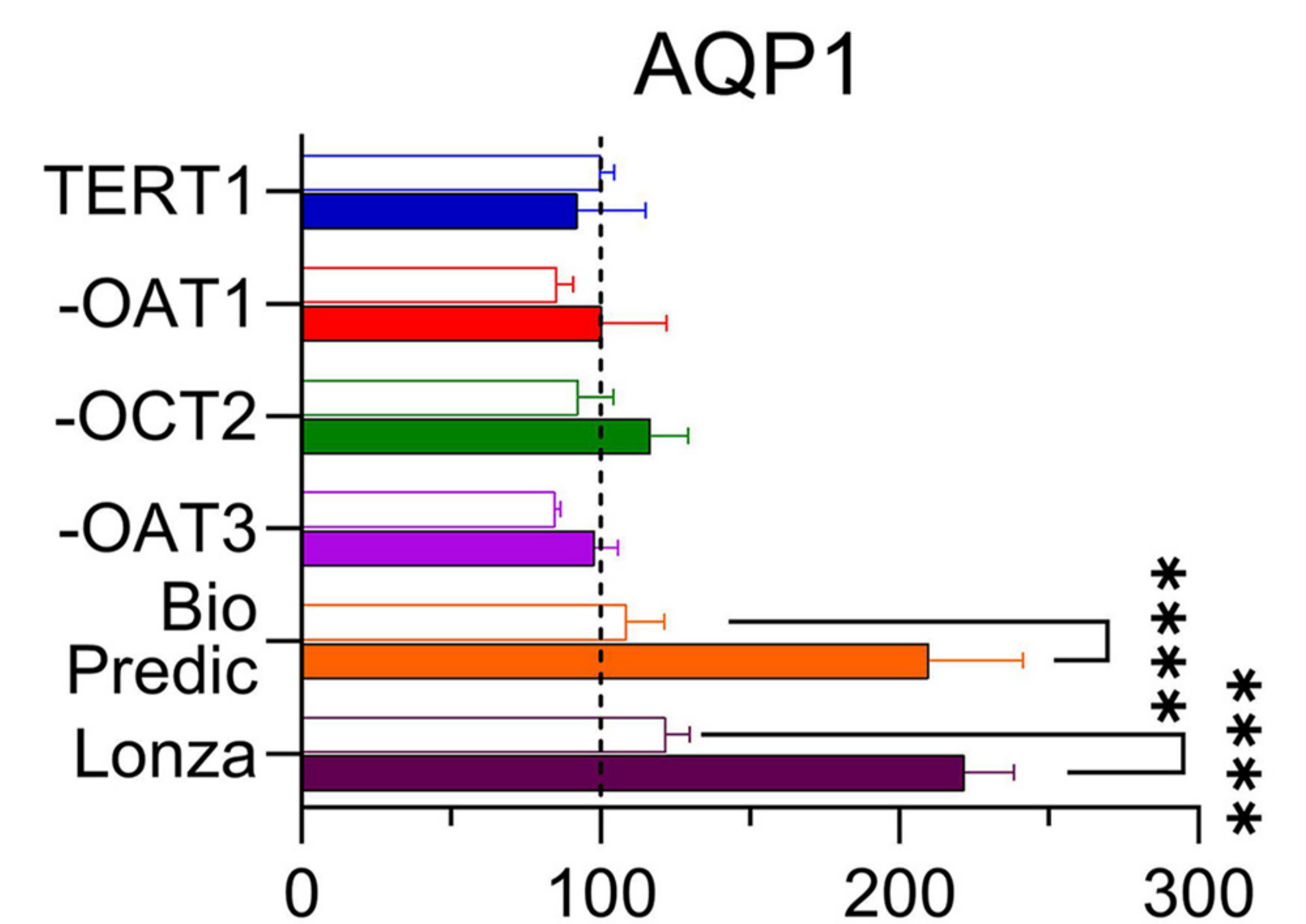
Figure 4



ZO-1



AQP1



SGLT2

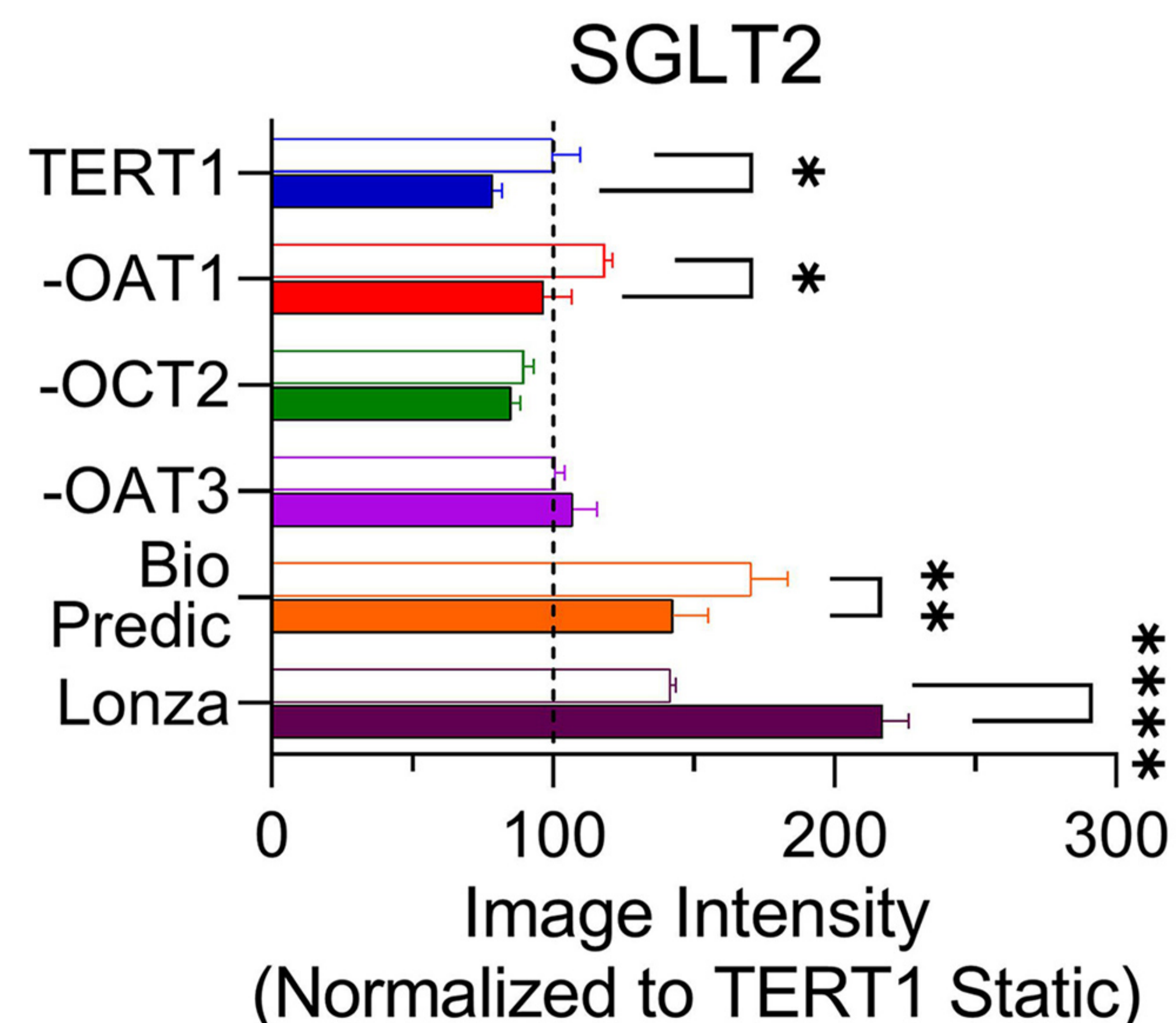


Image Intensity
(Normalized to TERT1 Static)

Figure 5

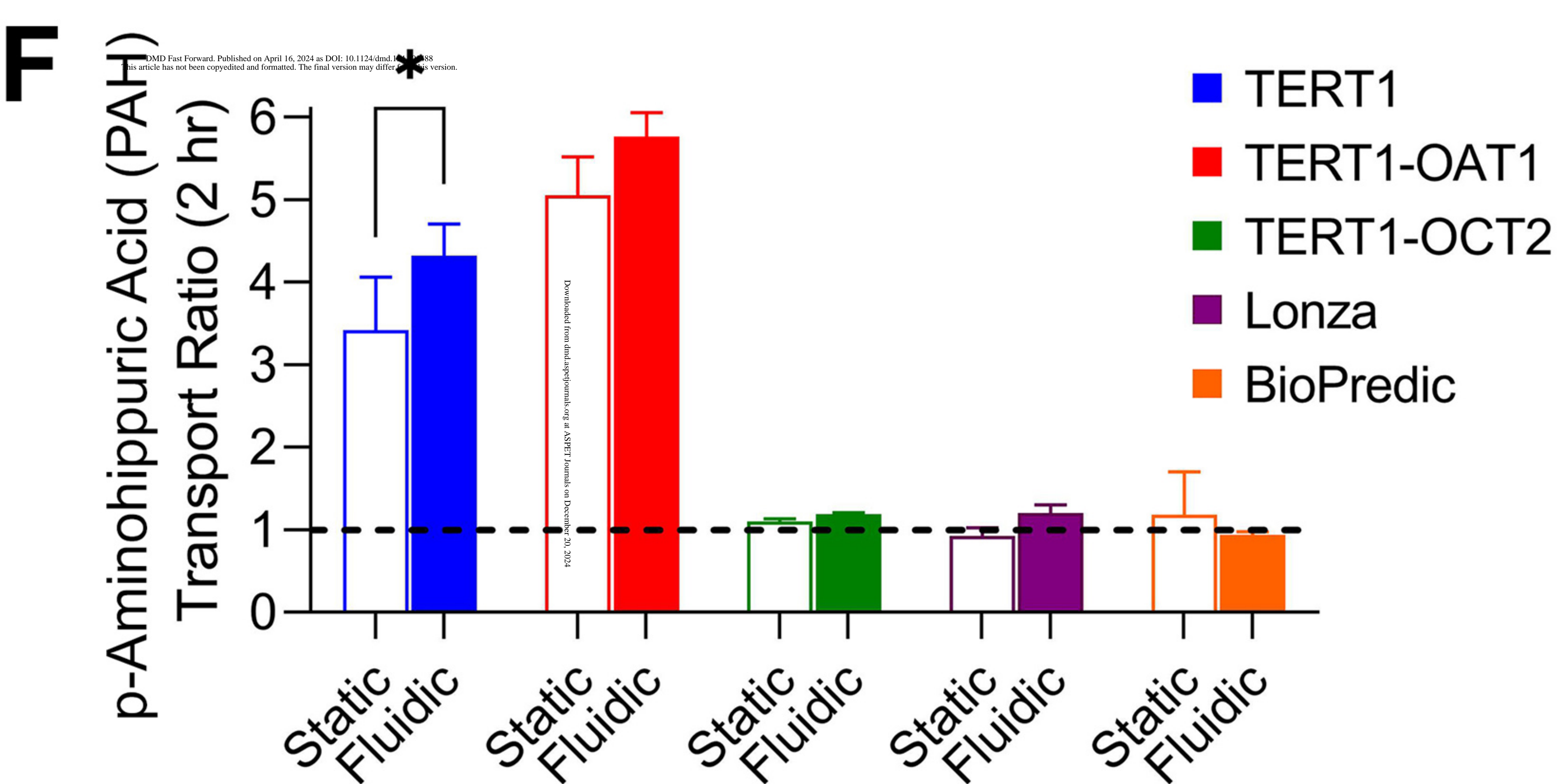
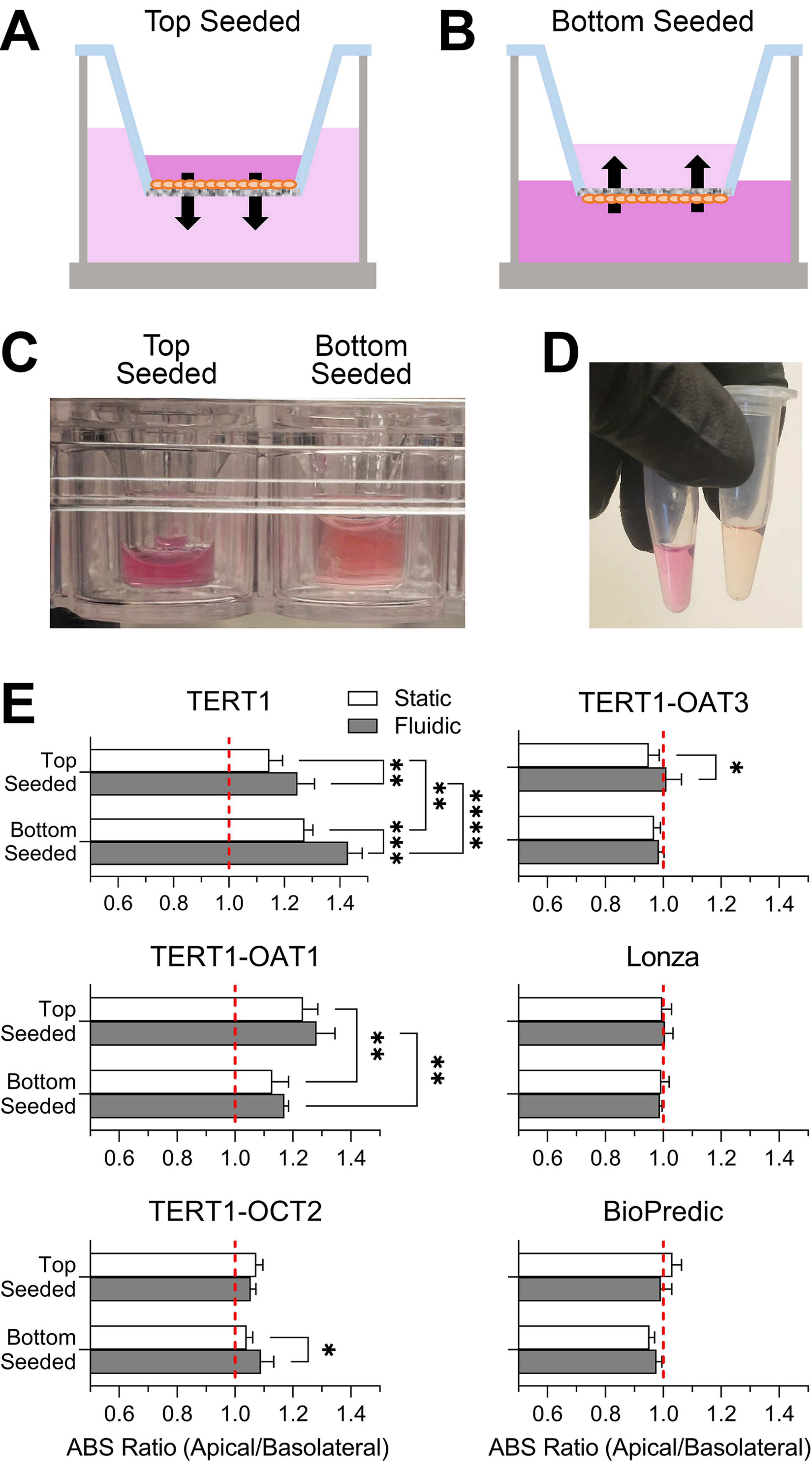
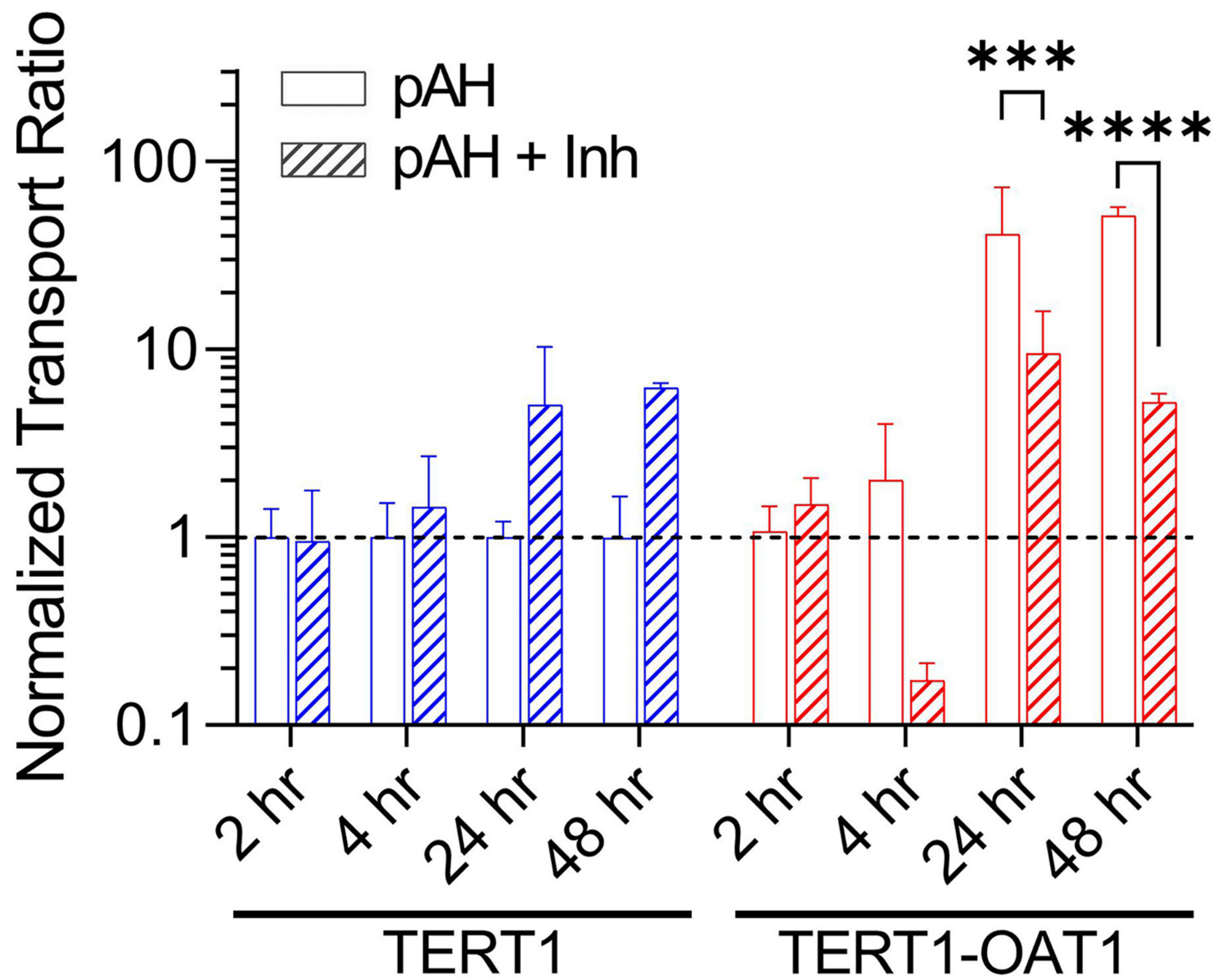


Figure 6

A

Static



B

Fluidic

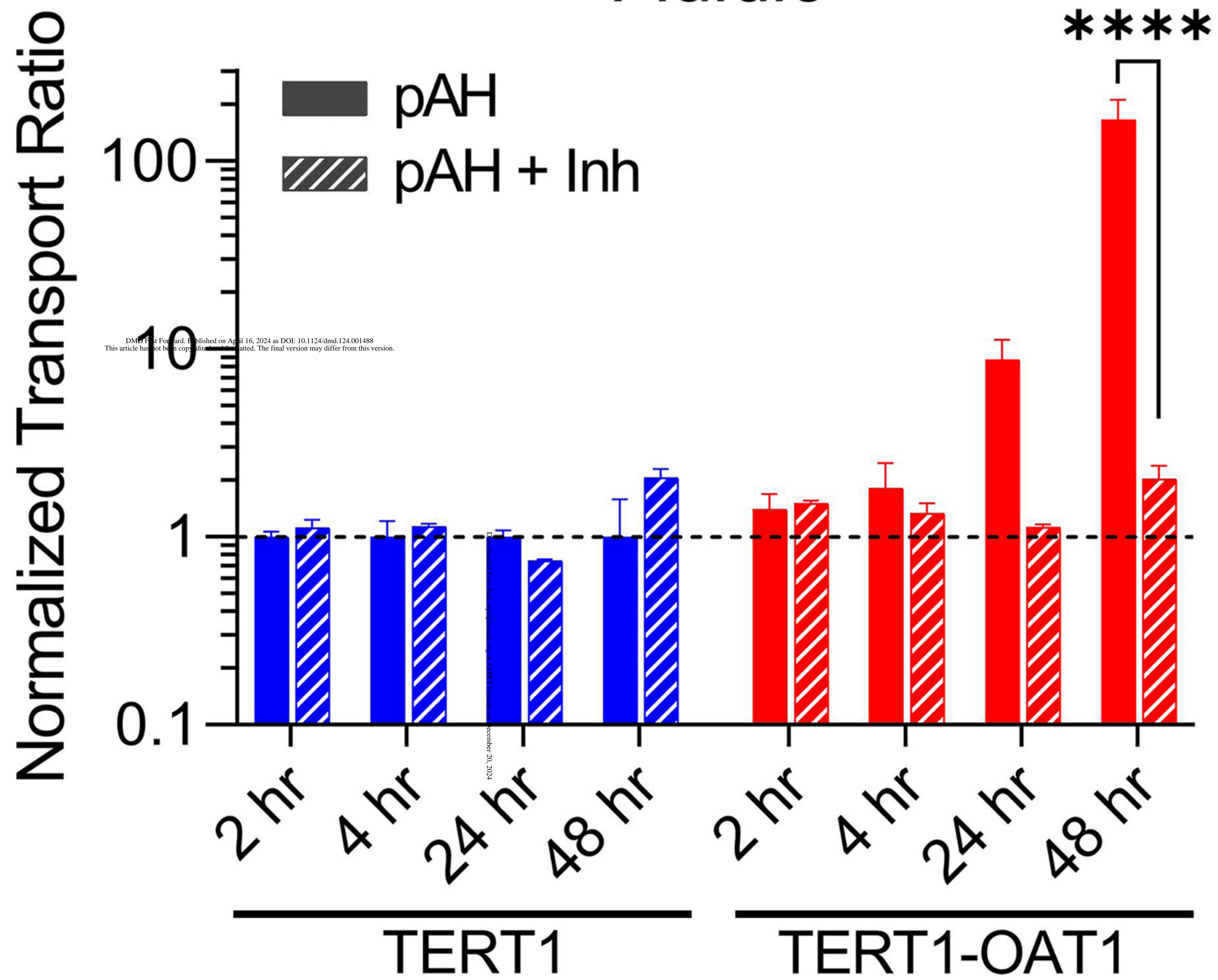


Figure 7

○ TERT1 Static, Bottom

● TERT1 Fluidic, Bottom

□ TERT1-OAT1 Static, Bottom

■ TERT1-OAT1 Fluidic, Bottom

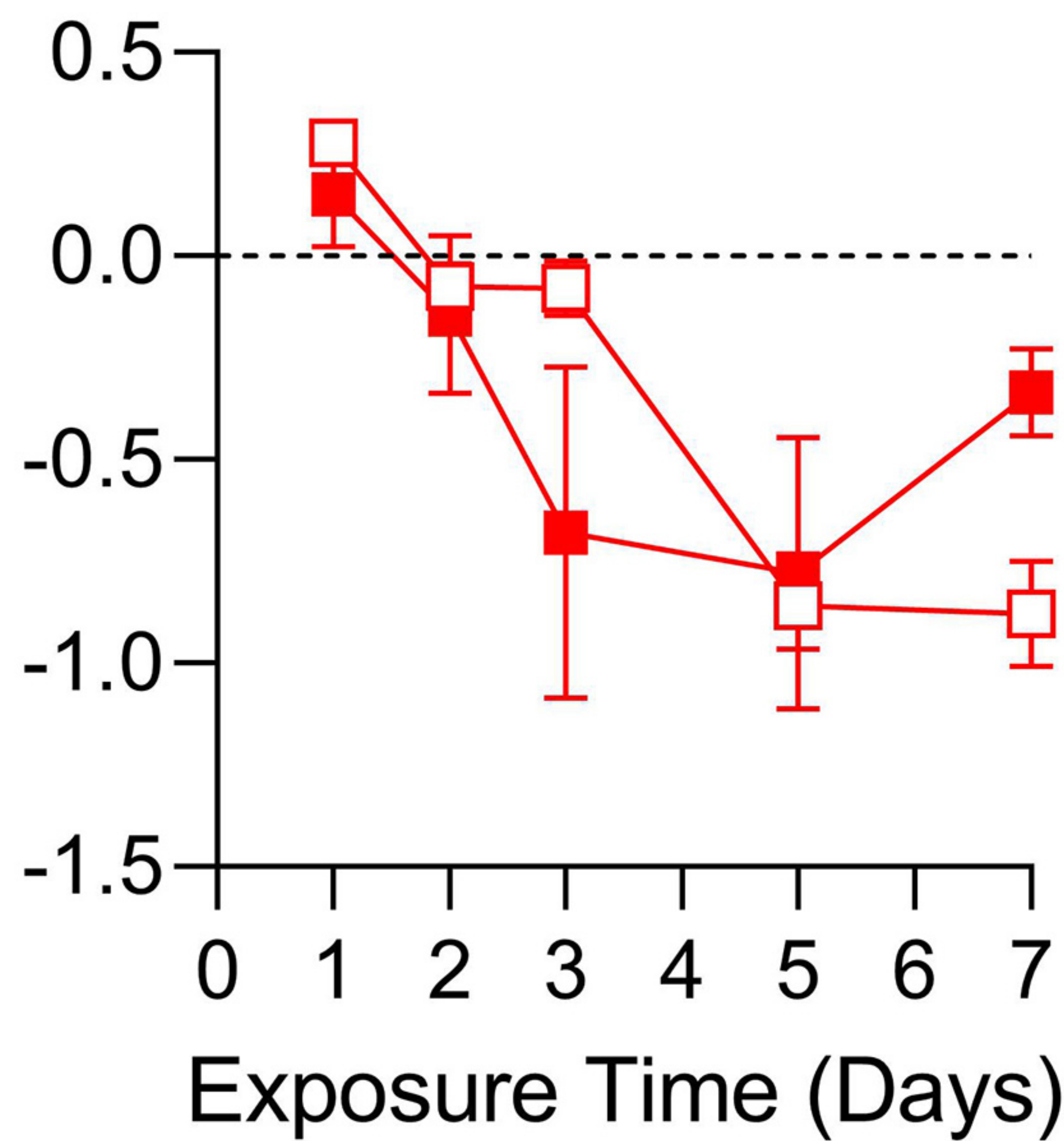
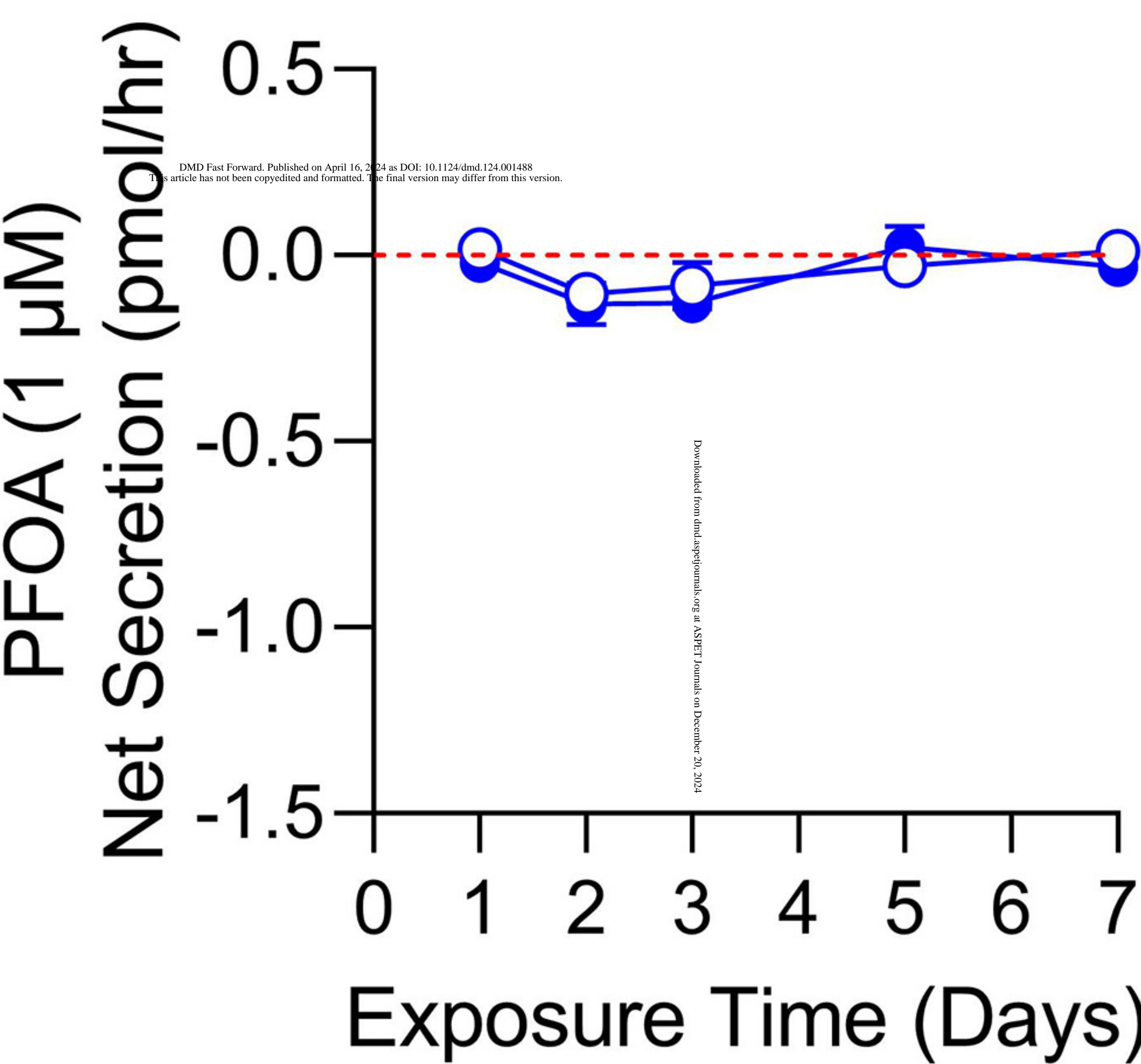
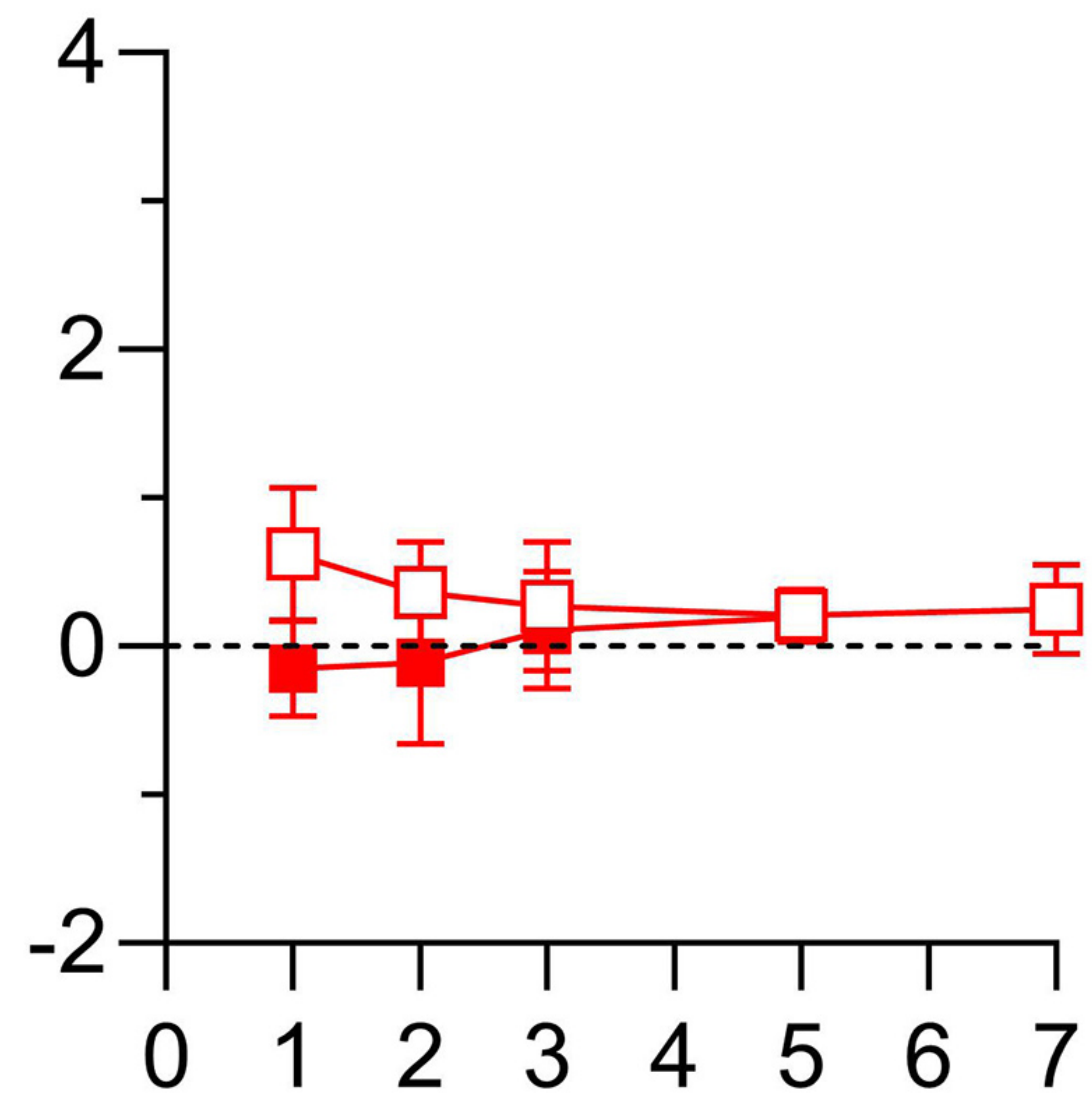
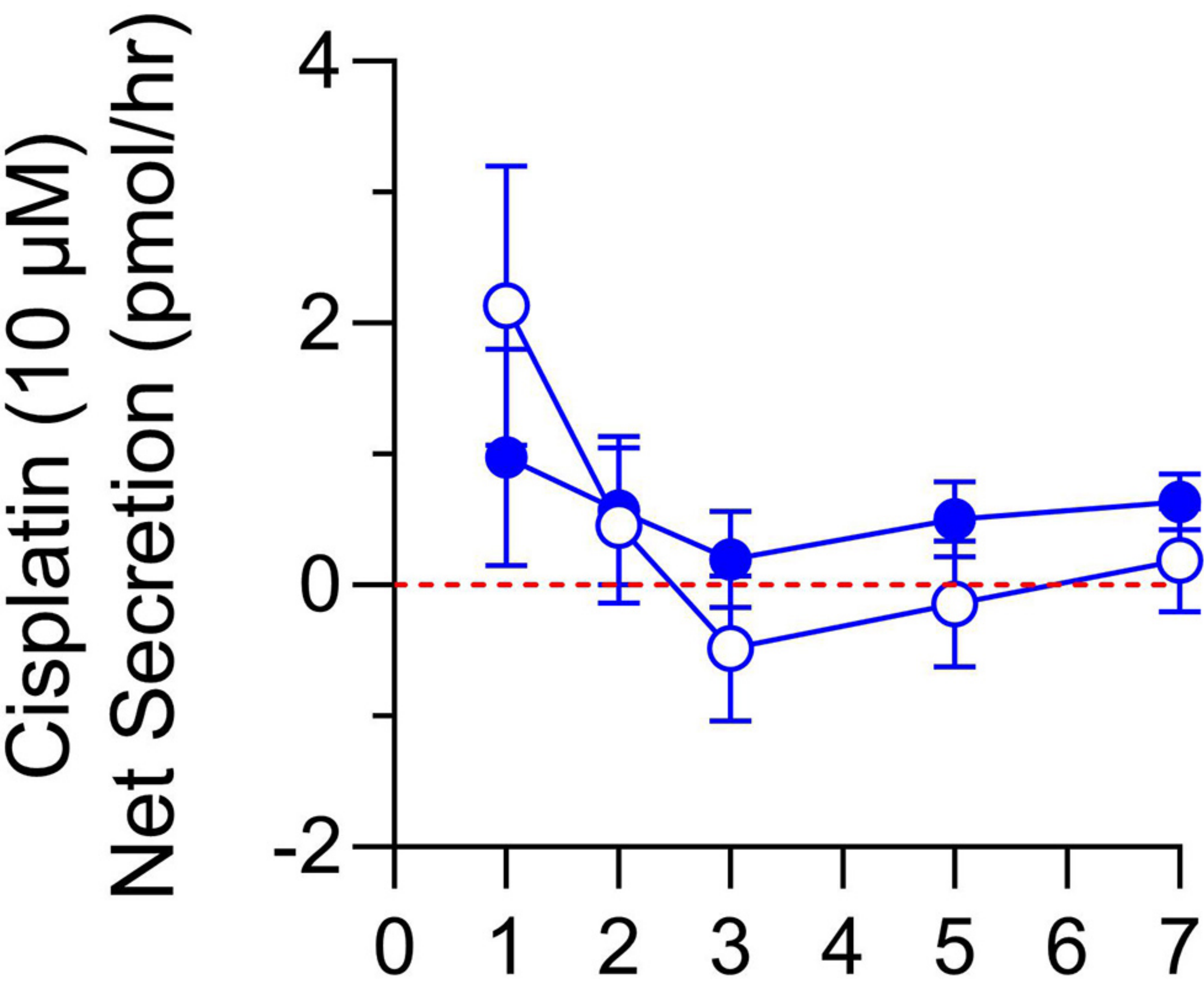
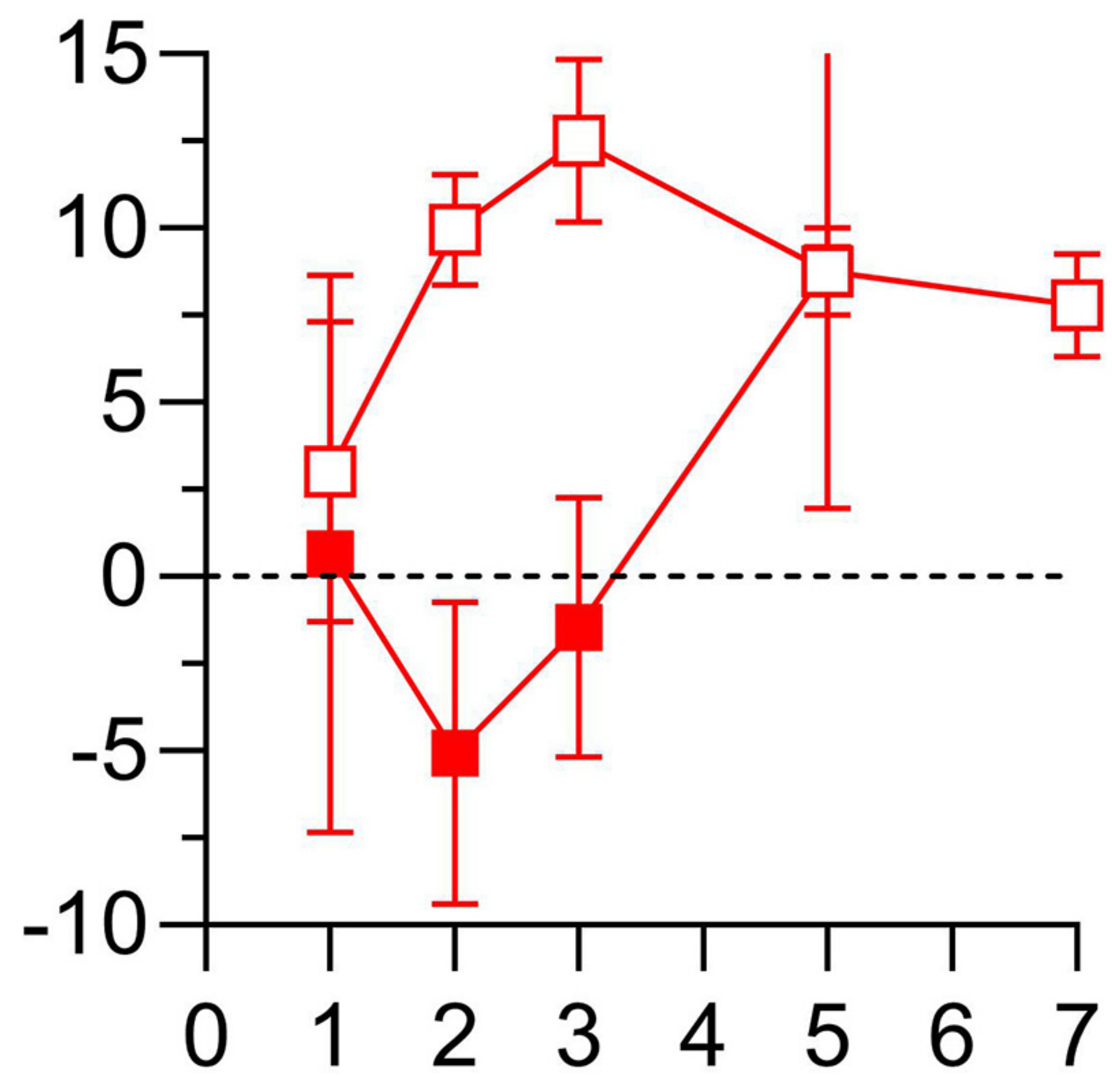
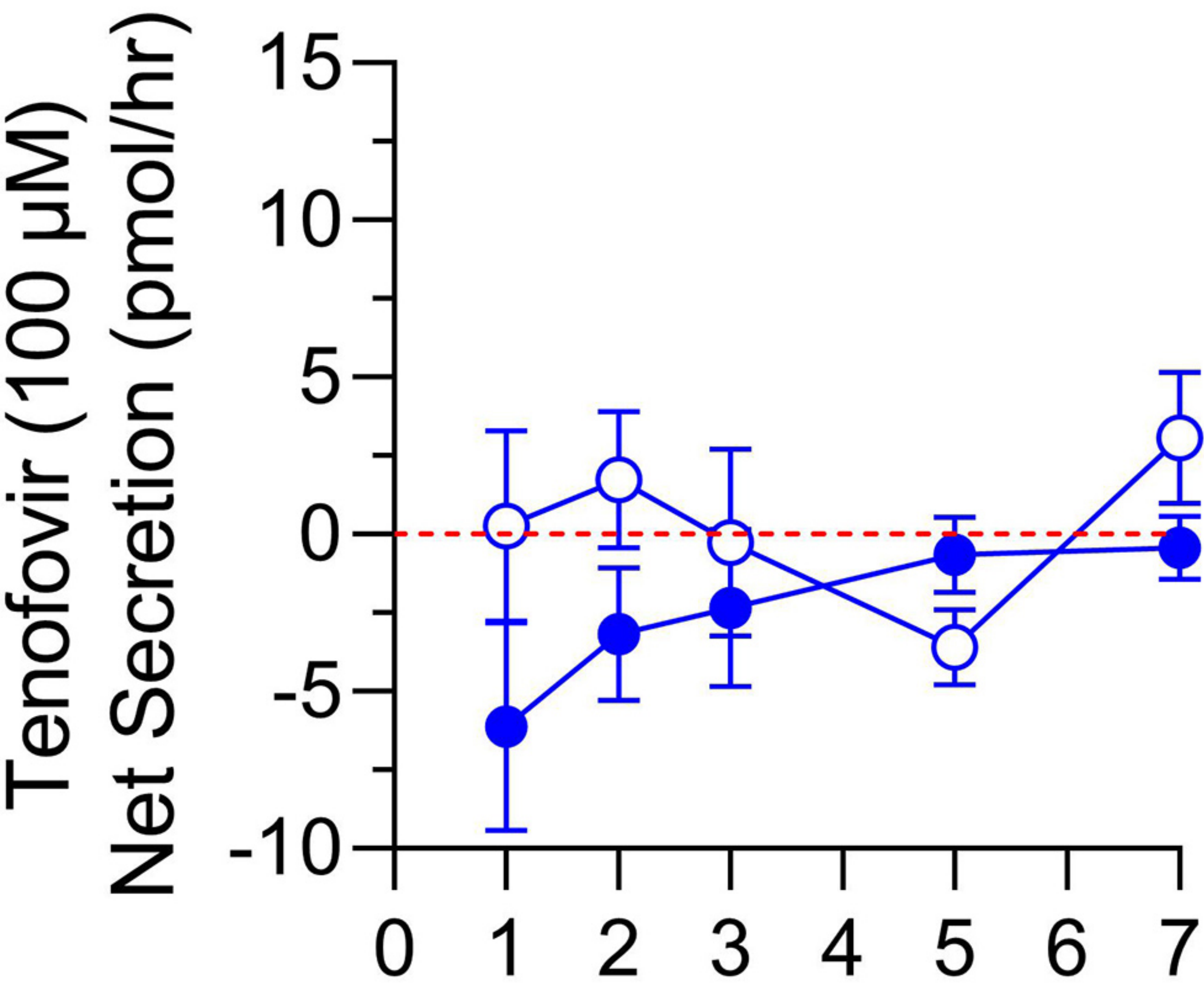
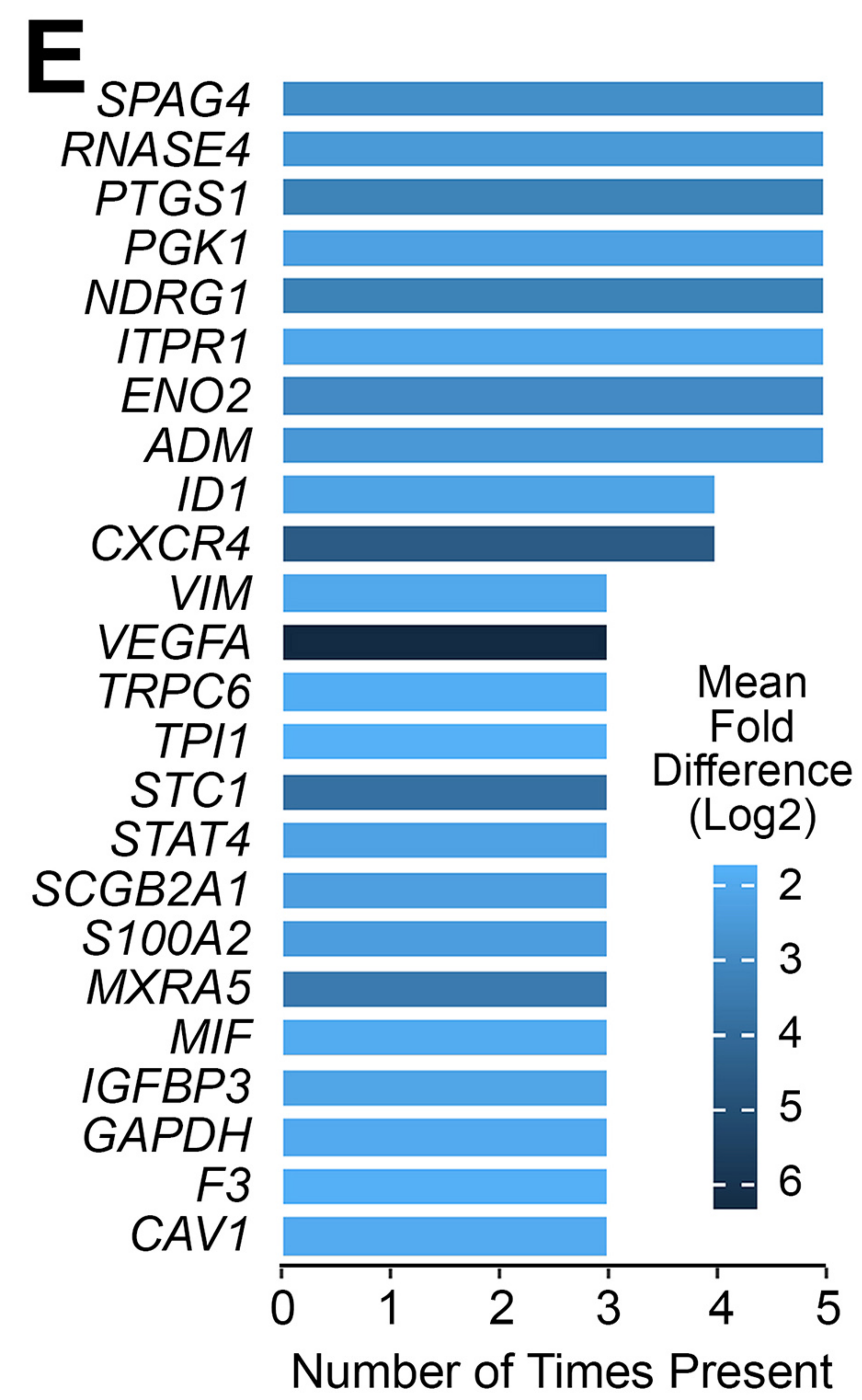
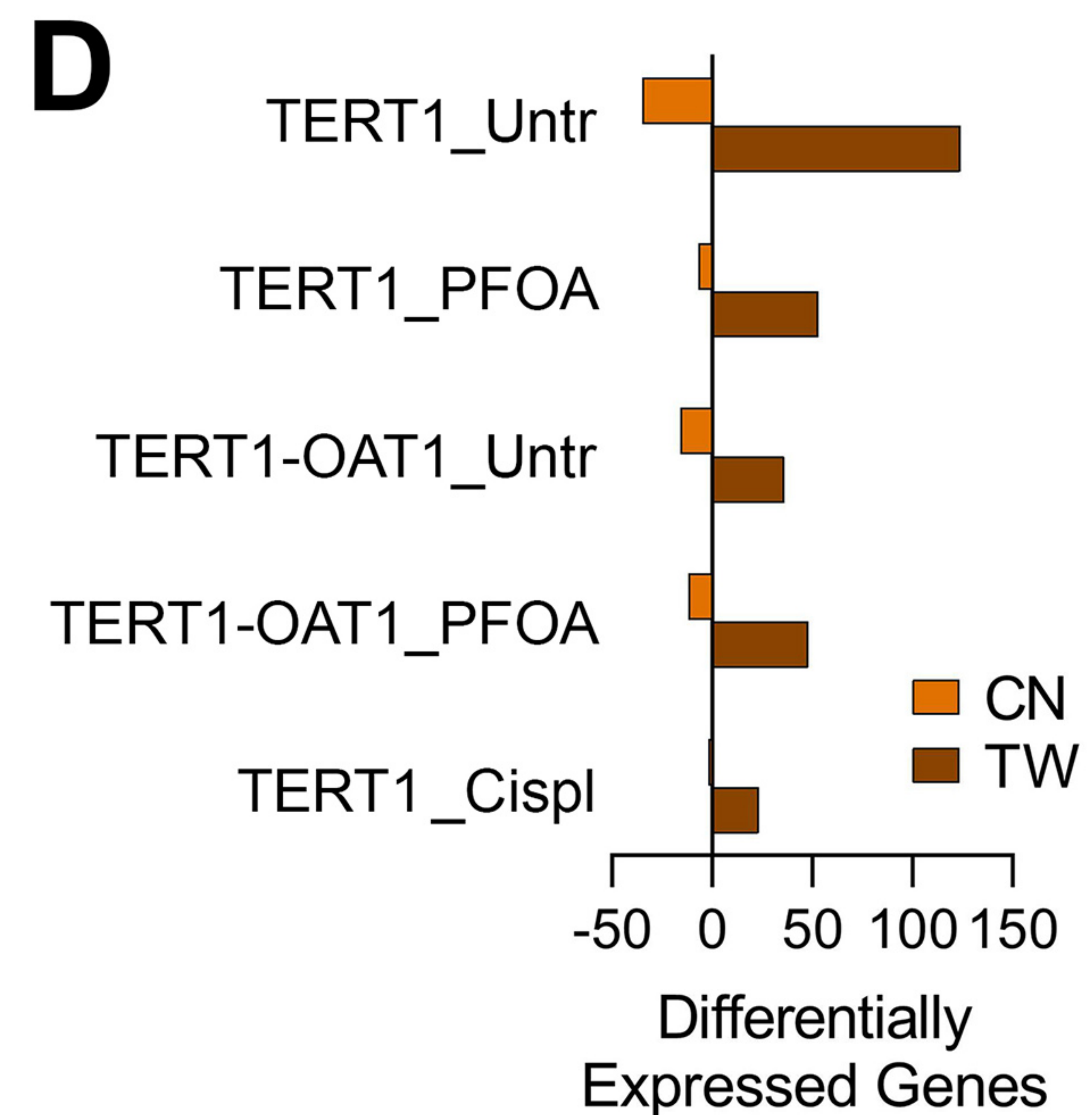
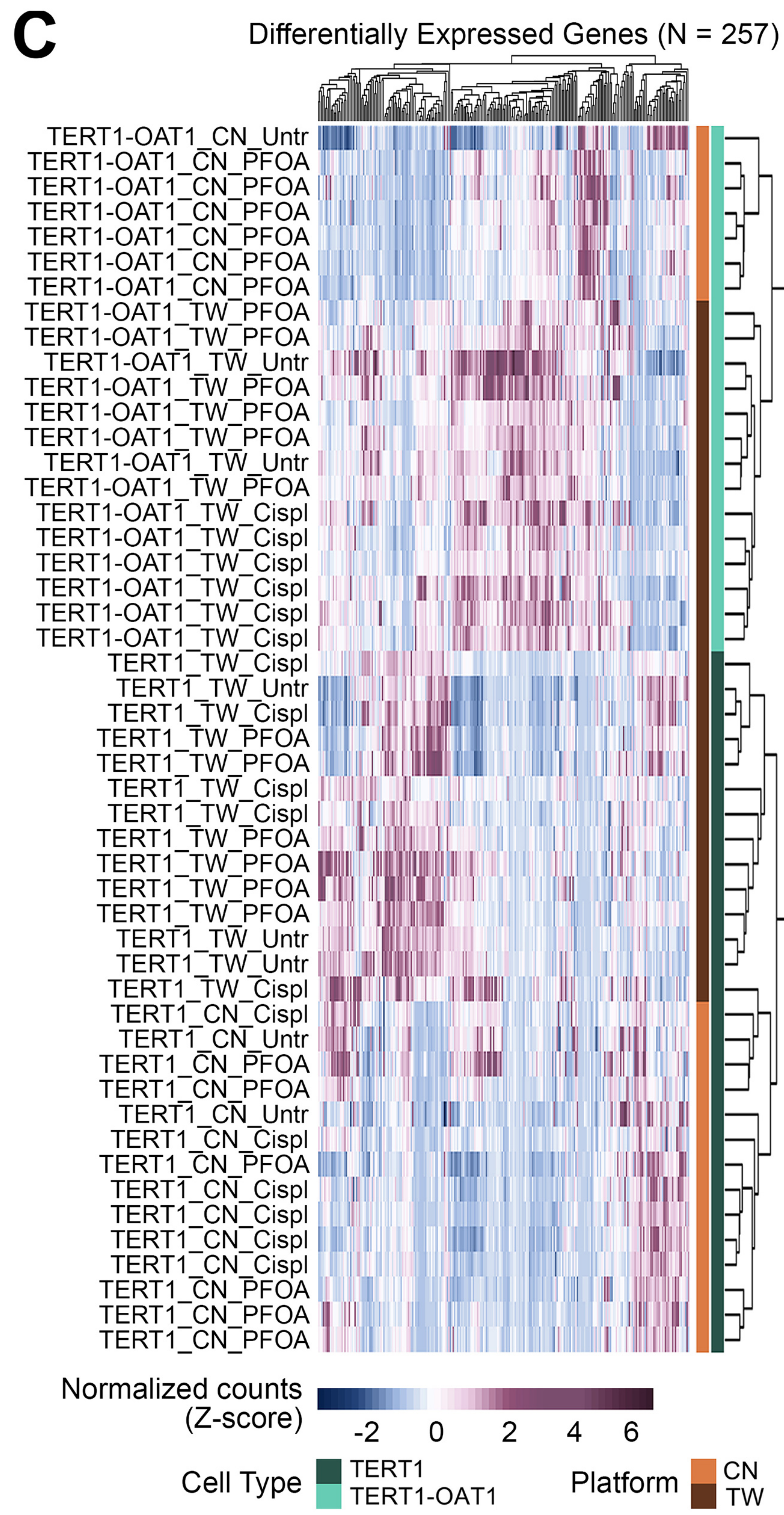
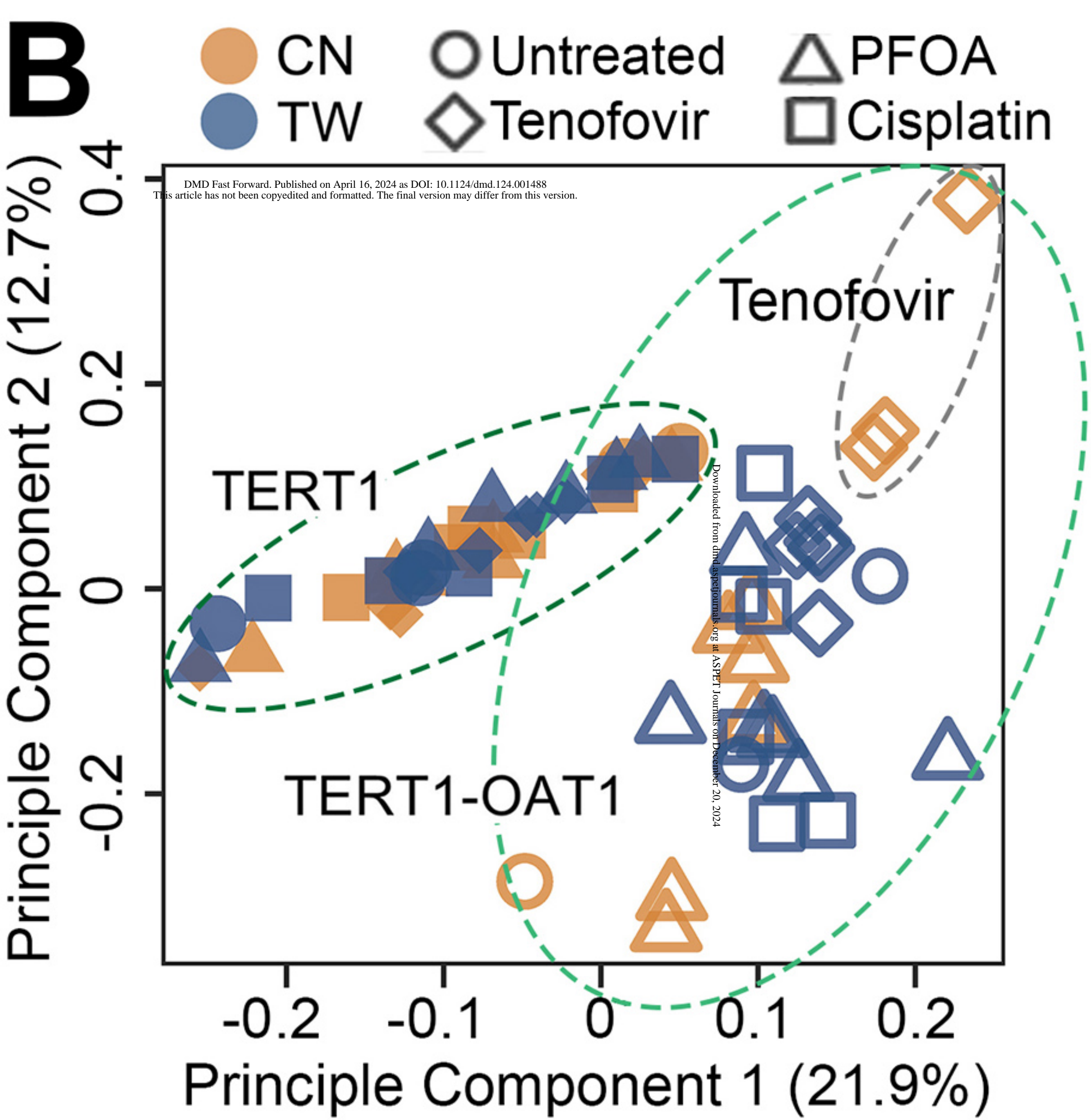
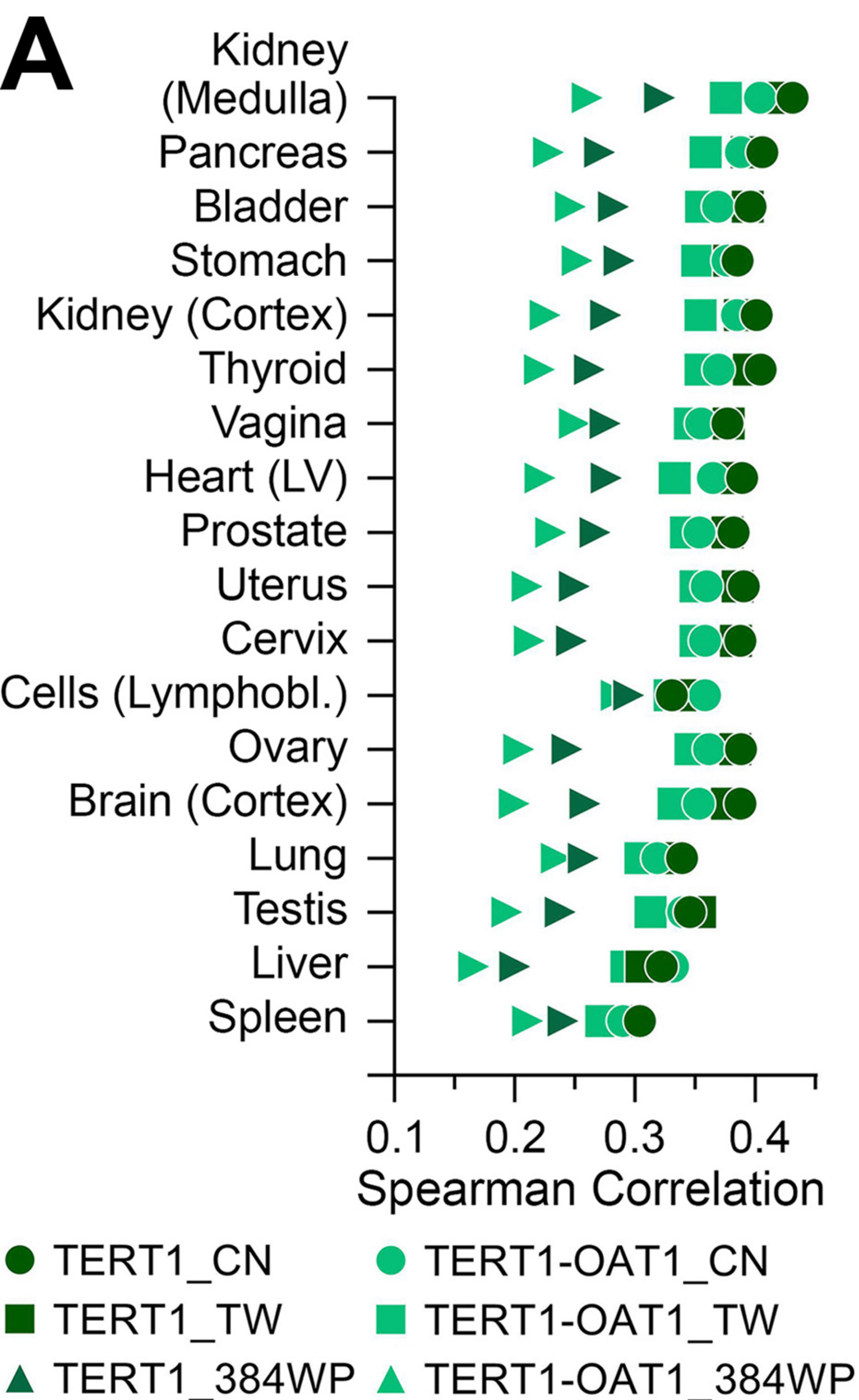


Figure 8

SUPPLEMENTAL TABLES AND FIGURES

Comparative Analysis of the Physiological and Transport Functions of Various Sources of Renal Proximal Tubule Cells Under Static and Fluidic Conditions in PhysioMimix™ T12 Platform

Courtney Sakolish,¹ Haley L. Moyer,¹ Han-Hsuan D. Tsai,¹ Lucie C. Ford,¹

Allison N. Dickey², Piyush Bajaj³, Remi Villenave⁴, Philip Hewitt⁵,

Stephen S. Ferguson⁶, Jason Stanko⁶ and Ivan Rusyn¹

¹Department of Veterinary Physiology and Pharmacology, Texas A&M University, College Station, TX 77843, USA

²Bioinformatics Research Center, North Carolina State University, Raleigh, NC 27695, USA

³Global Investigative Toxicology, Preclinical Safety, Sanofi, Cambridge MA 02141, USA

⁴Roche Pharma Research and Early Development, Roche Innovation Center Basel, F. Hoffmann-La Roche Ltd, Basel, Switzerland

⁵Chemical and Preclinical Safety, Merck KGaA, Darmstadt, Germany

⁶Division of Translational Toxicology, National Institute of Environmental Health Sciences, Research Triangle Park, NC, 27709, USA

Supplemental Table 1. List of studies included in each figure and the links to study protocols and data.

Figure(s)	Study Name in the Database	Direct Access URLs
2-5	CNBio_Proximal Tubule_Exp4 (6 cell comparison)	https://eve.eveanalytics.com/assays/assaystudy/596/
6	CNBio_Proximal Tubule_Exp9-pAH Transport [Transwell vs. CNBio, TERT1-parent, OAT1]	https://eve.eveanalytics.com/assays/assaystudy/1012/
7	CNBio_Proximal Tubule_Exp5 (3 Compound Tox/Transport)	https://eve.eveanalytics.com/assays/assaystudy/670/

Supplemental Table 2. Xenobiotic metabolism genes that were retained for the gene expression analysis regardless of their expression level across samples.

SYMBOL	GENENAME
<i>ABCC4</i>	ATP binding cassette subfamily C member 4
<i>MT2A</i>	metallothionein 2A
<i>ABCC5</i>	ATP binding cassette subfamily C member 5
<i>ABCC3</i>	ATP binding cassette subfamily C member 3
<i>PPARGC1A</i>	PPARG coactivator 1 alpha
<i>ABCC4</i>	ATP binding cassette subfamily C member 4
<i>NR1H4</i>	nuclear receptor subfamily 1 group H member 4
<i>SLC22A6</i>	solute carrier family 22 member 6
<i>GGT1</i>	gamma-glutamyltransferase 1
<i>SLC22A6</i>	solute carrier family 22 member 6
<i>NR3C1</i>	nuclear receptor subfamily 3 group C member 1
<i>SLCO2B1</i>	solute carrier organic anion transporter family member 2B1
<i>CYP3A5</i>	cytochrome P450 family 3 subfamily A member 5
<i>SLCO1B1</i>	solute carrier organic anion transporter family member 1B1
<i>CYP1B1</i>	cytochrome P450 family 1 subfamily B member 1
<i>ABCC2</i>	ATP binding cassette subfamily C member 2
<i>ABCC2</i>	ATP binding cassette subfamily C member 2
<i>NR1H3</i>	nuclear receptor subfamily 1 group H member 3
<i>ABCC3</i>	ATP binding cassette subfamily C member 3
<i>CYP3A5</i>	cytochrome P450 family 3 subfamily A member 5
<i>ABCB10</i>	ATP binding cassette subfamily B member 10
<i>SLC47A1</i>	solute carrier family 47 member 1
<i>GGT1</i>	gamma-glutamyltransferase 1
<i>CYP2B6</i>	cytochrome P450 family 2 subfamily B member 6
<i>SLC22A7</i>	solute carrier family 22 member 7
<i>ABCG2</i>	ATP binding cassette subfamily G member 2 (Junior blood group)
<i>NR1I3</i>	nuclear receptor subfamily 1 group I member 3
<i>SLC22A2</i>	solute carrier family 22 member 2
<i>SLC47A1</i>	solute carrier family 47 member 1
<i>SLC22A8</i>	solute carrier family 22 member 8
<i>KCNJ18</i>	potassium inwardly rectifying channel subfamily J member 18
<i>ABCB1</i>	ATP binding cassette subfamily B member 1
<i>ABCB1</i>	ATP binding cassette subfamily B member 1
<i>ABCB11</i>	ATP binding cassette subfamily B member 11
<i>ABCC1</i>	ATP binding cassette subfamily C member 1
<i>SLC10A2</i>	solute carrier family 10 member 2
<i>SLC22A1</i>	solute carrier family 22 member 1
<i>DPYS</i>	dihydropyrimidinase
<i>MT1G</i>	metallothionein 1G
<i>ATP1B1</i>	ATPase Na ⁺ /K ⁺ transporting subunit beta 1
<i>FN1</i>	fibronectin 1
<i>ARHGAP8</i>	Rho GTPase activating protein 8
<i>CDH1</i>	cadherin 1

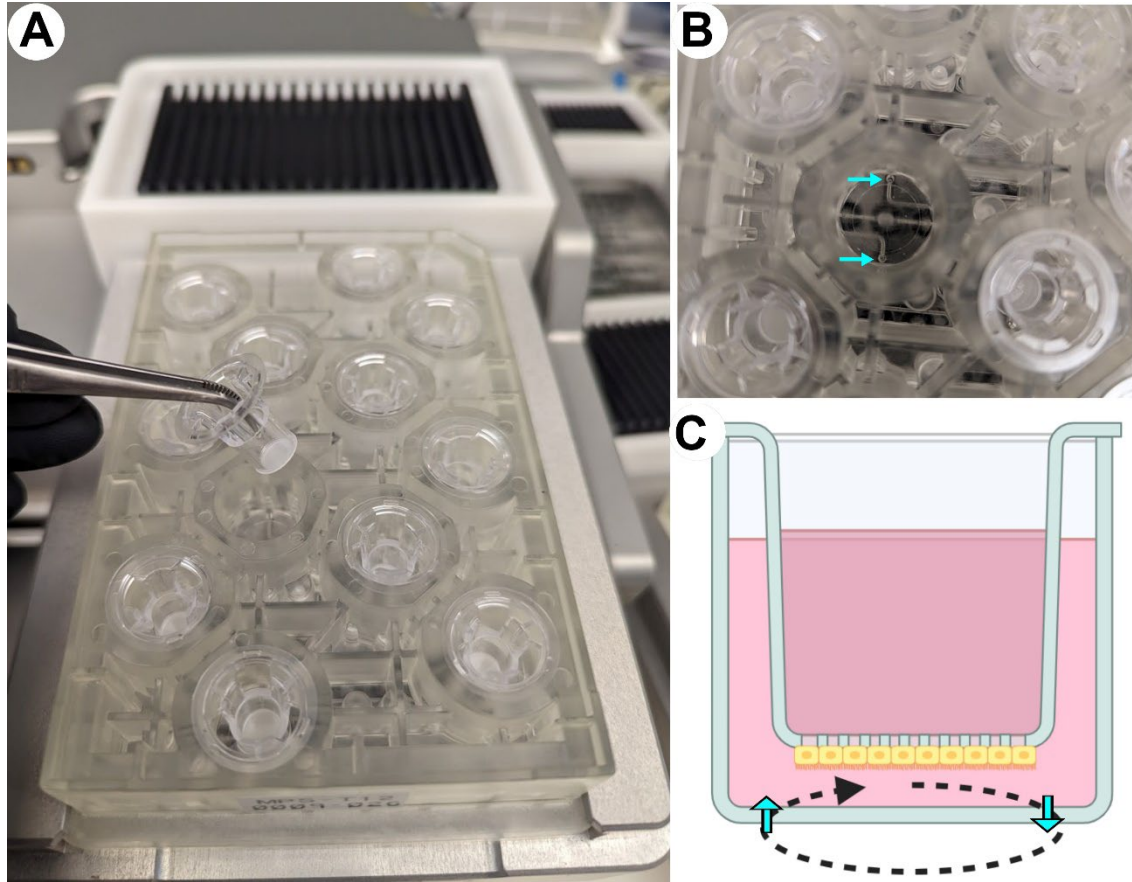
Supplemental Table 3. Top 9 genes shown in Figure 8E are listed with respect of their gene function and relevance to kidney function (a PubMed search for “gene” and “kidney”), as well as relative expression in human kidney as compared to other tissues using information from GeneCards (<https://www.genecards.org/>).

Gene	Gene Function	Kidney Association	Expression level in kidney
ADM	Vasodilation and blood pressure regulation	ADM is expressed in the kidney and is involved in renal vasodilation and regulation of renal blood flow.	moderate
ENO2	Glycolytic enzyme	ENO2 is expressed in various tissues, including the kidney, where it participates in metabolic processes.	moderate
ITPR1	Calcium signaling	ITPR1 is expressed in the kidney and contributes to calcium signaling, which is essential for renal function.	higher
NDRG1	Cell differentiation and stress responses	NDRG1 is expressed in the kidney and may play a role in renal cell differentiation and response to stress.	higher
PGK1	Glycolytic enzyme	PGK1 is expressed in the kidney and contributes to energy production in renal cells.	high
PTGS1	Prostaglandin synthesis	PTGS1 is expressed in the kidney and plays a role in renal prostaglandin production and regulation of renal blood flow.	moderate
RNASE4	Ribonuclease enzyme	RNASE4 may be expressed in the kidney and participate in RNA degradation processes.	moderate
SPAG4	Sperm function and male fertility	SPAG4 is not typically associated with kidney function but may have a role in other tissues.	moderate
CXCR4	Chemokine receptor	CXCR4 is expressed in the kidney and may play a role in immune cell recruitment during kidney inflammation.	moderate

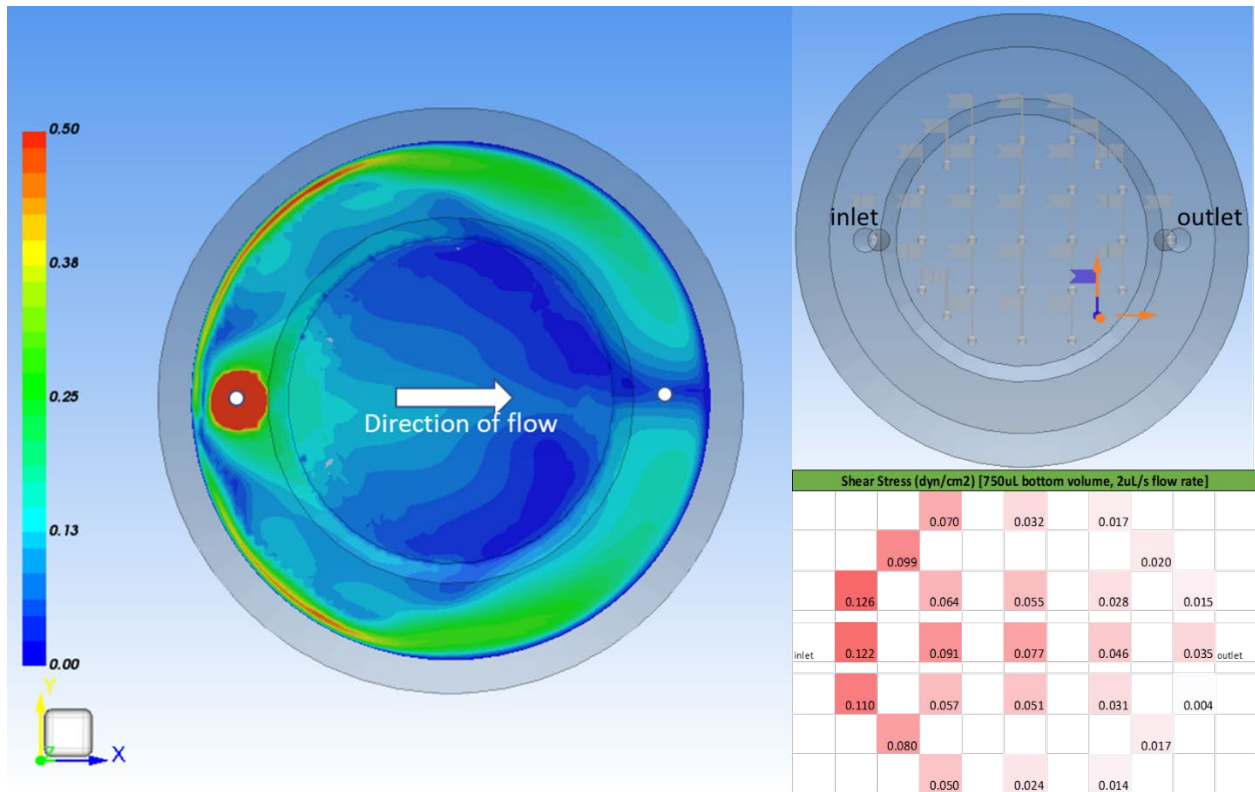
Supplemental Table 4. Significantly affected pathways derived from transcriptomic profiles shown in Figure 8D.

Significant Pathway	Genes in a Pathway	Group	#Overlap	p _{adj}
REACTOME_GLYCOLYSIS	<i>ALDOA, ENO2, GAPDH, PGAM1, PGK1, TPI1</i>	TERT1 untreated	6	7.10E-07
REACTOME_GLUONEOGENESIS	<i>ALDOA, ENO2, GAPDH, PGAM1, PGK1, TPI1</i>	TERT1 untreated	6	1.10E-06
KEGG_GLYCOLYSIS_GLUONEOGENESIS	<i>ALDOA, ENO2, GAPDH, LDHA, PGAM1, PGK1, TPI1</i>	TERT1 untreated	7	1.50E-06
REACTOME_GLUOSE_METABOLISM	<i>ALDOA, ENO2, GAPDH, PGAM1, PGK1, TPI1</i>	TERT1 untreated	6	3.50E-05
PID_HIF1_TFPATHWAY	<i>ADM, ALDOA, CXCR4, LDHA, NDRG1, PGK1</i>	TERT1 untreated	6	0.00037
PID_P53_DOWNSTREAM_PATHWAY	<i>BNIP3L, CAV1, IGFBP3, MDM2, NDRG1, S100A2, SFN</i>	TERT1 untreated	7	0.00088
REACTOME_METABOLISM_OF_CARBOHYDRATES	<i>ALDOA, ENO2, GAPDH, HS2ST1, PGAM1, PGK1, TPI1</i>	TERT1 untreated	7	0.0011
PID_HIF1_TFPATHWAY1	<i>ADM, CXCR4, NDRG1, PGK1, VEGFA</i>	TERT1 treated with cisplatin	5	5.40E-05
PID_HIF1_TFPATHWAY2	<i>ADM, CA9, CXCR4, FOS, LDHA, NDRG1, PGK1</i>	TERT1 treated with PFOA	7	3.00E-04
KEGG_GLYCOLYSIS_GLUONEOGENESIS1	<i>ENO2, GAPDH, LDHA, PGK1, TPI1</i>	TERT1 treated with PFOA	5	0.00078
PID_P53_DOWNSTREAM_PATHWAY1	<i>BNIP3L, BTG2, IGFBP3, NDRG1, S100A2, TIGAR</i>	TERT1 treated with PFOA	6	0.013
REACTOME_GLYCOLYSIS1	<i>ENO2, GAPDH, PFKP, PGK1, TPI1</i>	TERT1-OAT1 treated with PFOA	5	0.00012
KEGG_BLADDER_CANCER	<i>CXCL8, MDM2, MMP1, THBS1, VEGFA</i>	TERT1-OAT1 treated with PFOA	5	0.0016
KEGG_GLYCOLYSIS_GLUONEOGENESIS2	<i>ENO2, GAPDH, PFKP, PGK1, TPI1</i>	TERT1-OAT1 treated with PFOA	5	0.0016
REACTOME_GLUOSE_METABOLISM1	<i>ENO2, GAPDH, PFKP, PGK1, TPI1</i>	TERT1-OAT1 treated with PFOA	5	0.0016
PID_HIF1_TFPATHWAY3	<i>ADM, CA9, CXCR4, NDRG1, PGK1, VEGFA</i>	TERT1-OAT1 treated with PFOA	6	0.0016
REACTOME_INTERFERON_ALPHA_BETA_SIGNALING	<i>IFI27, IFI6, IFIT1, MX1, XAF1</i>	TERT1-OAT1 treated with PFOA	5	0.0022
NABA_MATRISOME	<i>COL12A1, CTGF, CXCL8, CYR61, MMP1, MXRA5, S100A2, SEMA5A, THBS1, VEGFA</i>	TERT1-OAT1 treated with PFOA	10	0.0027
NABA_CORE_MATRISOME	<i>COL12A1, CTGF, CYR61, MXRA5, THBS1</i>	TERT1-OAT1 treated with PFOA	5	0.0091
PID_P53_DOWNSTREAM_PATHWAY2	<i>BBC3, CAV1, MDM2, MET, NDRG1, S100A2</i>	TERT1-OAT1 treated with PFOA	6	0.014
REACTOME_INTERFERON_SIGNALING	<i>IFI27, IFI6, IFIT1, MX1, XAF1</i>	TERT1-OAT1 treated with PFOA	5	0.033
REACTOME_GPCR_DOWNSTREAM_SIGNALING	<i>ADM, CXCL8, CXCR4, MTNR1A, RGS2</i>	TERT1-OAT1 treated with PFOA	5	0.046

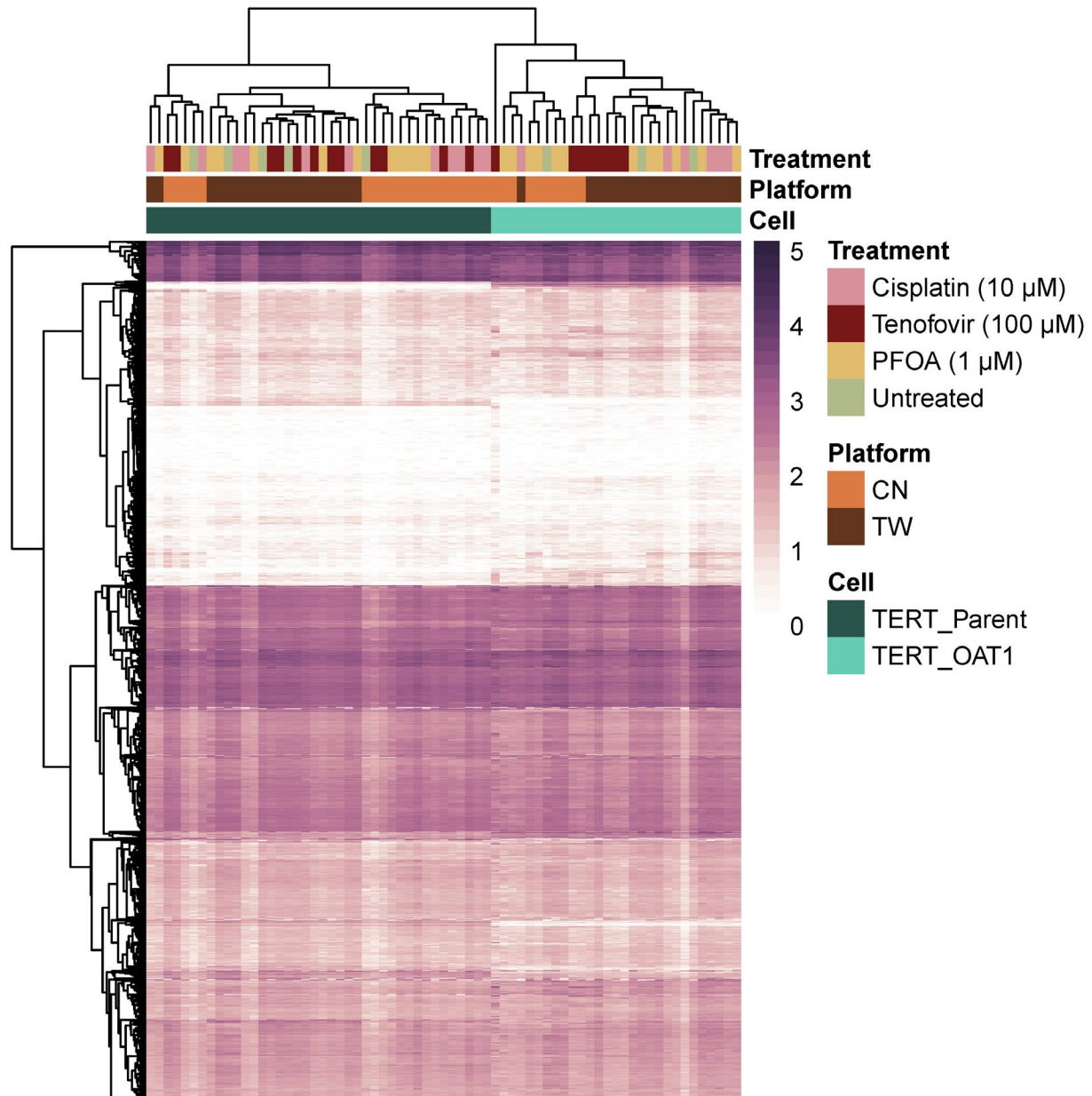
Supplemental Figure 1. Schematic of CNBio PhysioMimix T12 plate. **(A)** A photograph of a standard 24-well plate Transwell insert and how they fit into a single T12 plate (CNBio). The T12 plate is shown inserted into a dock that is connected to a controller (not shown) which regulates the media flow on each T12 plate. **(B)** A magnified image of the inside of each well of a T12 plate. Each well has a single inlet and outlet at the bottom (shown by the blue arrows) which allows for recirculation of the media and fluid flow (see Supplemental Figure 2) against the cells seeded on the bottom surface of the Transwell membrane. **(C)** A schematic drawing illustrating a magnified side view of a Transwell inserted into a well of a T12 plate with cells seeded on the bottom of a Transwell in the path of a recirculating media flow (dashed black arrow). Inlet and outlet locations are shown (blue arrows).



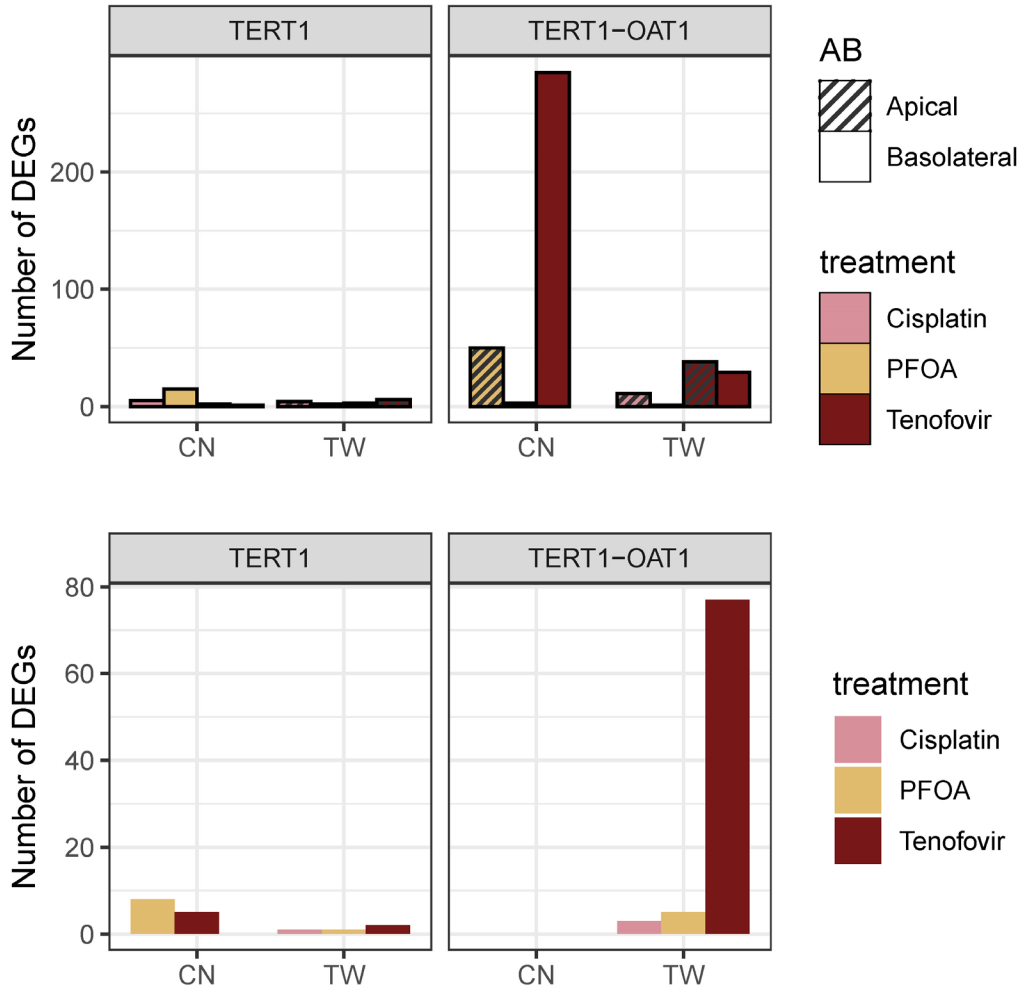
Supplemental Figure 2. Fluid dynamic modeling of shear stress in the PhysioMimix™ T12 platform under our experimental growth conditions (2 $\mu\text{l/s}$ flow rate, 750 μL volume in bottom chamber). Flow rate is thresholded to a max of 0.5 $\mu\text{L/s}$ to allow for gradient visualization. “Flags” were placed to probe fluid flow rate at evenly spaced locations across the membrane. Shear stress (dyne/cm^2) was calculated at each of these flagged locations, resulting in a peak of 0.126 dyne/cm^2 and average of 0.053 dyne/cm^2 .



Supplemental Figure 3. A heatmap visualizing expression of 2,311 genes across all samples passing quality control criteria (see Materials and methods for description). Color intensity represents $\log_{10}(\text{count} + 1)$ as input data matrix. Clustering of both genes (rows) and samples (columns) was performed using correlation distance and complete linkage. Cell sources are shown using shades of green (TERT1 – dark; TERT1-Oat1 – light). Culture conditions are indicated as static (TW) and fluidic (CN). Chemical treatments are also indicated by colors.



Supplemental Figure 4. Differentially expressed genes (DEGs) for pairwise comparisons among chemical treatments. **(Top)** The numbers of DEGs resulting from a comparison between treatment and control for each chemical separately for apical and basolateral treatments. Bars with patterns represent chemical treatments applied to the apical side, while bars without patterns represent chemical treatments applied to the basolateral side. **(Bottom)** The numbers of DEGs resulting from a comparison between treatment and control for each chemical between apical and basolateral treatment for each chemical.



Supplemental Figure 5. Expression levels of select xenobiotic metabolism genes in TERT1 (dark green) and TERT1-OAT1 (light green) cells cultured in static (TW) and fluidic (CN) conditions. Color represents relative expressions using $\log_{10}(\text{count} + 1)$ as input data matrix. Samples (columns) are arranged in the same order as the row order of Figure 8C, and genes (rows) are listed alphabetically.

